NTNU

Norwegian University of
Science and Technology

Effect of Fe and Si content in Aluminium Alloys as a result of increased recycling
Testing of high purity Aluminium Alloys in uniaxial tension

Marius Slagsvold

Materials Technology

Submission date: June 2011
Supervisor: Bjørn Holmedal, IMTE

Preface

This master thesis is the result of the final year of a 2-year master study at the department of material science, NTNU. The work is closely related to an ongoing project between Norsk HYDRO, SÄPA, NTNU and SINTEF supported by the Norwegian Research Department. The project was initiated to gain knowledge on the effects of alloying elements Fe, Si and Mg on aluminium alloys. In this work the approach is related to recycling and the quest to improve the recycling conditions and the search for new applicable recycled materials. Since few studies in recent times have been carried out under the same conditions, I am satisfied with my assignment and it has opened my eyes to the world of material science.

My background from mechanical engineering has been a challenge. Considerable time has been spent on gaining, to some elementary knowledge. This challenge has been accepted and I have tried to solve the task to my best abilities.

I would like to thank my supervisor, Bjørn Holmedal, for guidance and support throughout the duration of the work. Secondly, I would like to thank Pål Christian Skaret for his availability and help with the tensile testing. Sindre Bunkholt has been a great help with his wide material knowledge and clever "tricks", thank you. Many thanks to Pål Ulseth for offering supplies and help with sample preparations. A special thank you to Brit Wenche Meland who seems to genuinely care about all her students. Furthermore, thank you to Reidar Frog, Yingda Yu and Jarle Hjelen for their help. I would also like to acknowledge Norsk Hydro, Sunndalsøra for supplying the material used in this work.

Finally, I would like to thank Sofie and my family, friends and fellow students for their love and support throughout this project.

Trondheim, Norway, 20.6.2011

Marius Slagsvold

Abstract

The recycling of aluminium from used aluminium scrap leads to an unavoidable presence of pollutions in the form of elements of various amounts. Two such elements are iron and silicon. These will always be present to some extent in an aluminium alloy as they are introduced to the alloy during processing. Iron and silicon are accumulative elements, meaning that they can never be completely eliminated once introduced into the aluminium. Some alloys have very narrow compositional windows, they have strict regulations concerning amount of alloying elements allowed. This is of grave importance for the recycling process; to be able to produce specific alloys with limitations regarding content and mechanical properties. A project to uncover the effects of common elements in aluminium such as Mg, Si and Fe has been initiated by the industry. This work is closely related to the project and was carried out as a report during fall 2010 and continued as a master thesis during spring 2011.

The aim of this work was to study the effects of variation of small amounts of iron and silicon in 4 different alloys of high and ultra high purity (>99.7 and >99.999 wt% Al, respectively). The main focus was to uncover the effect of the elements on mechanical properties. Tensile test experiments with specimens in uniaxial tension were conducted to uncover the mechanical properties of the alloys. In addition to the tensile tests other parameters like texture, particles, recrystallisation and micro structure development were investigated. DC-cast, extruded flat profiles and rolled and recrystallised versions of the 4 alloys were used during the work.

The results from tensile tests performed on the rolled and recrystallised aluminium showed that an initial introduction of 0.066 wt % Fe and Si 0.068 wt % to an alloy containing no pollutions lead to a dramatic increase in strength properties (up to 100% for the tensile strength) and a mild decrease in elongation. The increased strength properties and reduced formability was traced to iron and silicon in solid solution. From the same tensile tests it was concluded that a further increase of iron and an introduction of a small amount of pollutions had close to no effect on the mechanical properties.

Abbreviations

Al5N	Ultra pure aluminium alloy, 5N > 99,999 wt% Al
Al5NFeSi	Ultra pure aluminium alloy 5N, as Al5N with the addition of small amounts of iron and silicon
Al2NFeSi	Commercially pure alloy 2N > 99.7 wt% Al, similar to Al5NFeSi with the addition of trace elements
Al2NFe2Si	Commercially pure alloy 2N > 99.7 wt% Al, higher amount of iron, silicon and trace elements compared to Al2NFeSi
Recrystallisation	Formation of new grains by heating a cold worked material[1]
YS and UTS	Yield strength (also referred to as R_{p02}) and Ultimate Tensile strength
Uniform elongation	Elongation during uniform decrease of the cross sectional area, prior to necking
Texture	A preferred crystallographic orientation for the grains in an alloy
ODF	Orientation distribution function
IPF	Inverse pole figure
PF	Pole figure
SEM	Scanning Electron Microscope
EBSD/EBSP	Electron Backscatter Diffraction/Electron Backscatter Pattern
EDS	Energy Dispersive Spectroscopy
PID	Proportional–Integral–Derivative controller

Table of Content

1. Introduction

1.1. Background

Recycling of aluminium is a preferable way to manufacture aluminium compared to the production from raw material. It comes with many benefits, the main ones being the environmental, economical and low energy consumption. The reduction process from bauxite to form alumina is a very energy consuming and polluting process. Recycling requires only 5% of the energy used in the bauxite process and the polluting process is eliminated. The melting temperature of aluminium is very low and this is one of the main contributing factors to the energy reduction.

Figure 1: Aluminium production furnaces (left)[2], aluminium production from raw material emits toxic gases illustrated by the chimneys (right)[3].

There is an ever growing focus on environmental issues in the industrial world, and the world in general, today. Regulations and directives from instances such as EU are sanctioned with the aim to both decrease the amount of toxic gasses released to the atmosphere and to utilise used metal scrap. Such directives are already in place in the material and metal industry today. It is likely that regulations, directives and laws will increase in the future to further reduce the environmental damage caused by material manufacturing processes. This is also visible in the aluminium industry. Terms such as "carbon footprint" are of grave importance when customers choose their suppliers. The carbon footprint refers to the amount of carbon dioxide released during production processes such as the alumina production from bauxite. Some companies require that a certain part of the end product should contain a large fraction of recycled material and a limited release of CO_2 emitted during production. In order to be a lucrative supplier in the aluminium industry in the future one must ideally limit the production from raw material and instead make use of as much used scrap metal as possible. Furthermore, the aluminium manufacturers believe that in the future the customers will order aluminium alloys with the desired quality and properties rather than focusing on the exact amounts of elements or if the material belongs to a certain group with a certain name. In this way, new alloys can be created to better suit the desired function and this makes the use of recycled material much easier. For aluminium, which is considered to be 100% recyclable, this would be greatly beneficial as the financial and environmental advantages are substantial[4].

Iron and silicon will always be present in any given aluminium alloy as they are accumulative elements, they will never be completely eliminated once introduced in the material and will only increase with further recycling. Some of the iron derives from the earth where the bauxite is found. Both iron and silicon are introduced through the aluminium casts and processing. Because it is

virtually impossible to prevent such elements presence in aluminium alloys it is essential to uncover the effects of iron and silicon in aluminium alloys. This is significantly visible when manufacturing low alloyed aluminium materials, such as 1xxx Al alloys. The window for allowed amounts of alloying elements is very narrow and it is difficult to control the amount of alloying elements. Furthermore, from a recycling perspective it is even more important to uncover the effects of Fe and Si. Before a material of aluminium is recycled it often arrives covered in dirt, material splinter, paint or coating. To reproduce an alloy which fulfils the requirements for the desired alloy type, the scrap has to be cleaned and distinguished by alloy and alloying elements.

Even elements of the order ppm can affect the properties of a material dramatically. In a lecture by Trond Furu[4], such an example was presented. By increasing the relative amount of Mn in an 8xxx aluminium alloy from 150 ppm to 280 ppm the tensile strength was found to increase by 35MPa (!). It is evident that the study of alloying elements and their effects are of grave importance. In figure 2, two examples are given on the mechanisms which may be present in alloys containing Pb or Cu.
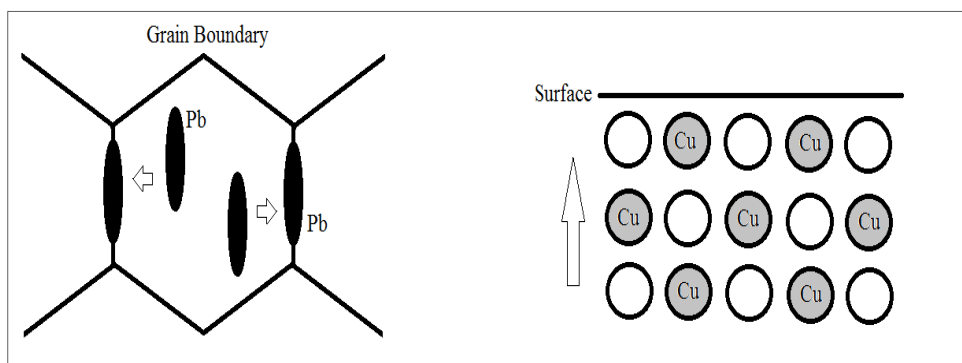

Figure 2: Strengthening of a material caused by diffusion of Pb toward grain boundaries (left) and diffusion of Cu toward the surface.

Säpa, Hydro, SINTEF and NTNU, supported by the Norwegian Science department, have initiated a project to gain knowledge and competence of the effect on variation of iron, silicon and magnesium (not covered in this work) in aluminium alloys. Specifically, the areas of interest include the effect on homogenisation, extrusion/rolling, forming and end properties. This paper is a continuation of a project work carried out by the author during autumn 2010. The project examined extruded flat profiles of high purity aluminium by means of tensile testing.

This thesis will concentrate on mapping the effects of very small amounts of iron and silicon in aluminium alloys of high and ultra high purity. Aluminium material of high purity containing varying degree of relatively small amounts of iron (0.0005-0.149 wt %) and silicon (0.0005-0.069 wt %), have been tested mainly by means of tensile experiments. The approach serves as a model for the recycling process, as more iron and silicon is introduced to the material by means of recycling. The fundamental question is then: are the effects on material properties from such small amounts of Fe and Si *substantial* or *negligible*?

1.2. Previous work

Marius Slagsvold's "*Study on the effect of Fe and Si content in Aluminium Alloys as a result of increased recycling - Testing of high purity aluminium alloys in uniaxial tension*"[5] was carried out during fall 2010. The work presented in the following pages is a continuation of a project work on the same material during fall 2010. As the results are directly connected and comparable they are referred to in sections where relevant. In section 6.1. the most important findings from the work are presented.

In his PhD, "*Work hardening and mechanical anisotropy of aluminium sheets and profiles*" from 2003, Øyvind Ryen[6] studied several aluminium alloys of the type AA6xxx and AA7xxxx. The main strengthening contribution for recrystallised alloys was found to be through Si, Mg and Zn in solid solution. The non-recrystallised alloys owed their strength to grain and sub grain size. Silicon was found to give rise to a high strengthening effect likely caused by a clustering. The extruded profiles investigated exhibited very strong textures, indicating variations in the Taylor factor in the profile plane. The consequence was that the materials showed a strong mechanical anisotropy, some profiles showed a strength variation of as much as 20-30%. The textures found in the recrystallised alloys were considered to be cubic, rotated cubic or Goss textures. The non-recrystallised alloys yielded a β-fibre texture. The extruded profiles had significant micro structural and textural gradients through the thickness, however, these were found to give only minor effects on the mechanical properties. In the non-recrystallised alloys the texture judged to be responsible for most of the strength anisotropy.

Frode Westvold's thesis, "*The effects of alloying elements on mechanical properties and formability of recycled aluminium sheet*"[7] from 2000, considered the effect of a selected group of common alloying elements (Fe, Si, Mn, Cu, Zn and Mg). The amount of elements of relevance to this paper, iron and silicon, were in the region 0.48-1.94 wt % and 0.16-0.50 wt % respectively. Westvold used tensile testing to determine the mechanical properties in a series of modified AA1200 alloys. A high density of coarse particles (due to high content of Fe and Si) in the alloys was found to display the best ability to distribute strain, i.e. postpone the onset of necking. Furthermore it was found that alloys with elements in solid solution strain hardened more at lower strains than the non-solute alloys, while at higher strains the behaviour was reversed. Alloys with a high density of coarse particles (and dispersoids) were found to maintain their strain hardening capacity at higher strains. Fe and Si were considered favourable for maintaining strain hardening abilities at higher strains.

The 1200 low alloyed materials and one 5050 alloy which contained 1.4% Mg in solid solution showed increased strength, both YS and UTS increased by 10MPa and 20MPa respectively with the introduction of a high density of coarse particles. The elongation, both uniform and total, was reduced by 85%. Further addition of dispersoids had a modest effect on uniform elongation. Total elongation, however, decreased noticeably for the alloys containing solid solution. Strain hardening behaviour was improved by elements in solid solution at low strains. However, the strain hardening decreased more rapidly at higher strains than for the non-solute alloys. Strain rate sensitivity decreased slightly in the presence of coarse particles, while the addition of dispersoids had a positive effect on the strain rate sensitivity. Elements in solid solution had a strong negative effect on the strain rate sensitivity.

Istvàn Kovàcs book *"Effect of Iron and Silicon in Aluminium and its Alloys"*[8] consists of numerous articles on the subject of iron and silicon effects in aluminium alloys in connection with an international workshop held in Balatonfüred in Hungary, May 1989. Some of the work is closely related to the present work. However, a summary of the findings in this extensive book will not be included here as it contains numerous partly relevant articles. The book will instead be used as a reference and a recommended read.

A study on AA6xxxx alloys yielded the following results regarding excess Fe, Si and Mg: the number density of inclusions increased with adding excess amount of Si, Mg and Fe. The inclusions were found to be composed of mainly Al, Fe and Si when Fe and Si were solely added. A part of the Si content was found to be consumed to form inclusions and the remained Si is effective for age hardening by forming the β"[9].

2. Theory

The most relevant and basic theory is covered in the following chapter. Firstly, some basic properties of aluminium are given; secondly, the strengthening contributors which may be present in aluminium alloys are presented. Finally, a more detailed description of the tensile test parameters is covered as they are the main focus of this work.

2.1. Aluminium

In this sub section some properties and relevant factors regarding aluminium are covered.

2.1.1. Purity

Aluminium with a purity of at least 5N, or 99.999 wt% Al, is called ultra pure aluminium. The formability is very good along with low strength; it is easily deformable by hand. Aluminium of commercial quality is required to have a purity of no less than 99.7wt% Al, or 2N. Commercially pure aluminium contains a much higher degree of alloying elements and trace elements (pollutions) and display higher strength and reduced formability depending on the type of alloying elements. As the name suggests, the commercial aluminium is the most widely used in the industry today. Alloying elements are chosen and added to design a material with the desired qualities, concerning strength, formability, conductivity and corrosion resistance. Ultra pure aluminium has a very low recrystallisation temperature due to the fact that it contains few inhibitors against grain growth. The conductivity is very good in addition to good resistance against corrosion. These factors limit the use of such alloys to a few areas like cans, wires and such, i.e. where high formability and low strength is desired[10].

2.1.2. Main alloying elements

The main alloying elements in this paper are iron and silicon. Both iron and silicon have a very low solubility in aluminium, as the phase diagrams in figures 3 and 4 below show. Si has a maximum solubility at 570 ^{o}C of roughly 1.5%, while iron displays an even lower maximum solubility of 0.04% in aluminium. The low solubility of the elements implies that most of the amount present in an aluminium alloy will form intermetallic compounds of Fe, Si and or Al[8]. However, since the material in this work is of high- and ultra high purity even very small amounts of elements in solid solution may affect the mechanical properties greatly.
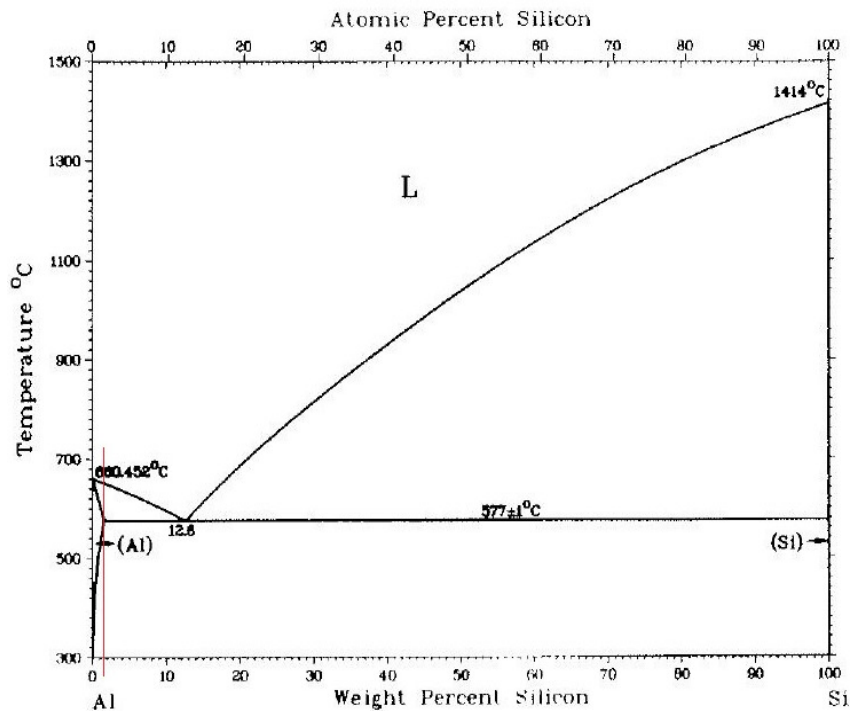
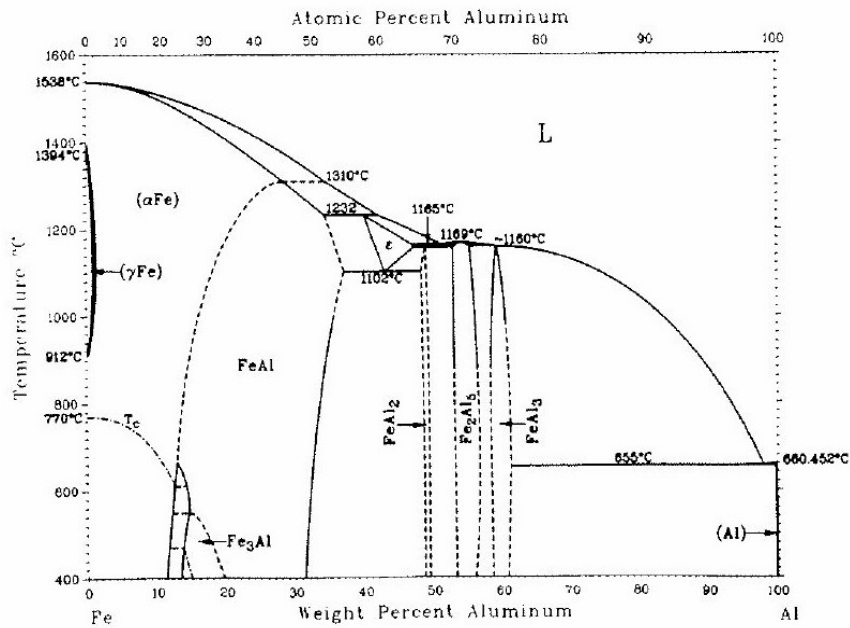*Figure 3: Phase diagram Al-Si.[10]*

Figure 4: Phase diagram Fe-Al.[10]

Some strengthening mechanisms in materials are related to the similarity in chemical properties. 2 such examples are solid solution and size misfit effect (size misfit is in reality a solid solution effect). For solid solution the length of lattice spacing is of importance and for strengthening from size misfit the size of an atom occupying space in a matrix' atom crystal lattice is important. Solid solution is easier when atoms have close to equal lattice spacing and a similar crystal structure. Strengthening through size misfit has an increased effect when the solute atom differs in size, it creates a strain field and the force of this field depends on said size. In table 1 below some key properties for aluminium, iron and silicon are given[11].

Table 1:Basic properties of aluminium, iron and silicon.[5]

	Aluminium	Silicon	Iron	Unity
Symbol	Al	Si	Fe	-
Density	2,71	2,33	7,87	$[g/cm^3]$
Atomic mass	26,98	28,09	55,85	[amu]
Atomic number	13	14	26	-
Melting point	660	1410	1536	$[C^o]$
Lattice spacing	4,04	5,43	2,87	[Å]
Structure	FCC	DIA/FCC	BCC/FCC	-
Glide plane	[111]	[111]	[110]	-
Glide direction	<110>	<110>	<111>	-

2.1.2. Extruded aluminium

A common way to produce aluminium in a wide range of shapes is through the process of extrusion. In short, a billet is introduced to a heated container, a ram pushes the billet against a steel die with the desired shape. The process is shown schematically in figure 5. When aluminium is deformed by means of extrusion the grains are elongated in the direction of extrusion and suppressed in the vertical direction. In addition the grains rotate and a fibre texture is created. This grain development leads to a strongly anisotropic material, i.e. the strength and mechanical properties are dependent on the direction of the deformation and not equal in all directions[1].
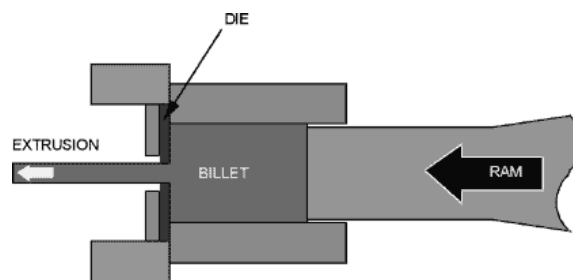

Figure 5: Basic principles of extrusion[5].

2.1.3. Cast aluminium

Casting is a simple procedure to produce various shapes and forms. Molten metal is introduced to a mold cavity, when the molten metal solidifies, it takes the shape of the cavity. The cavity comes in various shapes and casting offers a relatively uncomplicated and economical way to produce aluminium blocks and shapes. The most influential factors on the end casting product are the solidification, flow, heat transfer and mold material. Aluminium based cast alloys can be subjected to several hardening mechanisms and heat treatments which may result in alloys with a wide range of mechanical properties. Aluminium shrinks upon solidification while silicon precipitates. A clear disadvantage of the process is the presence of pours and segregations which cannot be completely avoided.[12]

2.1.4. Recycling

Recycling is an aluminium production method of great importance and will continue to grow in the future. Not only does it utilize used scrap aluminium which would otherwise go to waste (figure 6), but the advantages compared to the production from bauxite and alumina are massive. The production from raw material emits numerous pollutions through the reduction process, among them: green house gasses. Recycling requires 95% less energy compared to "raw" production and the economical benefits are substantial. As the polluting reduction process is excluded the environmental benefits are also of great importance. In addition, aluminium has several qualities which make it suitable for recycling. Aluminium has no "recollection" of its past and may therefore be recycled repeatedly without damaging the quality. Al also has a low melting temperature. [7]

Figure 6: Compressed used scrap aluminium and some examples of recycled products.[13-16]

Recycling used aluminium scrap to create specific alloys, which should not exceed certain requirements, is a challenge. Upon arrival the scrap metal is usually covered in dirt, coating and metal splinter. The scrap needs to be thoroughly cleaned and the alloy type needs to be distinguished in order to reproduce alloys with limitations with respect to alloy content, such as the 1050 alloy for example. Alloy content in the scrap may vary and it is a tedious process to uncover the amount of such for each scrap part prior to recycling. For alloys of high, super high and ultra high purity and in general low alloyed aluminium, recycling is even more challenging as the window for allowed alloying elements and pollutions is very narrow. Upon solidification from re-melting and further processing more pollutions and elements are introduced to the recycled

material. When recycling used scrap aluminium to form alloys with a low amount of elements and pollutions one must be very careful in order for the alloy to not exceed specific allowed levels.

2.2. Polycrystals

The crystallites in polycrystals are subjected to constraints when they deform plastically. Polycrystals must deform as a whole as opposed to single crystals where the response is made up of a set of individual crystals. In a polycrystal each grain has to participate in the deformation and each grain is affected by the shape change that the neighbouring grains undergo. A perfect fit of the crystals along their common grain boundaries must be fulfilled and this condition affects the strength and deformation of polycrystals.

In a polycrystal the grains have different orientations and when an external tensile stress is applied the initial deformation occurs in the grains which are favourably oriented. Less favourably oriented grains have not yet reached the critical resolved shear stress. An individual grain subjected to single slip deformation will change its shape; this shape change must be suppressed by elastic deformation causing rapidly increased internal stresses. The high internal stress eventually causes the neighbouring grains to reach the critical resolved share stress. To reach yield stress, all the grains in the polycrystal must deform plastically[17].

2.3. Strengthening mechanisms

In this section the most relevant strengthening mechanisms will be treated.

2.3.1. Strengthening from elements in solid solution

When a solute atom is introduced to a solid solution in the solvent-atom lattice the strength of the alloy is increased compared to that of the alloy without the solute atom. There are 2 main types of solid solutions. If the solute and solvent atoms are similar in size, the solute will occupy points in the solvent crystal lattice by substitution. This is *called substitutional solid solution*. Solute atoms which are much smaller than the solvent atoms will occupy positions between the solvent atoms in the crystal lattice. This is called *interstitial solid solution[11]*.

In aluminium the most common form of solid solution strengthening is by the substitutional variant. The strength contribution from elements in solid solution is due to interaction between mobile dislocations and the solute atoms. The atoms and the dislocations exert forces on each other. The solute atoms are centres of elastic distortion causing an elastic interaction with the dislocations.

The most important mechanisms for substitutional solid solution in aluminium are the elastic interactions caused by size misfit or modulus misfit between the solute and solvent atoms. Solute atoms which are larger than the solvent atoms create a strain field when occupying space in the solvent lattice. Edge dislocations have a hydrostatic strain field around their core and when these dislocations pass the solute atoms the two strain fields interact and energy arises between them.

The modulus misfit is related to the difference in elastic modulus between the solute and solvent atoms. A different bonding around the solute creates a soft or hard "spot" in the matrix and an elastic interaction with mobile dislocations is the result[6].

In addition to these two mechanisms solute atoms may also interact with dislocations through:

- Stacking fault interaction
- Electrical interaction
- Short-range order interaction
- Long-range order interaction

Of these interactions the size misfit, modulus misfit and long-range order interactions are relatively temperature insensitive. The other interactions represent short-range barriers and contribute strongly to the flow stress at low temperatures[11].

2.3.2. Substructure strengthening

The substructure of an aluminium alloy consists of a mixture made up of single dislocations and dislocation arrangements. During deformation, the mobile dislocations interact with the substructure and the mobility of the dislocations is reduced. As a result, the distance the dislocations travel before they are stored in the material, the slip length, depends on these interactions. When mobile dislocations are finally stored in the material, the total dislocation density is increased. A new substructure is built up and will act as barriers to slip, slip length is further reduced.

Even an annealed single crystal contains a great amount of dislocations in the form of a dislocation forest or a 3D network. If a mobile dislocation passes through such a forest of stored screw dislocations on its slip plane (figure 7), the interaction between them will leave behind short edge dislocation segments, or jogs, of length b. To enable the whole dislocation to move further, the jogs must climb. In order for climb to occur it requires a generation of vacancies behind the moving jogs. This is a thermally activated reaction which is difficult at low temperatures. In cold deformation of aluminium the glide of several screw dislocations through a forest of dislocations is the speed limiting reaction.
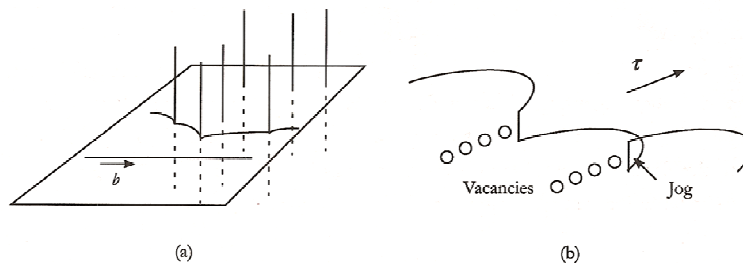
Figure 7 (a) A mobile screw dislocation moving through a forest of screw dislocations on a slip plane. (b) Vacancies in front of climbing jogs after the cutting[6].

A fine grained material, such as a polycrystal like pure aluminium, is stronger and more ductile than a material with larger, coarse grains. This is mainly due to the contribution from the grain boundaries. The effect from the grain boundaries is both a strengthening effect and an effect of distributing slip on different slip systems in neighbouring grains. To estimate the effect of the grain size on the yield stress of a material the Hall-Petch equation may be applied:

$$\sigma_0 = \sigma_I + k \cdot \frac{1}{\sqrt{D}} \qquad (1)$$

Where σ_0 refers to the yield stress, D the grain size and σ_I is the lattice friction stress. The final factor is the constant k, it increases with an increased amount of alloying elements and has a typical value of ~ 0.08 kP/mm$^{3/2}$ for pure aluminium and ~ 0.13kP/mm$^{3/2}$ for commercial purity[18].

2.3.3. Particle strengthening

A common classification of the different particles which may be present in aluminium alloys is given below.

- During solidification or homogenisation *primary* or *constituent particles* are formed. These are hard particles, not shareable by dislocations, with a radius of about 1µm or larger. The alloy composition and solidification rate determines their chemical composition.

- During homogenisation *dispersoids* are formed. In some cases however, they may also dissolve during homogenisation. In addition, dispersoids may also be precipitated during subsequent thermo-mechanical processing. Elements such as Zr and Mn precipitate in the form of intermetallic compounds with a typical size of 50-200 nm. The dispersoids impose a Zener drag on grain boundaries which implies that they prohibit recrystallisation and grain growth. As the primary and constituent particles, the dispersoids are hard and not shareable.

- Precipitates are formed by solution heat-treatment followed by aging. Except for the over aged incoherent phases, the precipitates are small (~10Å-200nm) and shareable by dislocations[6].

The materials in this work are of ultra high or high purity and the most relevant part of particle strengthening are the non shareable particles.

The Orowan mechanism (figure 8) is a common way to describe the strength contribution from non-shareable particles. A dislocation passing through 2 particles with a relatively big distance between them will bow out. Continued movement causes the bow to reach its critical configuration. Further dislocation movement causes the segments to meet on the other side of the particle. The segments are of opposite sign and form a loop around the particles while the dislocation carries on. The loops left behind lead to a structure strengthening of the material. When new dislocations pass more loops are left behind by the same mechanism. The Orowan mechanism has only been observed at lower strains, $\varepsilon < 2\%$. When a material is subjected to a strain above 2% the dominating mechanism becomes sub grains and deformation zones with a high density of dislocations[6].
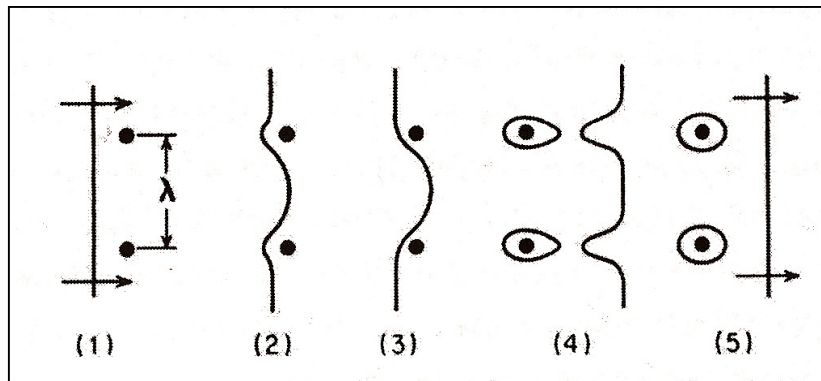
Figure 8: The Orowan mechanism. Dislocation passing non shareable particles. The passing dislocations leave behind loops around the particles which strengthen the material[11].

2.3.4. Strain hardening

The aluminium alloys in this work belong to a subgroup called non-heat treatable aluminium alloys, implying that these alloys do not gain strength or hardness by heat treatment. To improve the mechanical properties of such alloys an important industrial process called strain hardening or cold-working is used. The material hardens during deformation or strain. Several factors affect the rate at which the material strain hardens. Face and body centred cubic materials, for instance, hardens at higher rate compared to hexagonal close packed materials. Increased temperature decreases the strain hardening rate. Materials with elements in solid-solution may result in either increased or decreased strain hardening rate compared to the pure state of the material. The contribution depends on the type and amount of the elements involved. The tensile properties dependence on the amount of cold work is shown in figure 9.
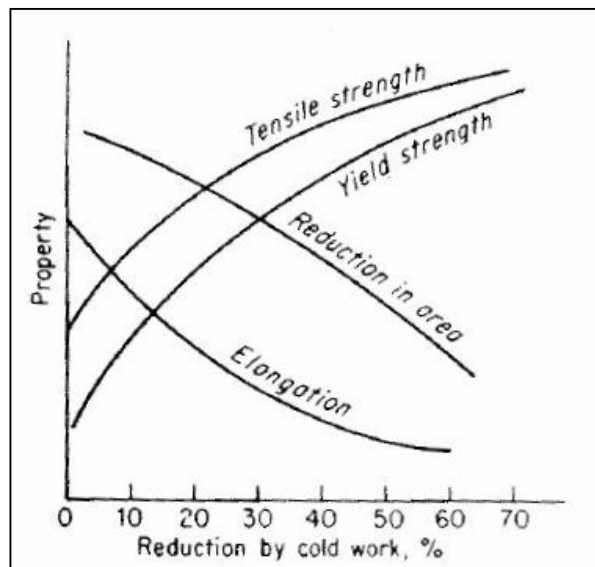
Figure 9: Graph showing the variation of tensile properties due to amount of cold-work[11].

In most cold-working processes one or two dimensions are reduced, while the remaining dimensions are increased. Cold-working produces elongation of the grains. This elongation follows the direction of working. The large deformation causes a reorientation of the grains into a preferred orientation.

A high rate of strain hardening is a result of mutual obstruction of dislocations gliding on intersecting systems. Such a state has three ways of forming:

- Through dislocation stress field interaction
- Through sessile locks, produced by dislocation interactions
- Through dislocation jogs, due to interpenetration of one slip system by another[11]

2.4.   The uniaxial tension test

The engineering tension test is used to establish basic design information regarding the strength and ductility of materials. In a tension test a specimen, machined in accordance to certain standards, is clamped in both ends. Force is applied in one end and the other end remains fixed while the specimen is elongated. During the test an extensometer, which is attached to the specimen, collects information and software linked to the tension machine logs parameters like time, displacement and force applied continuously. The software then calculates the nominal stress-strain curve based on the logged data from the tension machine and extensometer.
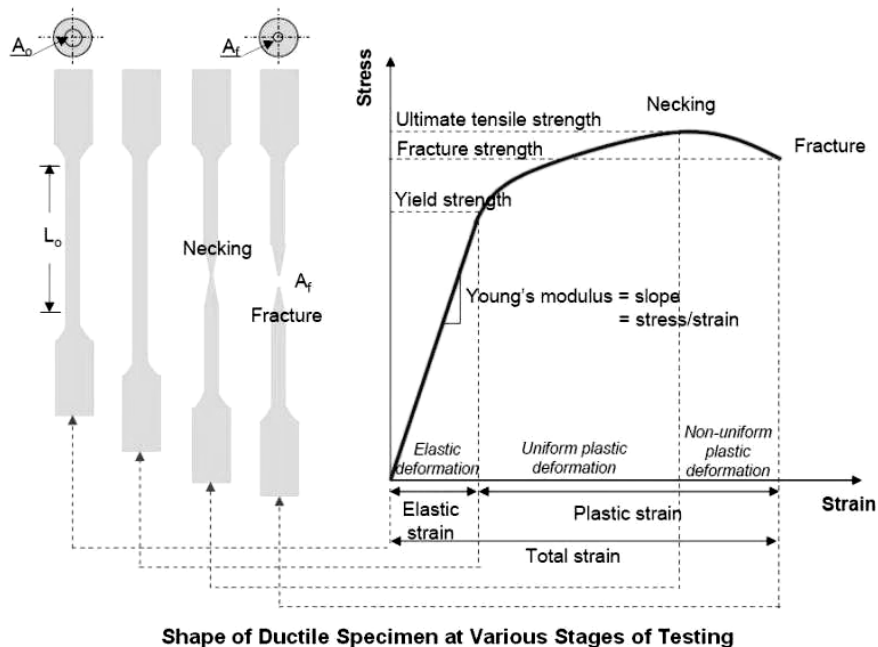
Figure 10: The nominal (engineering) stress-strain curve for a typical cylindrical tensile test specimen[5].

Figure 10 gives a good description of the relation between macroscopic geometry change and the engineering stress strain curve development during a tensile test. The initial section in the engineering curve is called the elastic region. In the elastic region the curve follows a linear development and Hooke's law applies. The recovery of the material in this region is known as elastic behaviour, once the applied force is removed the specimen returns to its original shape. Furthermore, when the behaviour ceases to be elastic, the elastic limit has been reached. This limit is defined as the largest stress a specimen can withstand without experiencing permanent deformation.

Beyond the elastic limit the deformation is permanent; the specimen does not revert to its original shape once the applied force has been removed. This is known as plastic deformation. A small permanent deformation of the specimen, usually equal to a strain of 0.002, is defined as the Yield strength of the material (also referred to as $Rp_{0.2}$). This is the limit of usable elastic behaviour and must be considered in cases where plastic deformation is undesired.

The stress required to continue plastic deformation will increase with increasing strain. In other words the material strain hardens. The volume of the specimen remains constant during plastic deformation and when the elongation increases, the specimen decreases uniformly along the gage length in the cross-sectional area. In the initial phase of plastic deformation the strain hardening compensates for this decrease and the stress continues to increase along with increased strain. After some time, the decrease in cross-sectional area is larger than the increase in deformation load due to strain hardening. This condition will occur at a point in the specimen which is weaker than the rest. Further plastic deformation will be concentrated around this "defect". The specimen will here start to "neck" down or thin locally. The deformation of the specimen in this region is now far greater than the increase in deformation load by strain hardening. As a result the load required, and subsequently also the stress, decreases until fracture occurs. The maximum load applied divided by original cross-sectional area is known as the tensile strength of the material, and is reached at the onset of necking[11].

The true stress-strain curve (the flow curve)

In a nominal stress-strain curve the stress and strain is calculated based on the original cross sectional area of the tested specimen. This is a valid method as long as the deformation is close to negligible, as is the case in the elastic region. However, beyond the elastic region the deformation is too great to ignore and must be corrected to sufficiently describe the development. Another method must be applied
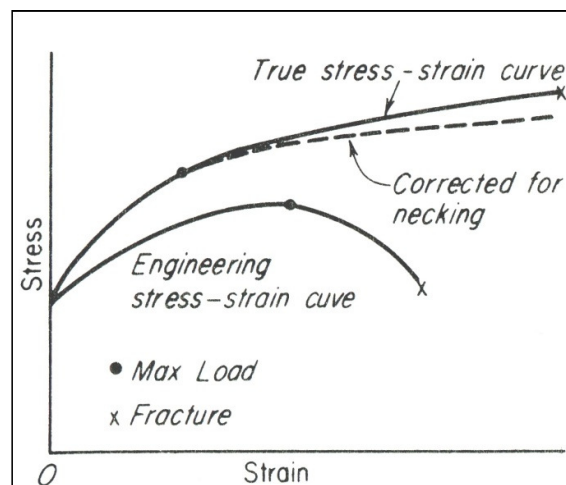
Figure 11: The true and engineering stress-strain curve and the true stress/strain curve[11].

The true stress –strain curve offers a more satisfactory approach to describe the deformation characteristics beyond the elastic region. . Figure 11 shows the difference between the true stress/strain curve and the engineering, or nominal, stress/strain curve. The stress and strain is calculated based on the load applied and the corresponding instantaneous cross-sectional area. As the software in the tensile test continuously logs the applied load and nominal elongation,

calculating the true values using some simple formulas is no struggle. Parameters such as tensile strength/ultimate tensile strength, yield strength and elastic limit follow the same principles as the nominal stress-strain curve[11].

Formulae[11]:

Nominal stress: $\qquad s = \dfrac{P}{A_0} \qquad P = force,\ A = area \qquad$ (2)

Nominal strain: $\qquad e = \dfrac{L - L_0}{L_0} \qquad L = length \qquad$ (3)

True stress: $\qquad \sigma = \dfrac{P}{A_0}(1 + e) = s(1 + e) \qquad$ (4)

True strain: $\qquad \varepsilon = \ln(1 + e) \qquad$ (5)

2.5.   Influence of testing machine on tensile test results

The hydraulic testing machine uses a movable crosshead to perform the tensile motion. There are certain aspects regarding the testing machine which may affect the results obtained by tension tests, for one the fact that testing machines deflect under load. As a result the velocity of the crosshead motion cannot directly be converted into deformation of the tensile specimen. Certain corrections are needed. A tensile test machine with constant crosshead velocity applies a constant strain rate which is the sum of three different strain rates:

- Specimen elastic strain rate
- Specimen plastic strain rate
- Strain rate caused by tensile machine elasticity

Based on these three contributors the preset crosshead velocity is usually different from the specimen's actual strain rate. The degree of miscorrelation depends on the rate of plastic deformation and the relative stiffness of the specimen and the testing machine. Therefore, to get an accurate result the experimentalist should consider involving the machine stiffness and material stiffness in calculations for true stress/strain values.

Rigid test machines are so called "hard machines" while the hydraulic machines are called "soft machines". The terms "hard" and "soft" are related to the spring constant, which is high in "hard machines". The different spring constant leads to a difference in accuracy for the upper and lower yield point. The "hard machine" will reproduce these points in good way, but the by the hydraulic machine these points will be smeared out so that only the extension recorded at constant load will be registered[11].

2.6.   Strain rate sensitivity & the "Haasen Plot"

The Haasen plot is a useful tool to distinguish between obstacles to dislocation motion when more than one set of obstacles may be present in a given material at the same time. The 3 main mechanisms in question are the thermal activation, dislocation density and particle density. Thermal activation in this context involves how easily dislocations can pass barriers (like atoms, other dislocations or particles). At elevated temperatures this passing/cutting becomes easier. The Haasen plot is a linear line based on abrupt changes in the strain rate. There are many variants concerning what to plot, but the more common version is by plotting $\Delta\sigma/\Delta\ln\dot{\varepsilon}$ as a function of $\sigma - \sigma_y$, where σ_y is the yield stress or R_{p02}. In the Haasen plot a positive intercept with the ordinate axis indicates the relative thermal profile of a set of obstacles. A negative intercept implies the existence of a set of obstacles which make dislocation-dislocation interactions "easier" than for thermal activation while a positive intercept indicates the presence of a set of obstacles which make thermal activation easier than dislocation-dislocation interactions[19, 20].

Experimentally the Haasen plot can be calculated by running a tensile test with sudden shifts between 2 different strain rates. Figure 12 shows the fit between such an alternating test and 2 plain tensile tests run at the corresponding strain rates. The fit is considered to be relatively good. However, an ideal fit should result in intersections between the upper and lower curves in the intervals between the instant shifts. This is hard to obtain in practice, and the fit in figure 12 is considered more than sufficient.
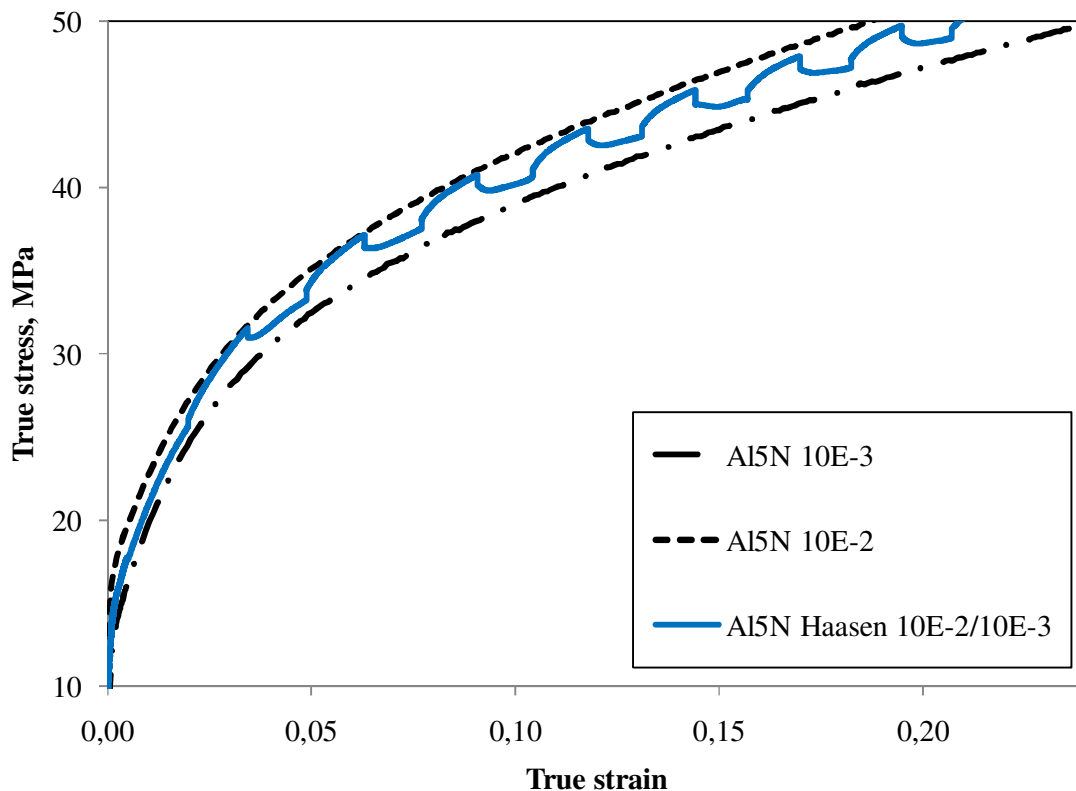
Figure 12: Alternating and 2 constant strain rate tensile tests for alloy Al5N[5].

One of the key parameters of interest in the Haasen test is the SRS or strain rate sensitivity, in most cases denoted *m*. It is important to distinguish between the strain rate sensitivity m, and the *instantaneous* strain rate sensitivity, m_i. The *strain rate sensitivity*, m, is only valid when the strain rate is kept constant. In figure 13 the red curve indicates a sudden shift in strain rate to a higher value. From such a test the *instantaneous strain rate sensitivity*, m_i, can be calculated. Also visible in the figure are the two different expressions for m and m_i. The instantaneous strain rate sensitivity will henceforth be referred to as *B* and can be found in the mathematical part of this section[21].
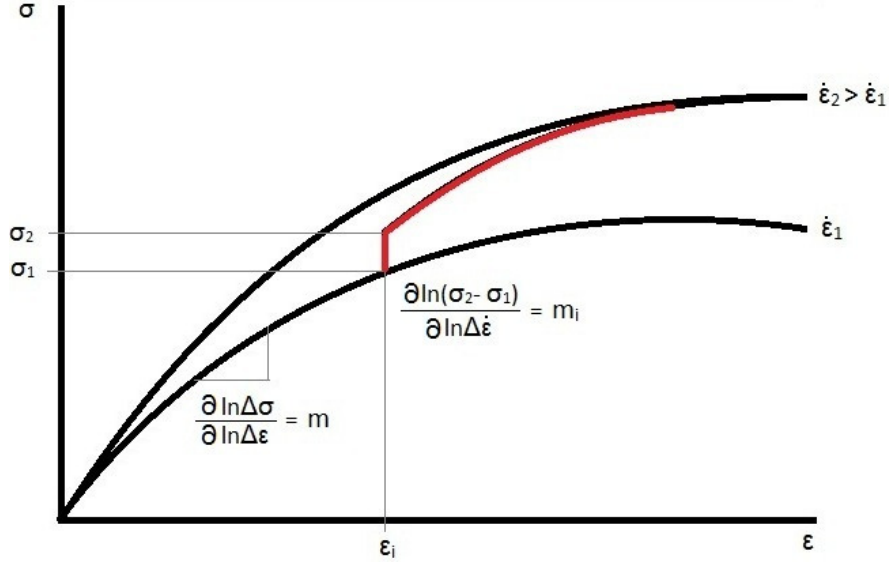
Figure 13: strain rate sensitivity, m, and instantaneous strain rate sensitivity, m_i.

There are several ways of approaching the Haasen method mathematically. Two ways are by considering how the strengthening contributions relate to the: total share stress or stress/strain rate. The total share stress approach is treated in the formulae below.

Formulae:

The share stress approach[21]:

$$\tau = \alpha G b\sqrt{\rho} + \tau_t(\dot{\gamma}, T) + \tau_p \qquad (6)$$

G and α are constants of the order 0.3-0.5 and b is the Burgers vector. τ_t is the thermal shear stress as a function of shear strain and temperature, while τ_p is the particle shear stress and ρ is the dislocation density. By considering the share strain and the thermal contribution we have the following equation:

$$\dot{\gamma} = \dot{\gamma}_0 \exp\left(-\frac{U - \tau_t V}{kT}\right) \qquad (7)$$

Where T is the temperature, k is the Boltzmann constant, U is the energy and V the activation volume. $\dot\gamma$ represents the shear strain. By solving equation (7) for τ_t we get:

$$\tau_t = \frac{U}{V} + \frac{kT}{V}\ln\dot\gamma - \frac{kT}{V}\ln\dot\gamma_0 \qquad (8)$$

The thermal sudden shift in the Haasen plot can be expressed as:

$$\left.\frac{\partial\tau_t}{\partial\ln\dot\gamma}\right|_{\rho,T} = \frac{kT}{V} \qquad (9)$$

By including the Taylor factor, M, we can solve for the corresponding stress and strain:

$$\frac{\partial\sigma_t}{\partial\ln\dot\varepsilon} = \frac{M\partial\tau_t}{\partial\ln\dot\varepsilon} = \frac{M\partial\tau_t}{\partial\ln\dot\gamma} \qquad (10)$$

The equation for the total activation volume, V, is:

$$\frac{1}{V} = \frac{\sqrt{\rho}}{\vartheta b^2} + \frac{1}{V_s} \qquad (11)$$

V is the activation volume and V_s is the activation volume from elements in solid solution. The activation volume is not a physical entity but is referred to as a volume because it is based on the burgers vector squared and the distance between dislocations. The distance included in V_s is the distance between the solute atoms.

By combination of equations (6, 8 and 11) we get:

$$\sigma - \sigma(0) = M\big(\tau - \tau(0)\big) = M\alpha Gb\big(\sqrt{\rho} - \sqrt{\rho(0)}\big) + \left(U + kT\ln\frac{\dot\gamma}{\dot\gamma(0)}\right)\cdot\frac{(\sqrt{\rho}-\sqrt{\rho(0)})M}{\vartheta b^2} \qquad (12)$$

Experimentally:

$$\frac{\Delta\sigma}{\Delta ln\dot{\varepsilon}} \approx \frac{MkT}{V} = A + B\big(\sigma - \sigma(0)\big) \qquad (13)$$

Where A and B are constants. For the recrystallised material the following assumption should apply: $\sqrt{\rho} \gg \sqrt{\rho(0)}$. This is a reasonable assumption based on the fact that most dislocations are removed by annealing and dislocations are rapidly generated during deformation work such as tensile testing.

$$\frac{MkT}{V} = A + BM\sqrt{\rho}\left(\alpha Gb + \frac{U+kTln\frac{\dot{\gamma}}{\gamma(0)}}{\vartheta b^2}\right) - M\sqrt{\rho(0)}\left(\frac{U+kTln\frac{\dot{\gamma}}{\gamma(0)}}{\vartheta b^2}\right) - M\alpha Gb\sqrt{\rho(0)} \qquad (14)$$

$$\frac{1}{V} = \frac{A}{MkT} - \sqrt{\rho(0)}\left(\alpha Gb + \frac{U+kTln\frac{\dot{\gamma}}{\gamma(0)}}{\vartheta b^2}\right) + \frac{B}{kT}\sqrt{\rho}\left(\frac{\alpha Gb + U+kTln\frac{\dot{\gamma}}{\gamma(0)}}{\vartheta b^2}\right) \qquad (15)$$

If the assumption of $\sqrt{\rho} \gg \sqrt{\rho(0)}$ applies and by considering equation (11) then:

$$\frac{1}{V_s} = \frac{A}{MkT} \qquad (16)$$

And:

$$\boxed{A = \frac{MkT}{V_s}} \qquad (17)$$

The constant A corresponds to the intersection of the linear Haasen line with the y-axis in the Haasen plot. While the contribution to the activation volume, V_s, is given in the formula above (equation 16).

By considering the section $\frac{\sqrt{\rho}}{\vartheta b^2}$ of equation (11) we can solve for the constants ϑ and B.

$$\frac{\sqrt{\rho}}{\vartheta b^2} = \frac{B\alpha Gb}{kT} + \sqrt{\rho}\left(\frac{U+kTln\frac{\dot{\gamma}}{\gamma(0)}}{\vartheta b^2 kT}\right) \qquad (18)$$

$$1 - \frac{kT ln\frac{\dot{\gamma}}{\dot{\gamma}(0)}}{\frac{B\alpha Gb^3}{kT}} = \vartheta \qquad (19)$$

$$\vartheta = \frac{kT - U - kT ln\frac{\dot{\gamma}}{\dot{\gamma}(0)}}{b^3 \alpha GB} \qquad (20)$$

$$B = \frac{1 - \left(\frac{U}{kT}\right) - ln\left(\frac{\dot{\varepsilon}}{\dot{\varepsilon_0}}\right)}{\vartheta \alpha \left(\frac{Gb^3}{kT}\right)} \qquad (21)$$

The constant *B* corresponds to the slope of the Haasen line in the Haasen plot, it is equal to the instantaneous SRS or m_i. B is affected mainly by the strain rate and temperature.

The Haasen plot is given as a linear line based on upward and downward shifts from the alternating tensile test. The diagram in figure 14 shows $\Delta\sigma/\Delta ln\dot{\varepsilon}$ as a function of σ - σ_y . The intersect with the y-axis corresponds to the constant A from equation (17), while the constant B corresponds to the slope of the linear line or the constant from equation (21). The linear line is based on the least square method and is back-extrapolated to cross the ordinate axis in the Haasen plots shown in chapter 5.3.3. and 5.6.
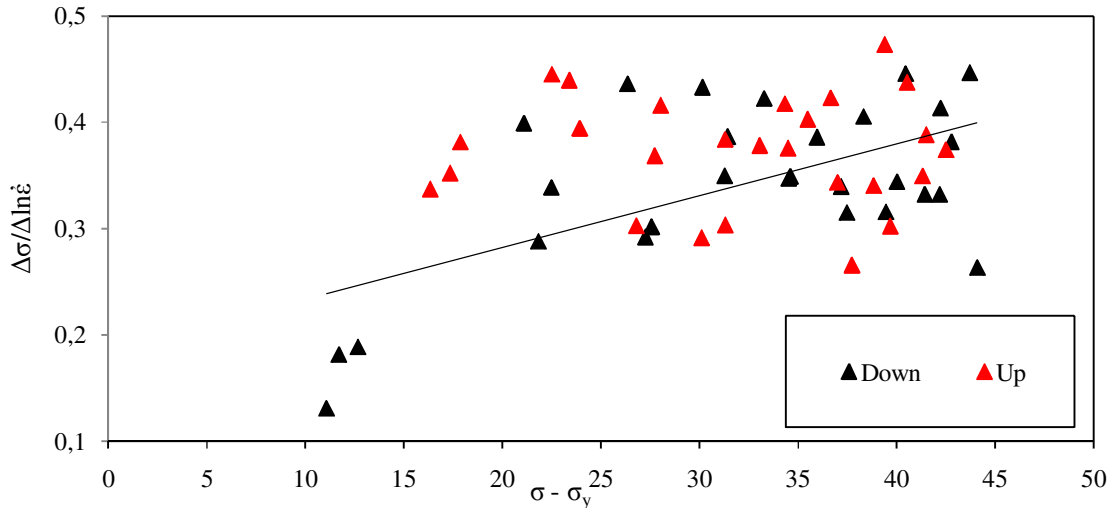
Figure 14: Haasen plot

2.7. Basic functions and techniques for SEM

The SEM, or scanning electron microscope, has a somewhat more complex set up compared to the optical microscope and therefore a short description of the most important principles for the scanning electron microscope by EBSD (electron backscatter diffraction) technique is given in this section in addition to a short section on determining crystallographic textures. The EDS (energy dispersive spectroscopy) is also used for particle investigation but will not be covered here.

2.7.1. The Scanning Electron Microscope by EBSD technique

Figure 15 (left) shows the inside of the vacuum chamber in a SEM. The sample is tilted 70 degrees to get a large amount of backscattered electrons and a big emission volume. A tilt of 70 degrees is considered the optimum to reflect (backscatter) as many electrons as possible onto the phosphor screen. The probe current hits the sample with a high amount of electrons, the backscattered electrons which are Bragg diffracted hit the phosphor screen and lights up showing Kicuchi bands. Only a small amount of the electrons are Bragg diffracted: when 70% (typical for 70 degree tilt) of the electrons are backscattered only about 2-3% fulfils Bragg's law and hit the screen.

The probe scans from left to right on the selected area of the specimen and moves downward. For indexing the step size is set by the operator and each scanning point gives a Kicuchi pattern as shown in the figure below on the right (fig.15). For one specific grain one specific pattern is representative for the crystal orientation of said grain. By Hough transformation we obtain the crystal orientations and grain distribution (offline/online indexing by the OIM analysis programme).
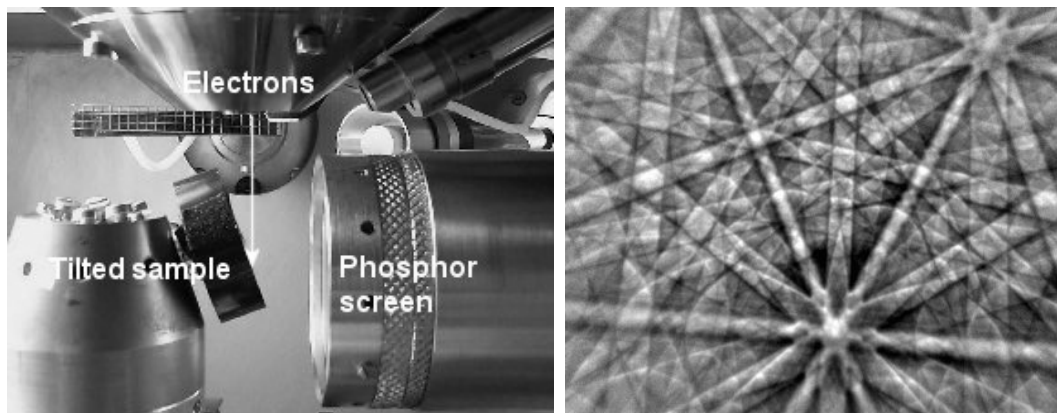
Figure 15: (left) inside the SEM specimen chamber[22]. (Right) Bragg diffracted Kikuchi bands light up on the phosphor screen[23].

2.7.2. Textures & texture determination

Crystallographic orientations or textures are terms which relate to the fact that most anisotropic materials have a preferred or dominating crystal orientation. When an EBSD scan has been performed and the crystal orientations for the grains in the scan have been indexed by analysis the texture can be established. A short description on how this is performed and the basic principles behind it is covered in this section.

Pole figures

Preferred orientations are often represented by a pole figure. A pole figure is a stereographic presentation and shows the distribution of crystallographic orientations relative to certain reference directions. These directions are normally described as rolling direction (RD), transverse direction (TD) and normal direction (ND). Figure 16 a) shows a 001 stereographic projection of a rolled sheet in the centre. The normal plane nodes from the (100) planes are projected toward a point at the bottom of the sphere. The intersections with the projection plane correspond to the black dots in figure 16 b) and represent the orientation for a single grain. In figure 16 c) the reflections from several grains from such projections are visible. By repeating these projections for a large number of grains a distribution of pole densities can be presented as a contour map as seen in figure 16 e). The intensity levels in figures d) and e) are relative to a randomly distributed texture, and thus making an assessment of preferred crystallographic orientation possible.
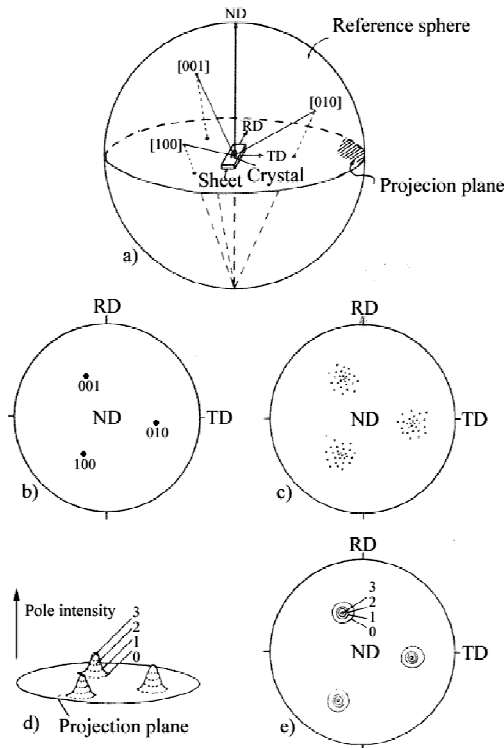
Figure 16: a) Projection reference sphere, b) projection of three poles representing a single grain, c) poles from several grains, d) pole intensities, e) pole density map[24].

For FCC- metals, like aluminium, the deformation occurs along the <111> planes and therefore the 111 pole figure is most commonly used to describe or judge the governing texture based on pole figures[24].

Orientation distribution function

To convert the 2D representation by pole figures to a 3D representation the so called orientation distribution function, or ODF, is used. ODF is a three-dimensional presentation of the texture and is based on several pole figures. A widely used orientation space is the Euler space made up by 3 Euler angles. This is the representation used for this work and only the basics are outlined in the following. A visualisation of the Euler angles, the Euler space and finally the transformation from Euler space to the ODF maps used in this work will be given. Firstly the Euler angles[24].

The Euler angles are defined by rotations in two different reference systems. The cube reference system is in turn rotated about the z-, x-, and C- (or "new z-") axis in the ABC reference system as shown in the figure below. The cube orientation in the left picture in figure 17 (a) is the same as in the right picture. However in pictures (b) and (c) this orientation is changed because of these two rotations.
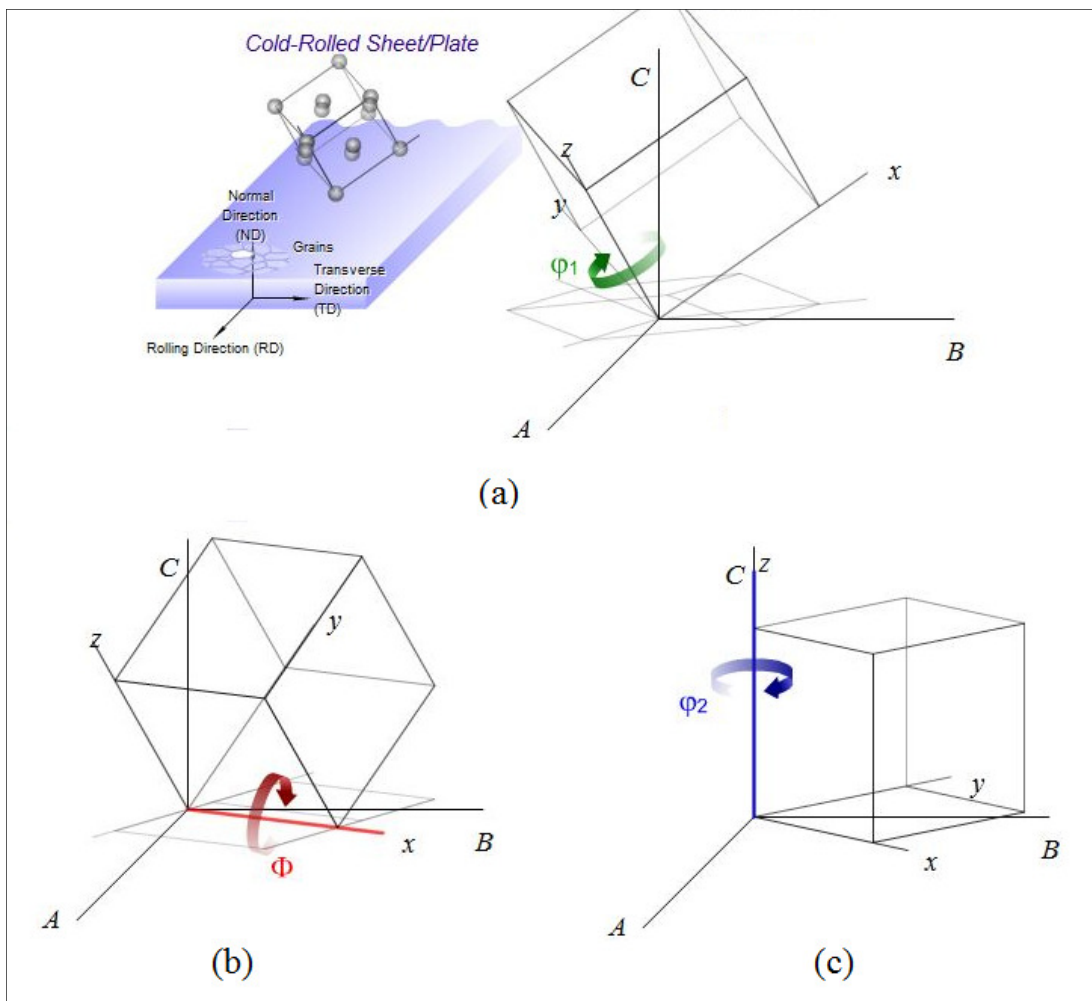
Figure 17: (a) Cube orientation and Euler angles (a-c)[25].

The Euler angles represented in the Euler space are shown in figure18. The intersection between the 3 coloured planes for a specific set of Euler angles correspond to a unique point in the Euler space. The euler angles in figure 18 are roughly $\varphi_1 = 42°$, $\phi = 90°$ and $\varphi_2 = 35°$.
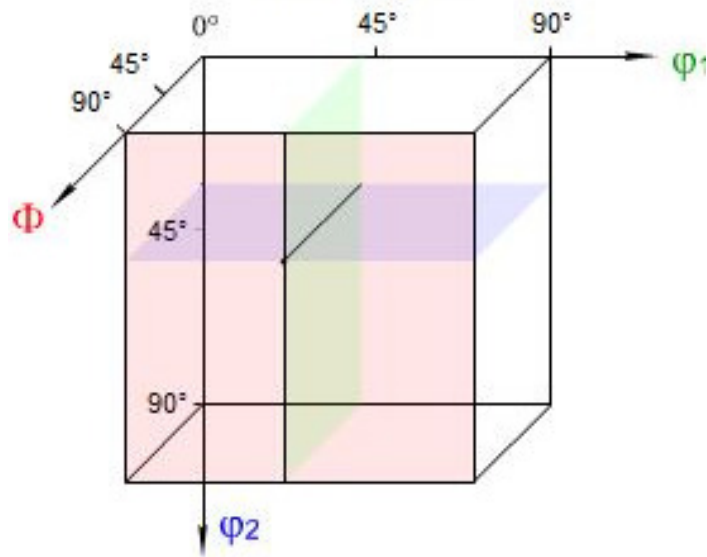
Figure 18: Euler angles represented in Euler space[25].

To convert the 3D representation Euler space into an ODF map the Euler space cube is divided into plane slices parallel to the horizontal top plane. The layers have a spacing of 5° in the vertical direction (or along the φ_2-axis). The slicing is shown in figure 19 (a), while the transformation to ODF is shown in figure 19 (b). The levels in the Euler space correspond to the slices and the intensity of the reflections is colour coded ranging from red (highest intensity)-orange-yellow-green-blue (lowest/no intensity). In the one dimensional slices the Euler angle φ2 is constant in each layer moving through region 0-90° by 5° intervals.
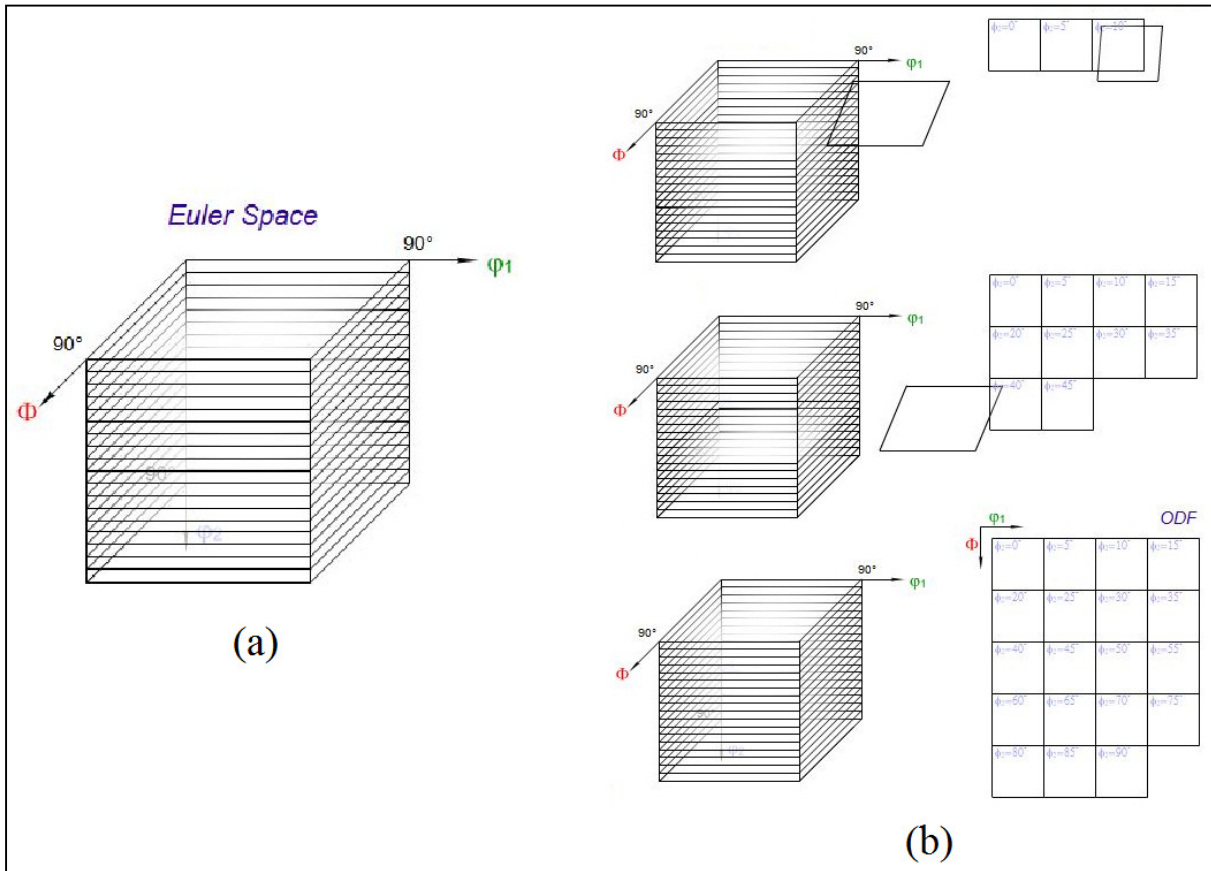
Figure 19: Transformation from Euler space to ODF map. (a) Euler space with sliced planes. (b) 2D slices from Euler space transformed to a series of one dimensional maps in ODF[25].

There are many different textures and these will not be treated here. Textures which are present in the findings in this work will be treated as they are found in chapter 5.3.

2.7.3. Particle determination by EDS

In this work the particles were studied in SEM by so called EDS (energy dispersive spectroscopy). In short, the energy arising from interactions between incident high energy electrons and the electrons in the shell is liberated as $K\alpha$ X-rays. These x-rays are picked up by a detector and transformed by the EDS software to characteristic peaks. These peaks are characteristic for each element and may be distinguished and quantified by EDS software[26]. The method will not be treated in further detail here but rather the interpretation of the results is the focus in this section as it is subject to discussion.

In his master thesis Sindre Bunkholt[26] collected a number of findings regarding the determination of α-AlFeSi and β-AlFeSi particles in Al-Mg-Si alloys. The findings and the conditions are given in table 2. The interpretations regarding the Fe/Si ratio is of interest since these values were calculated by the EDS software for the particles found in this work. Since the conclusions and conditions vary extensively from the different sources it is difficult to conclude whether the particle in question is a α-AlFeSi or β-AlFeSi, solely based on the values from the table. The particle findings in chapter 5.3.3. will be discussed by considering the table values.

Table 2: Relevant part of table from Sindre Bunkholt's master thesis from 2010[26]. The table contains the values of the iron/silicon ratio found in different experiments.

Source	Conditions	Fe/Si for α-AlFeSi	Fe/Si for β-AlFeSi
Samuel et al.(2004)	15, kV, not corrected	~ 0.7	~ 0.4
Claves et al.(2002)	15kV, not corrected	0.55	0.14
		1.71	0.81
Oasada (2004)	15kV, corrected	> 5.2	< 3.3

3. Material

The material used in this work was received in the form of DC cast aluminium ingots and in the form of extruded flat profiles. The materials are of high purity (>99wt% Al) and the varying factors are the content of iron and silicon in addition to various trace elements. Two alloys are of ultra pure quality and are referred to as *Al5N* and *Al5NFeSi*, where 5N indicates the amount of aluminium to be higher or equal to 99,999 wt%. In Al5NFeSi iron and silicon has been introduced and represents the separating factor from alloy Al5N.

The final two alloys are of commercially pure quality and resemble the 1xxx alloys. The distinguishable difference from the 5N alloys is the presence of multiple pollutions or trace elements and a slightly increased amount of iron. The trace elements consist of various impurities or elements of the ppm order. The commercial alloys are referred to as *Al2NFeSi* and *Al2NFe2Si*, where 2N indicates an aluminium content (purity) of 99 wt% Al or higher. A higher content of iron and small variations in trace elements is the difference between these 2 alloys. The exact amounts of elements present in the material are given in table 3 on page 29.

3.1. Fabrication

The aluminium alloys were produced at Norsk Hydro Sunndalsøra and partly in Bonn, Germany. When the aluminium was processed in Bonn the specifications regarding the amount of alloying elements, Fe and Si, were not followed in detail. Due to a misunderstanding between customer and manufacturer the content of iron and silicon, prior to the requested addition, was not clearly established. The result was that the 2 commercial alloys contained a higher amount of iron and silicon than specified. The main problem with the end products was that alloys Al5NFeSi and Al2NFeSi did not contain exactly the same amount of iron and silicon. The only difference between the 2 alloys should be that Al2NFeSi contained various amounts of other alloying elements in addition to Fe/Si. The error, however, was not considered to be of such a degree that good results could not be obtained and therefore the testing was carried out. Once introduced in alloy Al5NFeSi, the wt% Si is more or less the same also in alloys Al2NFeSi and Al2NFe2Si.

3.2. Material dimensions and prior treatment

The cast material had not been homogenised and arrived in the form of solid cylinders or *ingots* 230mm high with a diameter of 190mm. In theory the material should be homogenous and isotropic with a random texture. However, it is very likely that such a material contains segregations and other impurities due to the casting process.

The extruded material had been cast, homogenised at 500 ^{o}C and finally extruded to flat profiles prior to arrival. Measurements of the profiles were: 1000x70x5mm. Due to the production process, extruded profiles are strongly anisotropic due to the large deformation in the rolling direction they undergo during manufacturing. Specific crystal orientations and textures are dominant and the strength is dependent on these factors. Both the extruded material and the cast ingot are shown in picture 20 below.
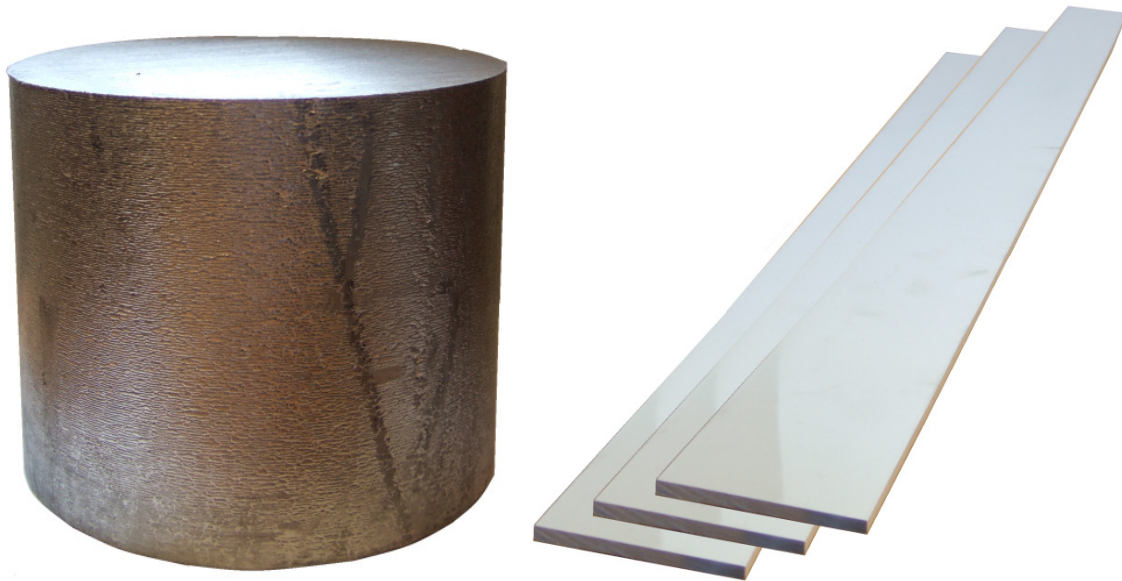
Figure 20: Cast aluminium block (left). Extruded aluminium profiles (right).

3.3. Chemical analysis

The basis and content of both cast and extruded aluminium are the same. From the chemical analysis values in table 3 we can see that the amount of trace elements in the 2 ultra pure alloys is roughly zero, 0-1 wt ppm. The most abundant trace elements for the 2 commercial alloys are Vanadium, Magnesium, Nickel, Gallium, Zinc, Titanium and Manganese. The contribution from each of these elements is questionable due to the amount. However, the collective effect of the trace elements may affect the mechanical properties of the alloys. Different elements affect the alloy in different ways depending on their properties, such as crystallographic orientation, lattice spacing, atomic size etc. Multiple other elements are present in the commercial alloys, but are not included due to their magnitude (of the order < 10 ppm).

Apart from the purest alloy, the iron and silicon content in the alloys is of the order 0.065 – 0.15 wt %. The alloy Al5N is used as a reference alloy so that any changes in material properties due to change in chemical composition is easily traceable. The introduction of various trace elements gives a more complete form of study as they are common in most aluminium alloys.

Table 3: Alloying and trace element content in the 4 aluminium alloys

Element →	Fe	Si	V	Mg	Ni	Ga	Zn	Ti	Mn
Alloy	wt %		wt ppm						
Al5N	<0.0005	<0.0005	0.2	0.9	0.2	0.1	1	0.1	0.1
Al5NFeSi	0.066	0.068	0.2	0.9	0.2	0.1	1	0.1	0.1
Al2NFeSi	0.094	0.069	89	34	33	92	27	42	16
Al2NFe2Si	0.149	0.065	118	49	45	119	47	37	19

4. Experimental Procedure

The basic principles and conditions for experimental work are given in this chapter.

4.1. Homogenisation

Before tensile testing the cast material was homogenised to remove any remaining dislocations, internal stress and to get a homogenous material. The material was held at 600 °C for 8 hours in a furnace (see figure 22) after an initial heating rate of roughly 100°C/hour. The homogenisation curve for the cast specimens is shown figure 21. The temperature sensor inside the furnace was located in the right upper corner in the back. In addition the actual heat in the furnace did not correspond with the temperature on the display, a mismatch found to be as much as 52 °C. To make sure that the temperature was in fact 600 °C a thermo element with a sensor wire was set up. The tip of the wire was placed in the middle of the sample holder inside the furnace. The thermo element had been checked prior to testing. The main objective of the homogenisation was to remove segregations due to the casting process, especially along the grain boundaries, and get as homogenous a material as possible.
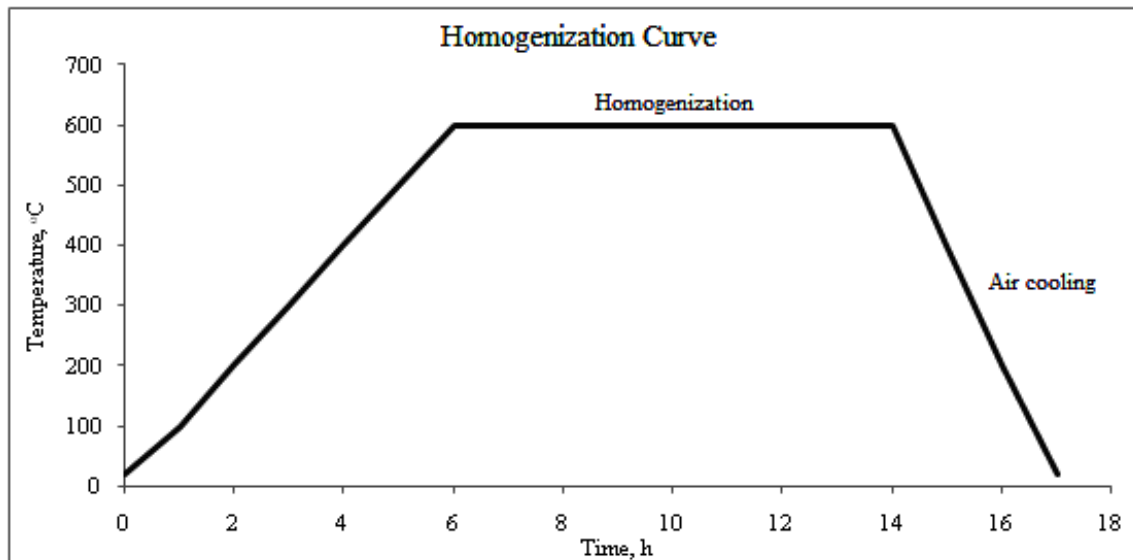
Figure 21: Homogenisation curve used for cast alloys. $600^{o}C$ reached by a speed of roughly $100^{o}C/hour$.
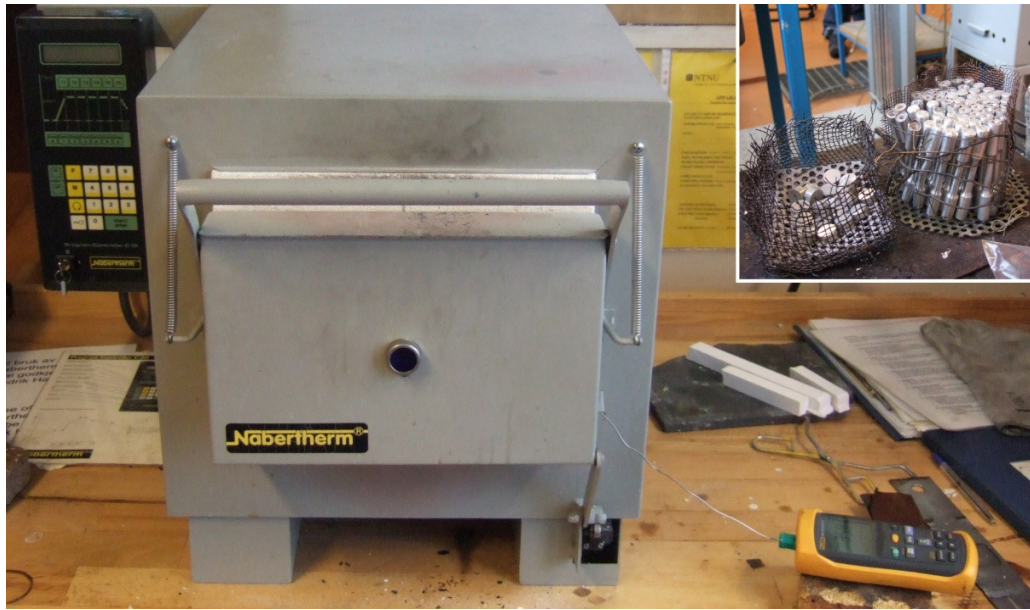
Figure 22: Furnace used for homogenisation with thermo element connected by a wire. In the upper right corner the cast tensile and microscope specimens can be seen after homogenisation.

4.2. Rolling

The extruded profiles were cold rolled in a rolling machine as seen in figure 23 below. 4 steps were used to obtain a 4mm reduction in thickness from the initial 5mm plates. The deformation steps are given in table 4 below. As the smaller steps may result in bending of the material, the third step was reduced so that the final step would yield reasonably flat plates. The speed of the rolling cylinder was roughly estimated to be about 0.27m/s, based on the diameter of said cylinder. The speed was slightly increased before the 2 last steps, because the machine stopped.

Table 4: Reduction intervals during rolling.

Step	Thickness	Unity
0	5.00	mm
1	3.78	mm
2	2.74	mm
3	1.98	mm
4	1.10	mm

Figure 23: The rolling machine.

4.3. Recrystallisation

After rolling the extruded flat profiles were recrystallised. A standard method was used to find the most suitable heat treatment for the alloys. Small square specimens were cut out from each material, measuring roughly 50x30mm. These were lowered into a salt bath and held there for 30 minutes before being quenched in water. By using different temperatures and measuring the hardness, the treatment yielding satisfactory conditions for recrystallisation can be established. A typical recrystallisation curve, hardness as a function of temperature, will increase slightly before dropping rapidly until stabilisation. The ideal recrystallisation temperature is the one located close to the start of stabilising. When the recrystallisation is complete further annealing may result in grain growth and this is not desirable. If the temperature or time is too low the specimen may only be partly recrystallised. Based on these 2 outcomes it is important to find the balance to obtain the desired result. In figure 24 the recrystallisation development as a function of temperature is given along with the recovery and grain growth stages.
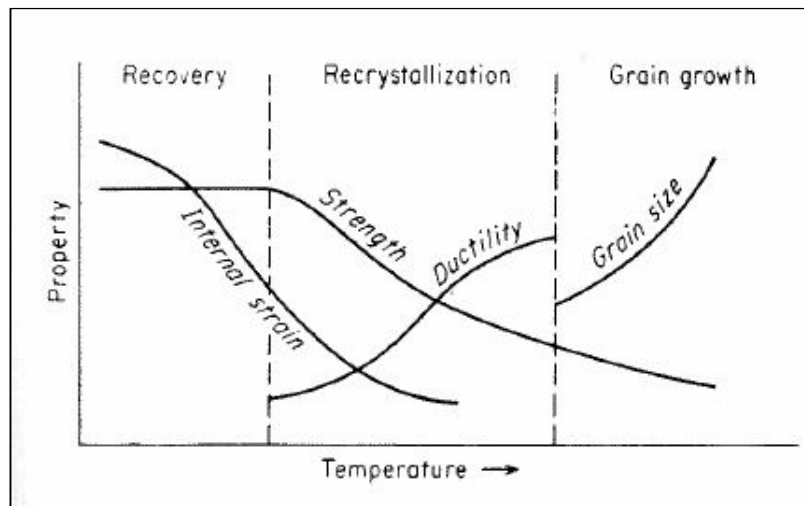
Figure 24: Mechanical properties as a function of temperature [11].

4.4. Hardness measurements

After each heat treatment for the recrystallisation test the specimens were measured for hardness in the Vickers hardness machine. 5 impressions were made on each type of alloy with a spacing between impressions of 2 mm. The amount of impressions was chosen because of the possibility of hitting different areas of the grain structure or dirt which may yield different results. Since the material is so soft it was sufficient and necessary to use 0.5kP force to form the diamond impressions. Hardness measurements were taken to quantify and register the development during heat treatment to find a suitable recrystallisation temperature.

4.5.   Microscopy and sample preparation

In this section the various preparations and machining of microscope samples are treated. For grain measurements a simple method was used by counting the number of grain boundaries crossing a measuring line. By measuring this line relative to the scale bar and dividing it on the number of grains one gets an average grain size. Several such measurements were made for each sample to get a more accurate result.

4.5.1. Cast aluminium samples

As mentioned earlier, the cast aluminium arrived as large cylindrical blocks. When fabricating microscope samples, a 10mm thick disc was firstly cut out from the middle of the block. The outer 10mm region was then removed before cylindrical samples measuring 10x15mm were cut out. The same procedure was used for all 4 cast materials. The process along with an actual sample is described in figure 25 below. Prior to polishing and grinding the samples where homogenised as described in section 4.1. The coarse nature of the cast material presented problems during grinding; it proved difficult to obtain a smooth, even surface during grinding. After embedding the samples in ClaroCit the results were improved greatly. The upper part of the sample was left free of embedding so that about 50% of the sample was sticking out. In further treatment, such as anodizing or electro polishing, it is essential that good contact between the anode and the sample is established.
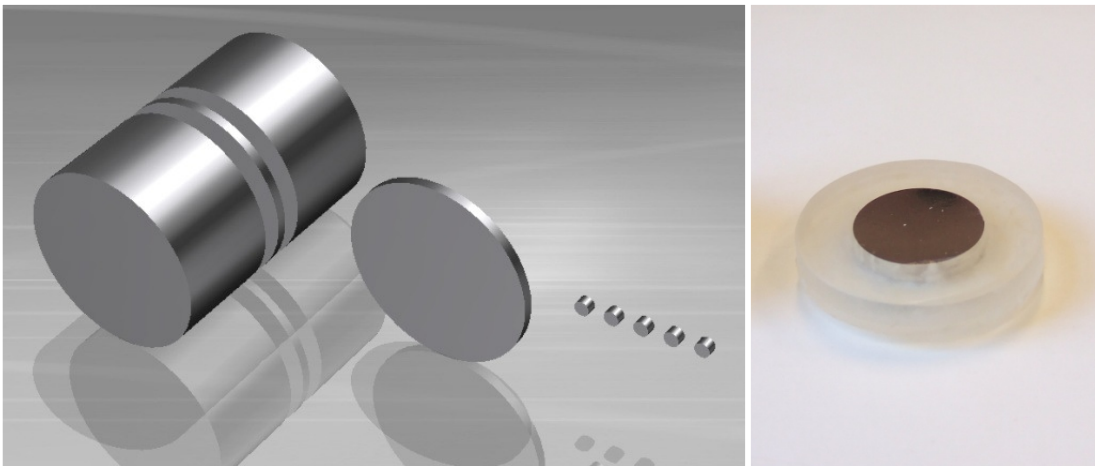
Figure 25: Origin of cast microscope samples in the cast block (left), embedded microscope sample with a 15mm diameter (right).

4.5.2. Extruded aluminium samples

The extruded microscope samples were cut from the side edges of the extruded flat profiles. In figure 26, below, the black square area indicates the origin of the sample, while the arrow tip indicates the surface studied. This "side-in" view is the most relevant as the grain structure is strongly dependent on the extrusion direction.
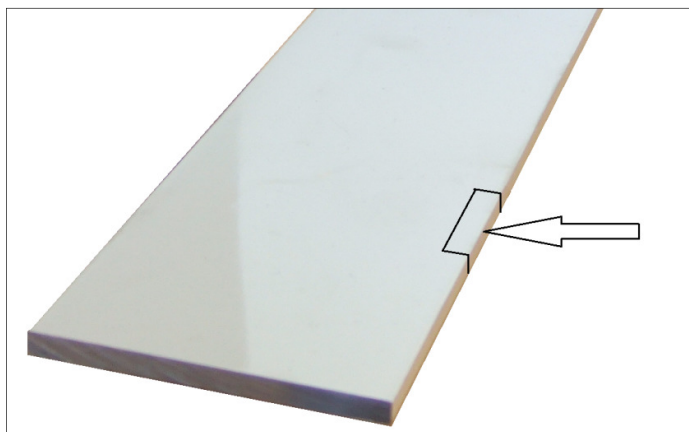
Figure 26: Extruded aluminium with microscope sample area highlighted.

4.5.3. Rolled and recrystallised aluminium samples

After rolling the extruded material was recrystallised. The samples used to make sure that the recrystallisation had been successful were simply square cuts from the rolled material. A side-in view in the microscope was preferable and since the rolled material only measured about 1mm in thickness, the samples were embedded in ClaroCit. In the same way as for the cast embedding, a part of the sample was left free. In figure 27 the sample embedded is shown on the right, while the picture on the left indicates where the specimen was cut from by the red square and the arrow. The arrow indicates the surface of side edge which was examined in the optical microscope. The specimen measurements were roughly 40x10x1mm.
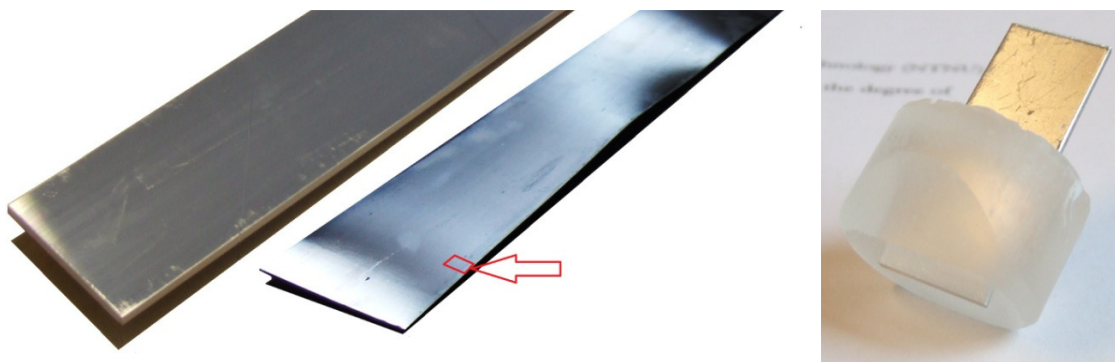
Figure 27: Extruded and rolled material (left). Annealing experiment sample embedded (right).

4.5.4. The optical microscope

The following grinding papers and polishing cloths were used for both the cast and extruded material: 500sic, 800sic, 1000/1200sic, 2400sic (with soap), 1µm. The soft aluminium was relatively uncomplicated and fast to grind. However, because of its softness the final polishing step with diamond spray (1µm) resulted in multiple diamond particles logged in the surface of the samples. To avoid this, the polishing cloths were thoroughly cleaned prior to use and as little diamond as possible was added. The results were good but it was a far more time consuming process. Soap was used to collect particles and dirt in front of the sample while using the 2400sic paper, which gave very good results and made the need for 6µm and 3µm polishing cloths unnecessary. The best way to prepare the samples proved to be through electro polishing after the 1µm treatment. Not only did the amount of diamond particles decrease significantly, but the surface was in essence free of grinding and polishing scratches and stripes. The procedure for electro polishing is more thoroughly covered in the section 4.5.5.

To clearly distinguish the grains and grain boundaries in the optical microscope the aluminium samples were anodized and studied with polarized light. The anodizing time required to obtain good results varied from sample to sample and cast/extruded/rolled, but 1-2 minutes were found to be satisfactory for the rolled and extruded aluminium. The cast aluminium required anodising times of up to as much as 5-6 minutes to obtain good results, partly because of their size. The anodising fluid H_2O 950ml, HBF_4 50ml was used along with a voltage of 20kV.

4.5.5. SEM & EBSD

The SEM used in this work was a FESEM Zeiss Ultra 55 limited edition. For the optical microscope polishing with 1µm cloth is sufficient to gain good results. In the SEM microscope the backscattered electrons, which creates the backscattered pattern for EBSD technique, originate from the top 10-50nm layer of the sample surface. The need for more extensive sample preparation is therefore critical. Electro polishing offers a convenient and satisfactory method to achieve good results. However, as many factors influence the result it may prove difficult to find a standard set up, reproduction is difficult. The optimal temperature of the cooling liquid, flow rate, voltage, type of electrolyte and surface area must be found by a "try & fail"-method, more or less.

To avoid the creation of defects from oxygen, such as pours from bubbles, masks which were larger than the samples were used to allow the oxygen to escape. Alternatively the mask was removed completely and a copper plate with a wire and a clamp (figure 28) was used to "fool" the anode allowing the sample to be held freely by hand as it was lowered into the electrolyte. The anode was drawn to the side and put on top of the copper plate, the wire was entangled in the plate in one end and a clamp was connected to the sample in the opposite end. The sample was clamped and lowered into the electrolyte bath allowing all the oxygen to escape easily.
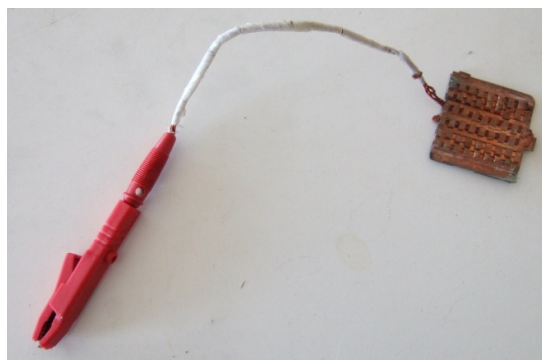
Figure 28: Equipment used for electro polishing: modified sample holder.

The electrolyte used for electro polishing was C1. C1 was a mixture containing 20% Perchloric Acid ($HClO_4$) and 80% Ethanol (CH_3OH). The general settings for the LectroPol machine were as follows; cooling liquid holding -33^oC, holding time 10 seconds, voltage 20V. The flow rate and area of the mask opening was regulated according to the size of the specimen and its metal surface area (most samples were embedded in ClaroCit). Once the suiting electrolyte had been found and the critical parameters set, the process was efficient and timesaving. The softness of the material required short treatment in the electrolyte, only about 10seconds. The results were superior compared to the treatment ended at the 1µm polishing step.

4.6. Tensile specimens

The pure state of the aluminium alloys used in this work presented several challenges related to machining and fabrication of samples. As some of the material is bendable by hand or small forces it needs to be handled carefully to avoid undesired deformation prior to testing and examination. Different types of specimens were machined based on the shape and condition of the material (cast, rolled and extruded).

4.6.1. Cast aluminium

Figure 29 explains how the tensile specimens were formed and where they were cut from in the block. Firstly the block was cut into 3 parts, 2 smaller blocks and one disc for microscope samples. The outer shells of the new cylinder blocks were removed before cylindrical specimens were cut out from the remaining core, with a diameter of 10mm. Since the cast material should be homogenous and isotropic no strict requirements regarding where the microscope samples were taken from applied. The removal of the outer shell was made in case of non-uniform solidification during casting along the edges of the cast mold and the possibility of inclusions in the cast mold. Finally tensile specimens with dimensions in accordance to the NS-EN ISO standard[27] were machined at the work shop by qualified personnel. Other than a few initial problems with the softest alloy, the machining of the tensile specimens were fabricated to fulfil the ISO Standard requirements. The parallel area was 28mm to make sure that the extensometer of 25mm had a good fit.
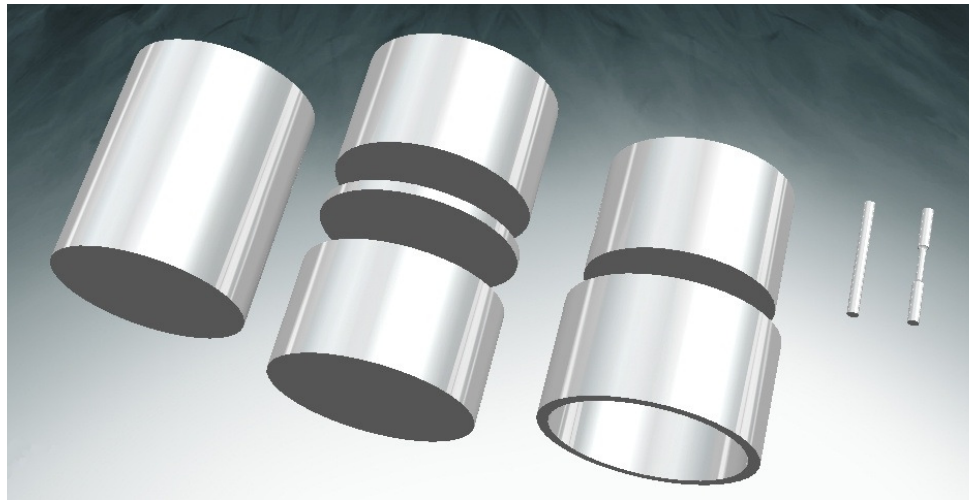
Figure 29: Cast block, cut block, removed outer shell, cylindrical milling specimen and turned tensile specimen.

In figure 30 the dimensions of the cast tensile specimens are given in millimetres. The specimens were fabricated by means of turning.
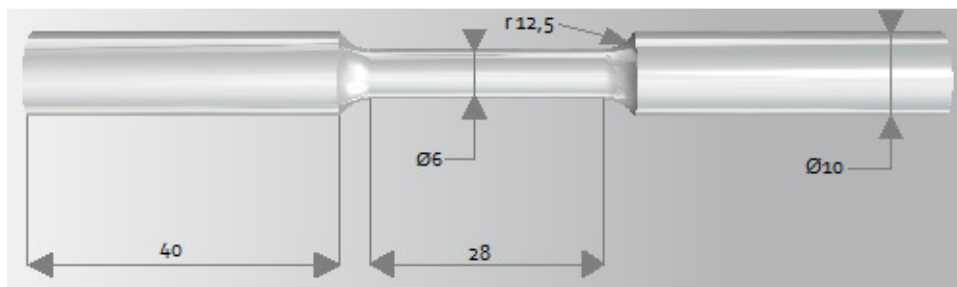
Figure 30: Cast tensile specimen dimensions (mm).

4.6.2. Rolled and recrystallised aluminium

The tensile specimens fabricated from the rolled and recrystallised material were machined so that the gage length was parallel to the extrusion and rolling direction. Extruded and rolled material is strongly anisotropic and strongest along the direction of the deformation. The rolling procedure yielded somewhat varying results with respect to geometry of the rolled sheet profiles. Some bending, of variable magnitude, occurred at several areas along the edges. As the access to rolled material was bountiful, the areas where the bending was extensive were discarded. The need for equal geometry of the specimens is critical to get good correlation in results. Following the recrystallisation, specimens were milled from the rolled profile sheets. The ISO standard was used to make sure regulations were followed. The picture below shows the direction from which the tensile specimen was cut in the rolled material (figure 31). The dimensions of the specimen are shown in figure 32.
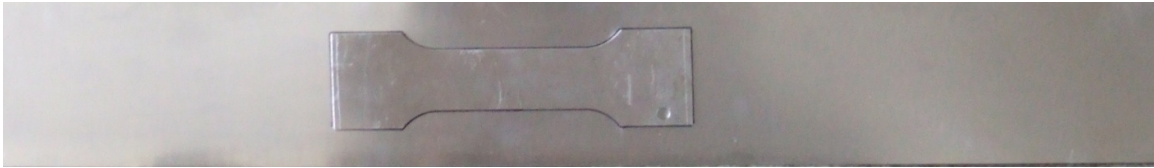
Figure 31: Rolled material with tensile specimen lying on top.
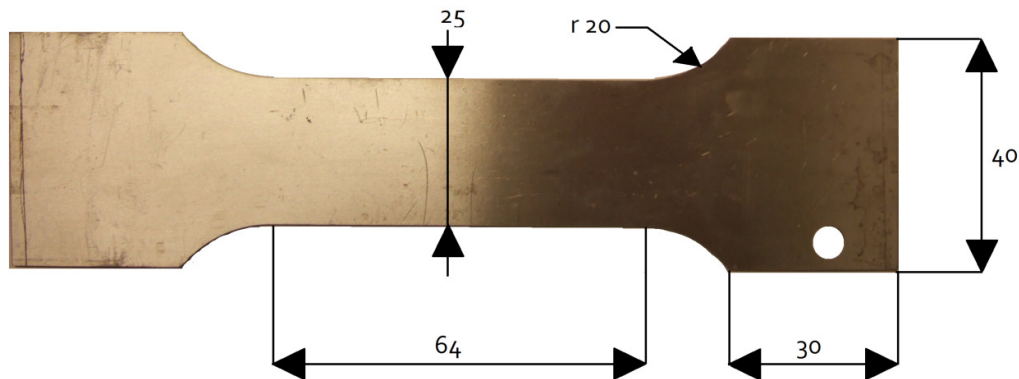
Figure 32: Rolled tensile specimen dimensions (mm).

4.7. Tensile testing

For the tensile tests two different types of tests were used. Constant strain rate experiments with displacement control in addition to a tensile test which was programmed to run in loops alternating between a "fast" and a "slow" strain rate. The latter was also controlled by the displacement method, although a different tensile machine was used. In the 2 sections below the procedures are treated in more detail.

4.7.1. Displacement control at constant strain rate

The MTS 810 tension machine was used with constant strain rate set-up for both cast and rolled material. 2 different constant strain rates were used, $\dot{\varepsilon} = 10^{-2}s^{-1}$ and $10^{-3}s^{-1}$. For both material types, 3 specimens were tested per alloy for each strain rate. A loading cell of 5kN was found sufficient, based on calculations of a maximum applied force during testing of slightly above 2kN. All tensile tests where run at room temperature, $20^{\circ}C$. The set-up for the tension tests can be seen in figure 33. 2 extensometers were available at the work shop, the 25 and 50 mm extensometers. The 50 mm extensometer was chosen for the thin rolled specimens, while 25 mm was used for the shorter cylindrical cast specimens.

In the tensile test the force and elongation is registered and plotted by the software as a force/displacement diagram. The cross head registers force applied and displacement relative to starting conditions, while the extensometer also logs displacement. To describe the entire development of the stress and strain some calculations and conversions are needed. By applying the formulas (2-5) from the theory section a conversion of the data from nominal values to true stress and strain values was performed.
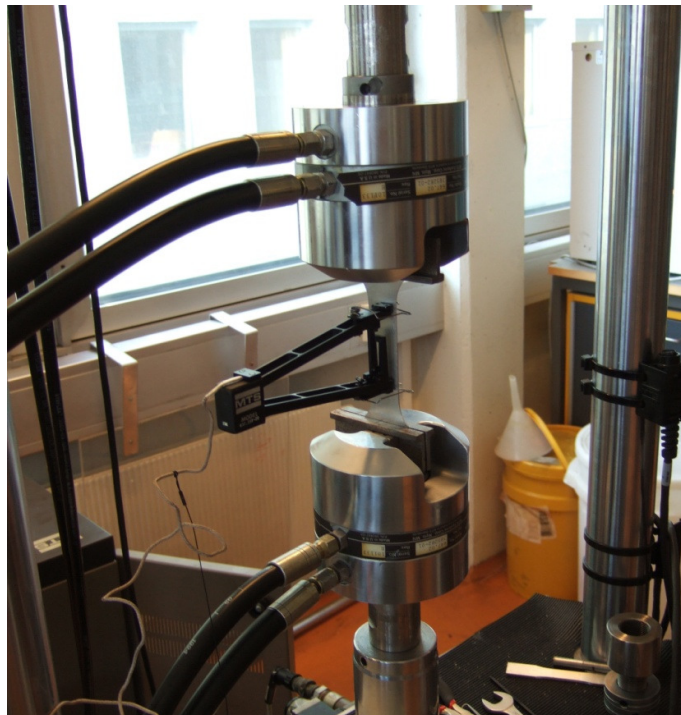
Figure 33: Tensile specimen with 50mm extensometer in the MTS 810 tension machine.

4.7.2. Haasen plots, abrupt shifts in strain rates

For the alternating strain rate testing, needed to calculate Haasen plots, some rather complex programming and fine tuning was required. Due to problems with the MTS 810 machine in connection with such a test, the MTS 880 with manual attachment of the specimens was preferred.

To optimise the test parameters for the tensile test with alternating strain rate a commercial alloy AA1200 was used. Simple rectangular specimens of equal length and width compared to the recrystallised tensile specimens were used. However, the difference in thickness was larger. The AA1200 alloy had a thickness of about 6mm compared to the 11,1mm specimens for the 4 alloys Al5N-Al2NFe2Si. Around 30 specimens of the dummy material were run before satisfying conditions for P, D and I (proportional, integral and derivative control) settings were reached. In this alternating strain rate test the area of interest was the transition between the strain rates and in some cases the logging finds it difficult to gain sufficient points during this abrupt change. Undershoot and overshoot of the curves occurs frequently and should be minimized by PDI control and logging/buffer rate. In the area close to the change both prior and post change the slope of the curve may vary and the experimentalist must judge whether it is due to settings or to a physical response in the material. One way to establish this is by studying the strain rate and whether it remains constant or not.

As mentioned above, some programming of the software was needed. An initial strain rate was set at the start of testing before the first loop was initiated. The start rate was set to 10^{-2} so the first jump was downward to a strain rate of 10^{-3}, set to run for a certain amount of elongation (1.5%) before shifting upward to the fast strain rate. The loop then repeated itself until the test was terminated manually, at the onset of necking. The duration of the steps at low strain rate were set to run slightly longer than the fast rate steps to more clearly distinguish the development. Additional information about the programming can be found in appendix page B.

All tensile tests where run at room temperature, 20°C. A 50mm extensometer along with a 5kN loading cell was used.

5. Results

In this chapter the results from conducted experiments will be presented.

5.1. Optical microscopy: grain structure

Strength and ductility properties of a material are strongly dependent on the microstructure. Therefore, an assessment of the grain size and distribution of the alloys used in this paper is covered in the following sections. As we are dealing with polycrystals, the grains must all deform during destructive testing such as tensile experiments. If the grain structure is not homogenous throughout the material, the results from such testing will likely be heavily affected[17].

NOTE: For all the microscope pictures included in this work regarding deformed specimens (rolled and extruded) the direction of deformation is parallel to the horizontal vector of the pictures.

5.1.1. Cast and homogenised aluminium

The cast material contained no grain refiner and had not been homogenised. These factors should result in an isotropic material with a random grain structure. To support this theory the 4 cast alloys where investigated in the optical microscope. The cast microscope specimens proved notoriously difficult to prepare for microscopy and the images in the following sections are of lesser quality compared to the other material.

Al5N
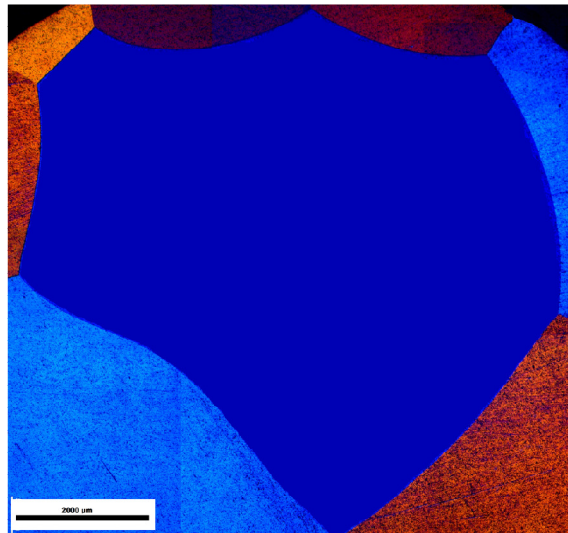
Figure 34: Grain measuring 8mm in alloy Al5N at 2.5X magnification. The picture is a collection of 9 smaller pictures and the area inside the big grain has been edited to conceal the overlapping images.

Figure 34 is a collection of pictures to illustrate the large size of the grains, as the options for the optical microscope are limited regarding small magnifications. It must here be mentioned that the

picture has been edited to hide the intersecting lines from the many pictures. Only the area inside the biggest grain has been edited, without affecting the actual grain boundaries or any surrounding grains. The big grain measures about 8mm, and some observed grains from different specimens were even bigger. The small grains close to the edge are due to the cutting, where the alloy has been subjected to deformation and altering of the grain structure. The magnification in the picture was set at 2,5X and the measuring band is located in the bottom left corner (measures 2000µm). One sample studied in the optical microscope showed a microstructure containing only one grain over the whole of the surface. This grain must subsequently be of the size 15mm in diameter or larger, as that is the diameter of the specimen surface. To give a further visualisation of the magnitude of the grains in Al5N figure 35 shows an "over-anodised" microscope specimen which has been magnified roughly 4.5 times. "Over-anodising" implies far longer holding times in the anodising fluid than required to distinguish grains in the OM. The shape of the big grains indicate recrystallisation and subsequent uninhibited grain growth.
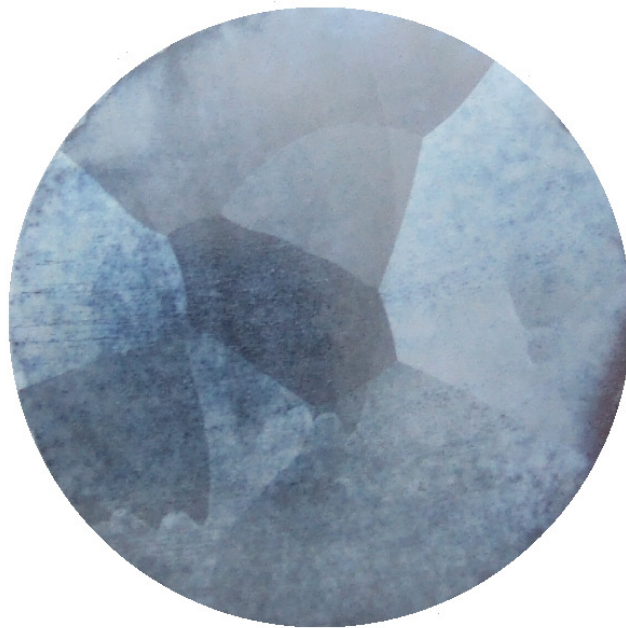
Figure 35: Al5N microscope sample surface after (over)anodising. Grains and grain boundaries are clearly visible. The diameter of the sample is 15mm.

Al5NFeSi

The grain structure in alloy Al5NFeSi consists of significantly smaller grains compared to the large grains in alloy Al5N. The grains seem to be distributed quite randomly along the examined surface and they vary in both size and shape. The grain size of the larger grains were in the region 500-1000µm. The smaller grains measured 75-300µm. The grain structure in alloy Al5NFeSi is shown in figures 36 (optical microscope) and 37 (over anodised sample, macro picture).
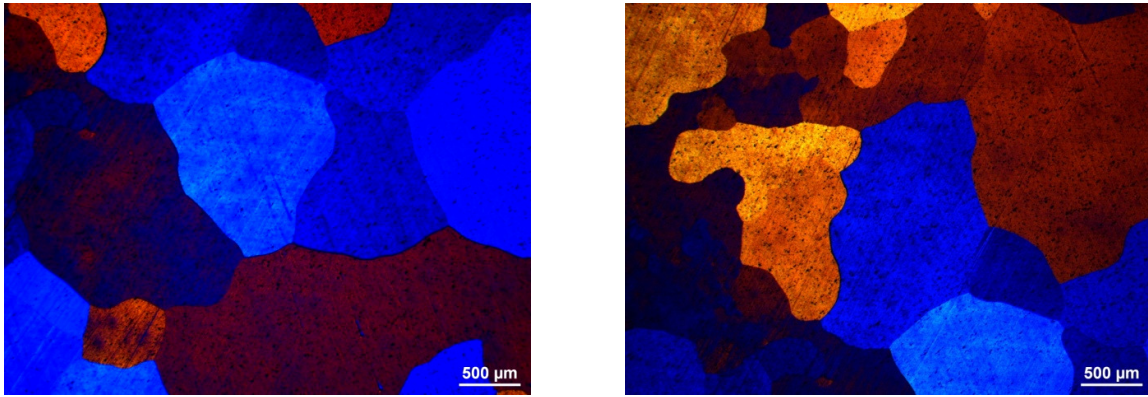
Figure 36: Cast Al5NFeSi at 2.5X magnification (left and right).

The shape and size of the grains indicate that initiation of recrystallisation has been started but not been completed. Figure 37 shows a macro image of an over-anodised Al5NFeSi microscope specimen
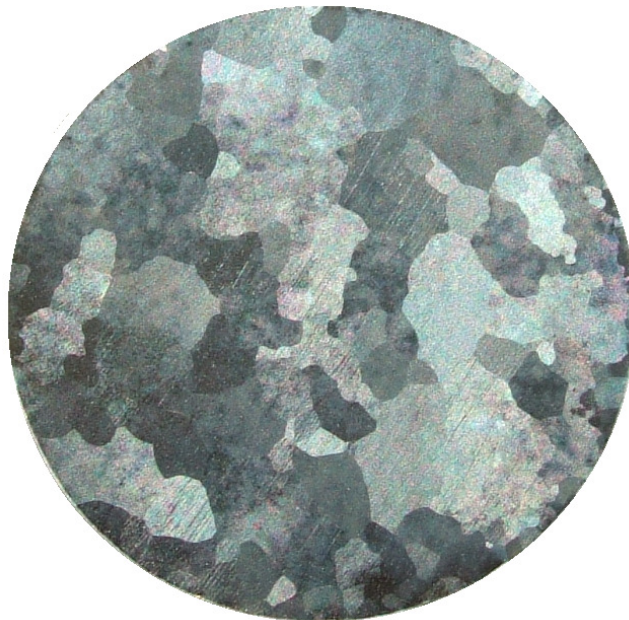
Figure 37: Al5NFeSi microscope sample surface after (over)anodising. Grains and grain boundaries are clearly visible. The diameter of the sample is 15mm.

Al2NFeSi

The governing grain structure in alloy Al2NFeSi seemed to be greatly affected by the casting process and saturation seen in figure 38. Large grains which seem to "flow" across the surface with no distinctive shape are dominant. These are most likely large segregation zones. In addition to the large grains smaller grains have started to form along several grain boundaries. The small grains were measured to be between 50-400µm and are likely due to recrystallisation initiation based on the purity of the material and their location on grain boundaries. The grain structure is far from uniform.
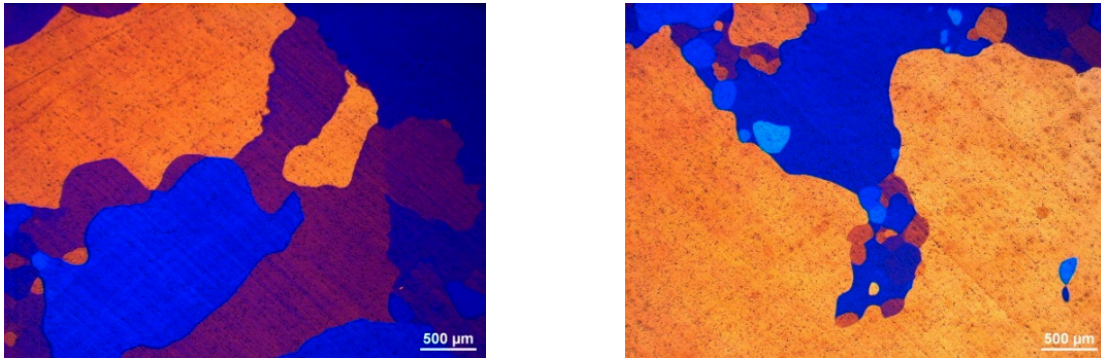
Figure 38: Large grains in alloy Al2NFeSi (left), small grains formed at grain boundaries in alloy Al2NFeSi (right).Magnification 2.5X.

Figure 39 shows a macro image of the grain structure in alloy Al2NFeSi.
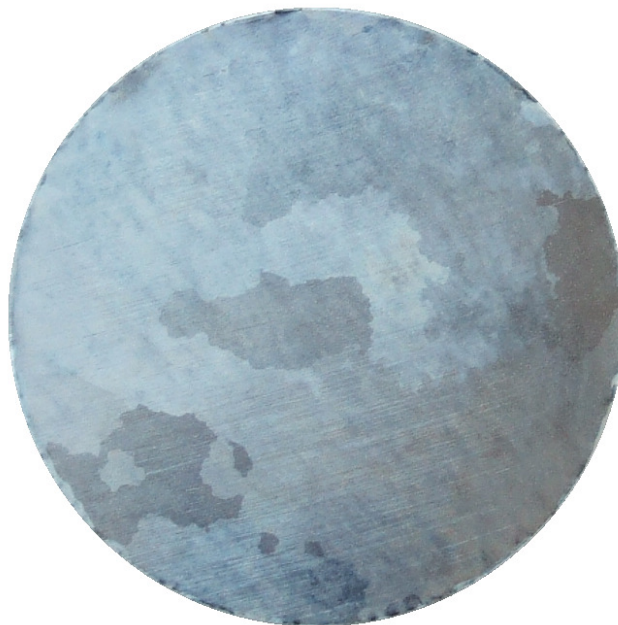
Figure 39: Al2NFeSi microscope sample surface after (over)anodising. Grains and grain boundaries are clearly visible. The diameter of the sample is 15mm.

Al2NFe2Si

In alloy Al2NFe2Si the effect of the casting process is even more evident than for alloy Al2NFeSi. In the same way the structure is dominated by large coarse grains with smaller grains formed at grain boundaries in some areas believed to be nuclei caused by initiation of recrystallisation. The large grains, segregation zones, are smaller compared to the previous alloy. The grain boundaries for the dominant large grains deviate from the straighter lines found in alloy Al5N and Al5NFeSi. The grain boundaries show visible signs of segregation (see figure 40). The smaller grains have more distinct and straight grain boundaries and measurements from 20-800 micron. However, the smaller grained regions are few and far between.
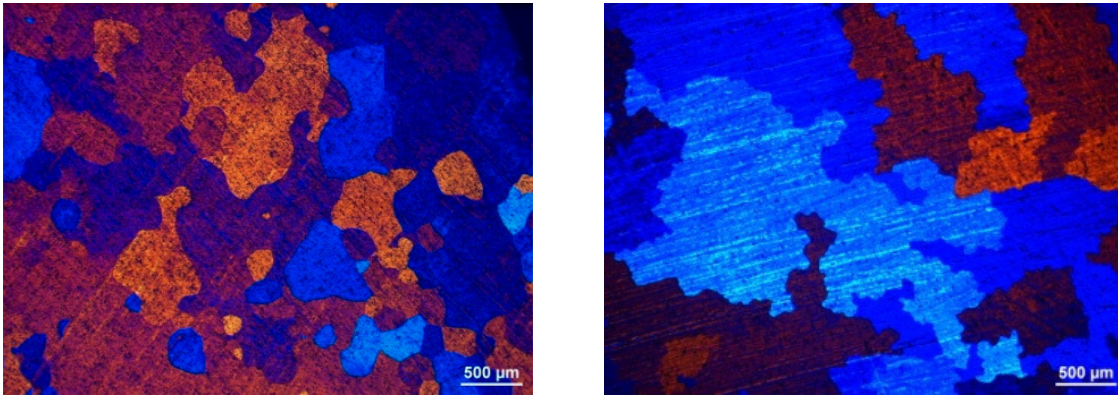
Figure 40: Small grains in alloy Al2NFe2Si (left) found in some areas of the specimen, large grains in Al2NFe2Si (right). Magnification 2.5X

Figure 41 shows a macro image of the grain structure in alloy Al2NFe2Si.
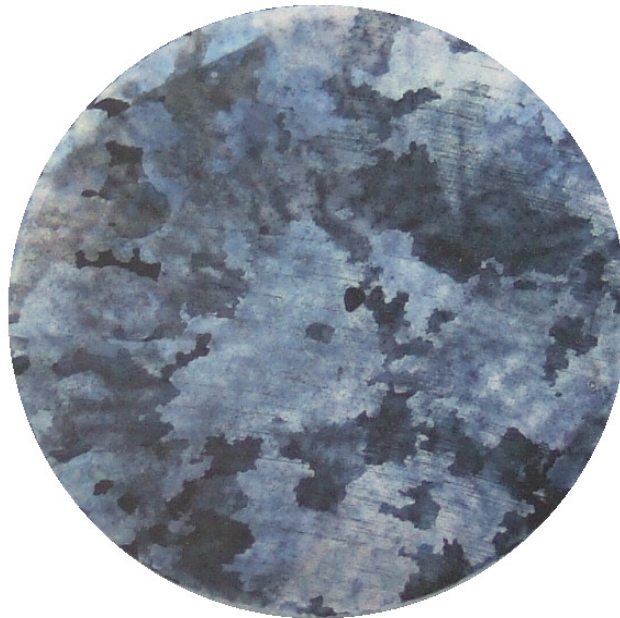
Figure 41: Al2NFe2Si microscope sample surface after (over)anodising. Grains and grain boundaries are clearly visible. The diameter of the sample is 15mm.

Table 5 shows an estimate of the average grain size in the 4 cast alloys along with a grain structure description. The measurements are rough estimates as the random grain distribution in the cast specimens was difficult to measure by the average approach. They are still included as they give an idea of the relative differences between the alloys.

Table 5: Grain size and grain structure description for cast aluminium alloys. Due to the coarse nature of the grains and the random structure it is difficult to conclude an average size. The 2N alloys have a few regions of smaller grains which lead to a lower average size value.

Alloy	Average grain size		Structure description
Al5N	5600	µm	Extremely large grains.
Al5NFeSi	830	µm	Random structure. Significantly smaller grains compared to Al5N
Al2NFeSi	1420	µm	Mixture of large "flowing" grains and smaller equiaxed grains. Segregation structure.
Al2NFe2Si	530	µm	Saturation/segregation structure.

5.1.2. Extruded and homogenised aluminium

The alloys in this section have been extruded. In most cases where aluminium is deformed in this way, the result is a fibre like grain structure or areas with large narrow grains in the deformation direction. The pictures are included to illustrate the grain structure prior to rolling. In the project work[5] performed by the author during fall 2010, the alloys used were these extruded ones.

Al5N

Figure 42 shows the grain structure in the extruded alloy Al5N. Although the alloy has been extruded there are few traces of this deformation work in the grain structure. Large equiaxed grains and a reasonably uniform distribution seem to dominate.
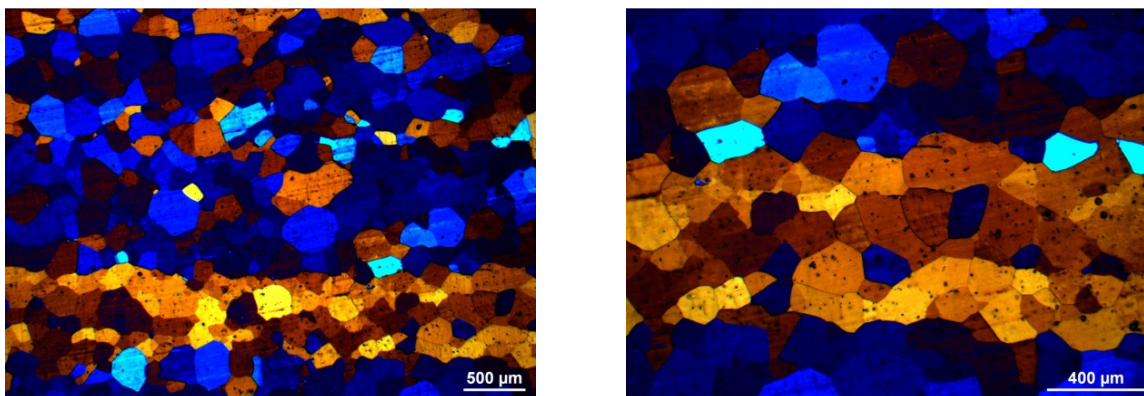
Figure 42: Grain structure of extruded Al5N at 2.5X magnification (left), grain structure of extruded alloy Al5N at 5X magnification (right).

Al5NFeSi

Alloy Al5NFeSi appears partly recrystallised (figure 43). The structure arising from the extrusion process is clearly visible by the large narrow areas which dominate. Smaller grains have started to form inside these narrow grains.
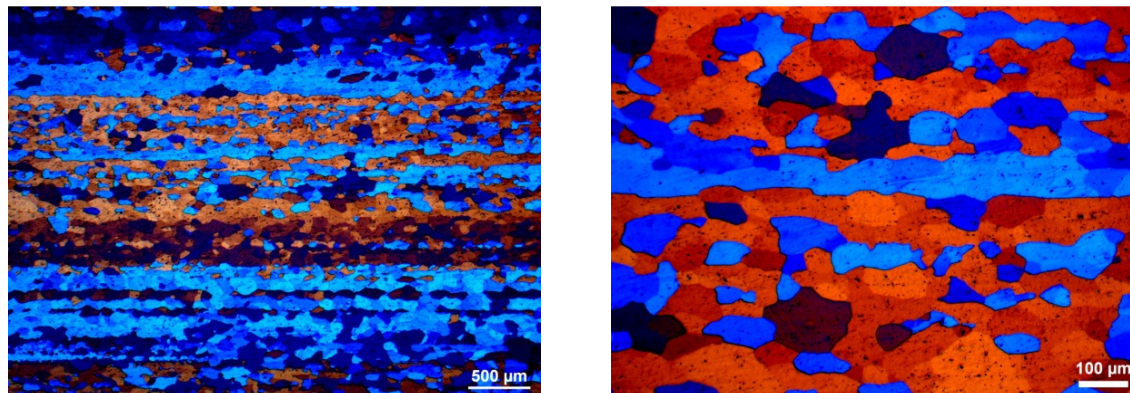
Figure 43: Grain structure of extruded Al5NFeSi at 2.5X (left) and 10X (right) magnification.

Al2NFeSi

The microstructure of alloy Al2NFeSi is very similar to that of the previous alloy as seen in figure 44. The alloy is also considered partly recrystallised.
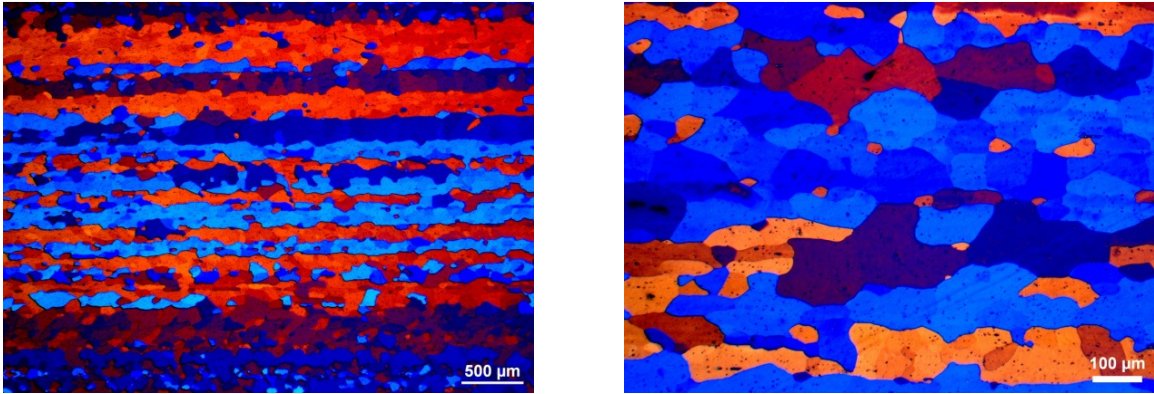
Figure 44: Grain structure of extruded Al2NFeSi at 2.5X (left) and 10X (right) magnification.

Al2NFe2Si

The governing grain structure in Al2NFe2Si is the fibre like large narrow grains, visible in figure 45. Al2NFe2Si seems to be the alloy which has been most heavily affected by the extrusion process. Few smaller grains appeared at the lower magnifications (2.5-10X). The few grains which are visible are most likely initiation of recrystallisation and have formed at grain boundaries.
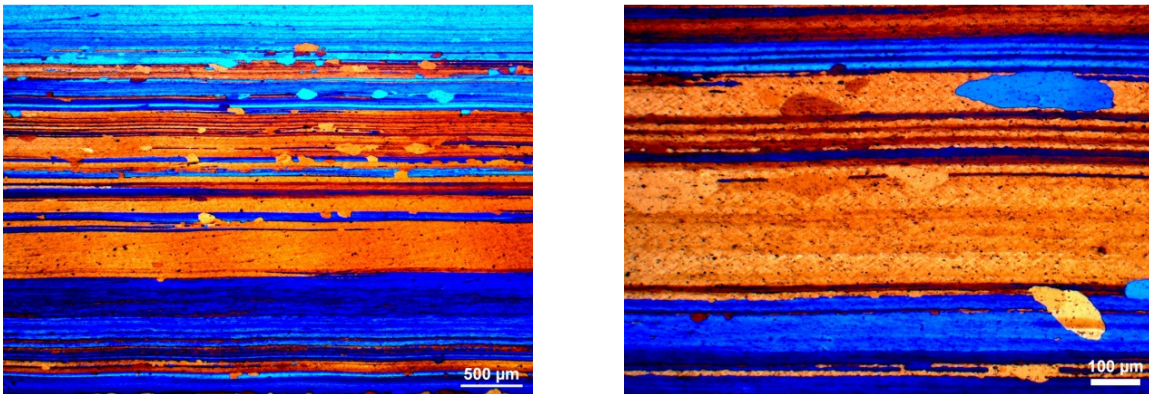
Figure 45: Grain structure of extruded Al2NFe2Si at 2.5X (left) and 10X (right).

Larger magnification (20-50X) revealed what appeared to be a sub grain structure. A multitude of smaller grains, i.e. sub grains, were visible in alloy Al2NFe2Si. In figure 46 they are vaguely visible, especially in the blue regions.
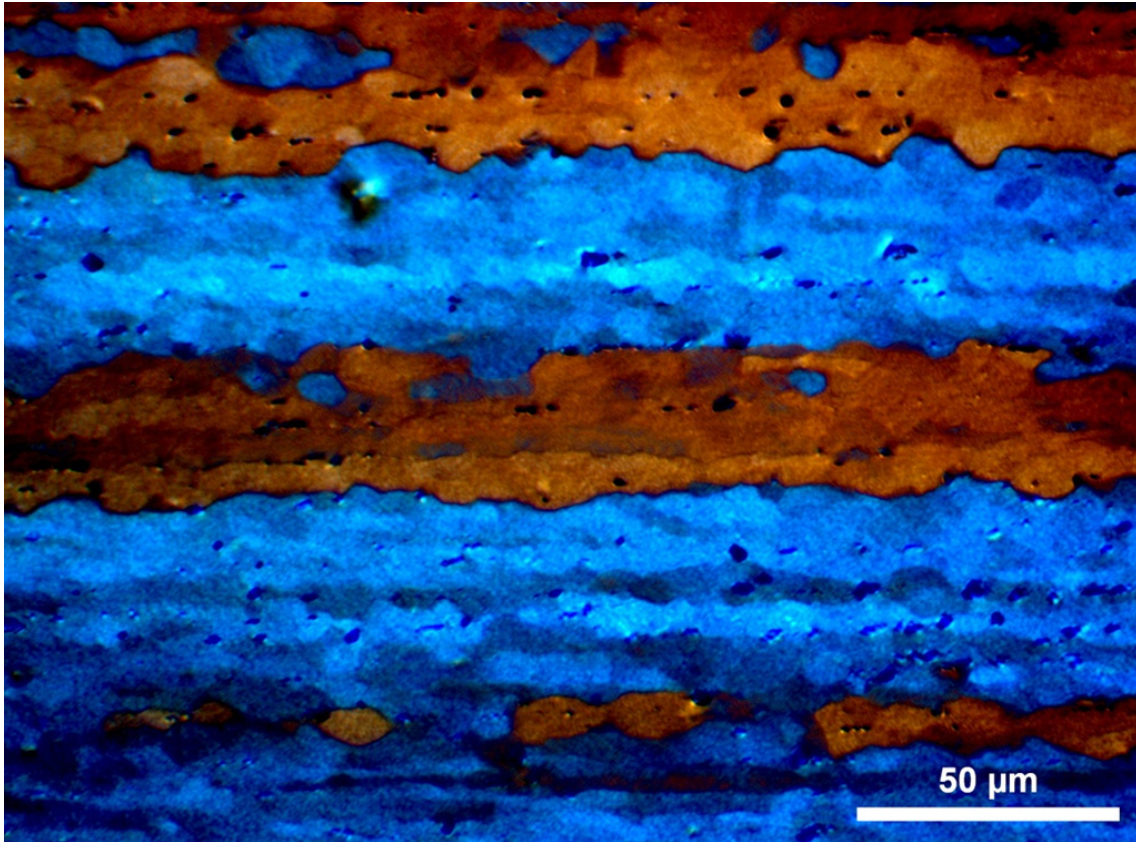
Figure 46: Sub grains in alloy Al2NFe2Si at 50X magnification.

5.1.3. Recrystallisation of rolled aluminium: hardness and micro structural development

The extruded aluminium was rolled and prior to the tensile testing the material was recrystallised. In this section the development of the grain structure at various annealing temperatures are covered to elaborate how the recrystallisation temperatures were decided.

The results from hardness measurements after annealing at various temperatures showed that the ideal temperature for recrystallisation should be within the area 325-400°C. The results are given in figure 47 below. After an initial increase in hardness, it drops drastically and when it starts to stabilize the material should be recrystallised. The exception from this behaviour is the least alloyed material, Al5N, which appears to be recrystallised at room temperature. Few inhibitors against grain growth result in large grains which do not deform in the same way as more alloyed materials during extrusion. Dynamic recrystallisation during extrusion or recovery may be an explanation.
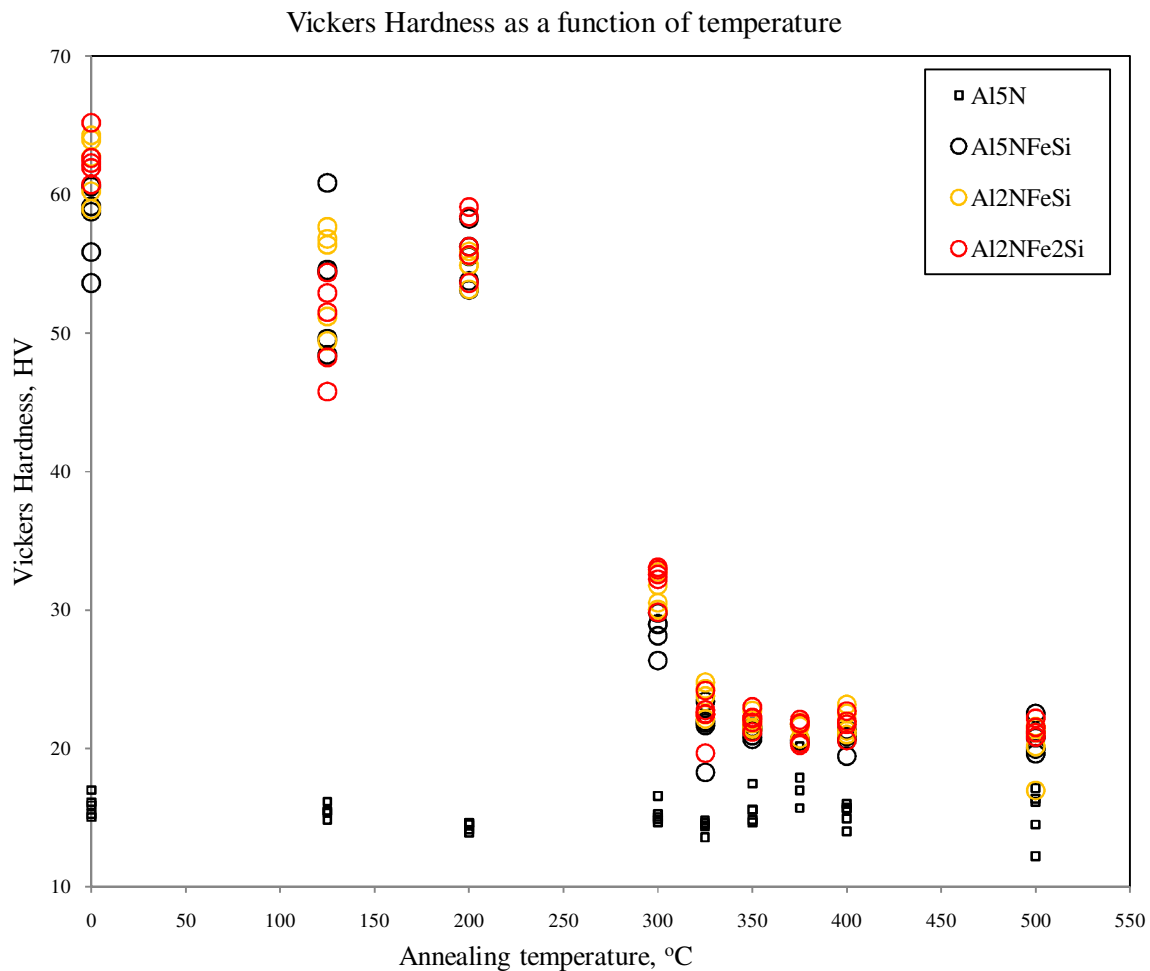
Figure 47: Vickers hardness as a function of temperature. The alloys were held in a salt bath for 30 minutes for each investigated temperature. 5 hardness impressions per alloy were made after each treatment.

A suitable temperature must be established in order for the material to recrystallise completely. To be certain, the microstructure must be examined in the optical microscope. Alloys Al2NFeSi and Al2NFe2Si appear to increase their hardness slightly beyond 375°C, this is likely due to the Hall-Petch effect (1).

50

Microstructure

350 ^{o}C

Al5N, Al5NFeSi, Al2NFeSi and Al2NFe2Si annealed for 30 minutes in salt bath holding 350°C. The horizontal direction in the pictures corresponds to the rolling and extrusion direction of the material profiles.

Al5N

Figure 48 shows that alloy Al5N contains very large grains and it is unlikely that annealing will cause any recrystallisation, nor any hardening. However, the risk of grain growth is present. The grain size development must subsequently be monitored.
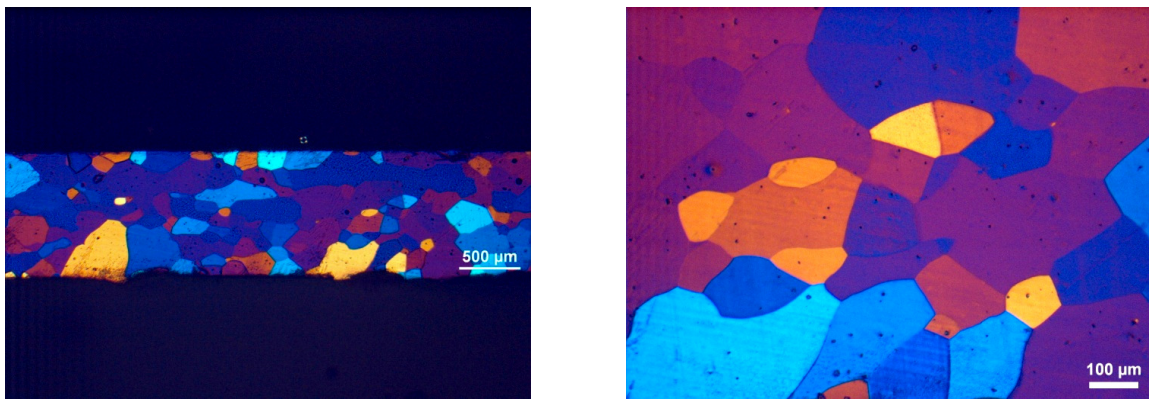
Figure 48: Al5N annealed at 350°C at 2.5X (left) and 10X (right) magnification.

Al5NFeSi

The grain structure for alloy Al5NFeSi is shown in figure 49. Areas showing large narrow grains indicate that the alloy had not been completely recrystallised and therefore 350 ^{o}C is not a sufficiently high temperature. The light-blue coloured grains seem to be dominant as an underlying layer, deriving from either the extrusion or rolling process.
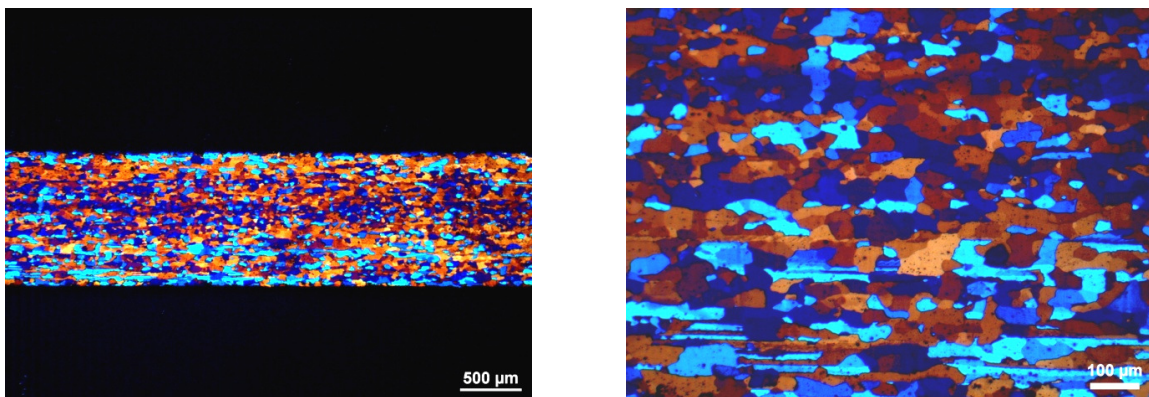
Figure 49:Al5NFeSi annealed at 350°C at 2.5X (left) and 10X (right) magnification.

Al2NFeSi

Figure 50 shows the grain structure in alloy Al2NFeSi at 2 magnifications. As for Al5NFeSi there is still evidence of deformation structure in alloy Al2NFeSi, complete recrystallisation not fulfilled by annealing temperature 350°C.
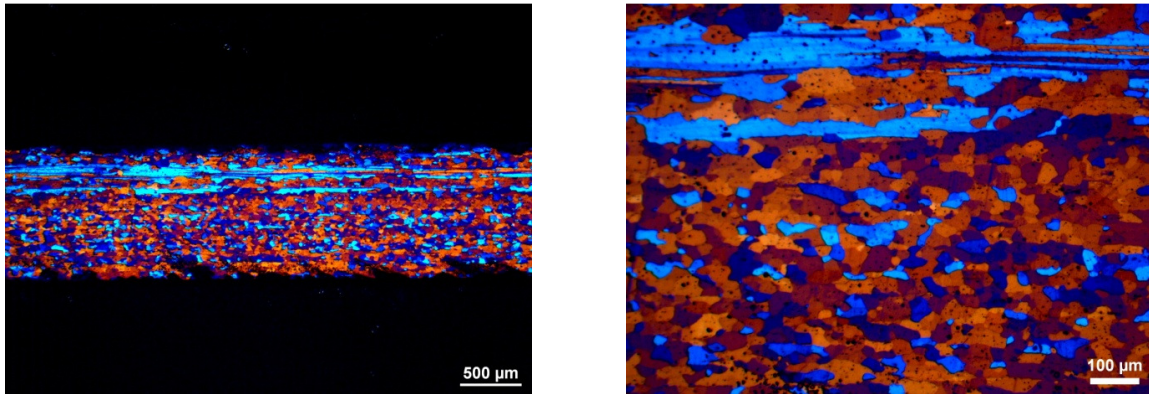
Figure 50: Al2NFeSi annealed at 350°C at 2.5X (left) and 10X (right) magnification.

Al2NFe2Si

Al2NFe2Si, complete recrystallisation not fulfilled by annealing temperature at 350°C (fig. 51). The deformation structure is still visible in several areas.
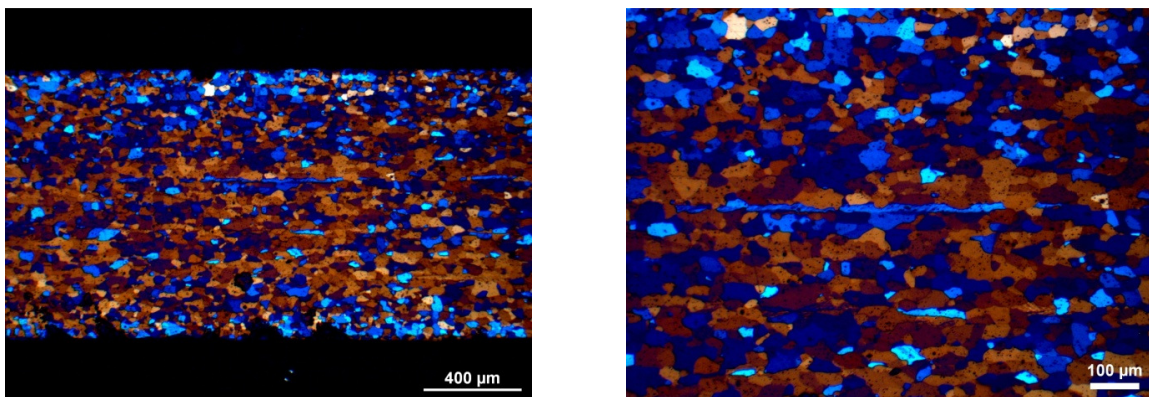
Figure 51: Al2NFe2Si annealed at 350°C at 5X (left) and 10X (right) magnification.

375 ^{o}C

Both alloys Al5NFeSi, Al2NFeSi and Al2NFe2Si showed debris of the texture formed during rolling or extrusion, i.e. large narrow grains, and therefore complete recrystallisation had not been fulfilled. New specimens were annealed in salt baths with the temperature at 375°C. Alloy Al5N was treated in the same way, even though no significant changes should occur during annealing because of the large grains.

Al5N

The grains are finer and more equally sized size compared to the structure after annealing carried out at 350°C (figure 52). However, the average grain size is substantially larger.
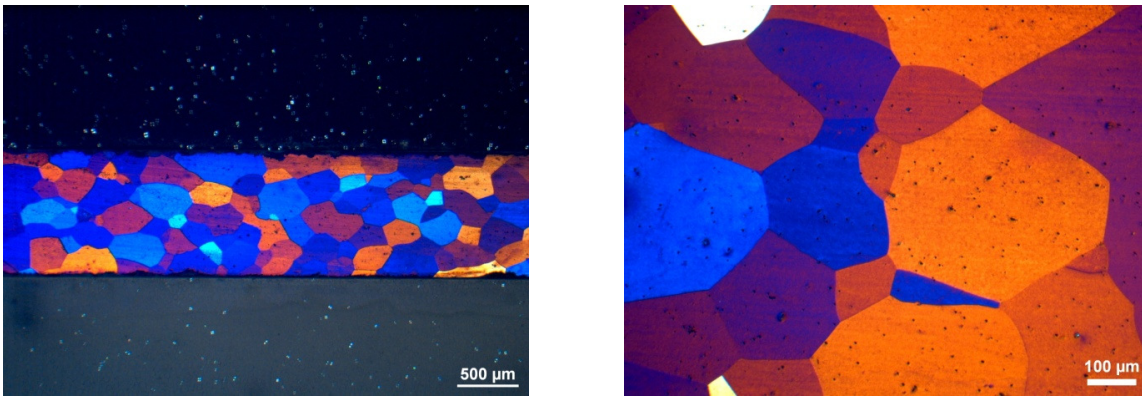
Figure 52: Al5N annealed at 375°C at 2.5X (left) and 10X (right) magnification.

Al5NFeSi

Al5NFeSi show no traces of deformation structure and appears fully recrystallised (fig. 53). The pictures show a typical recrystallised grain structure for aluminium.
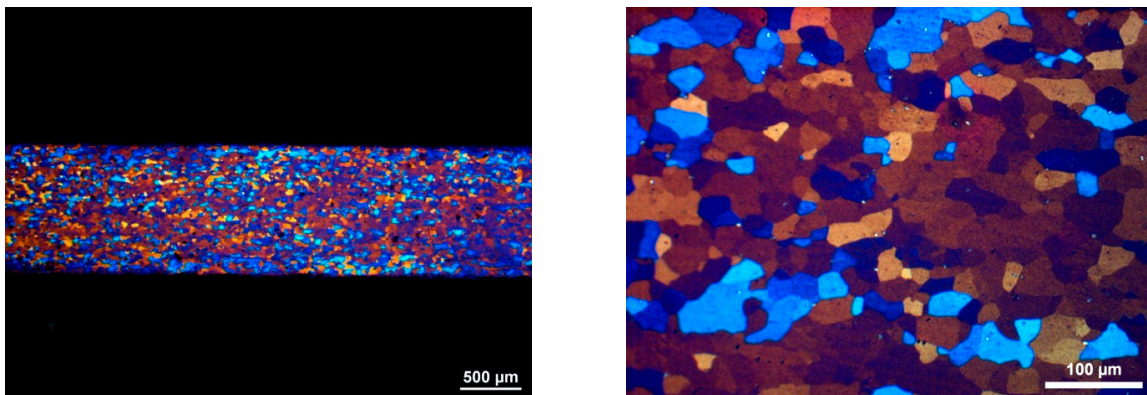
Figure 53: Al5NFeSi annealed at 375°C at 2.5X (left) and 20X (right) magnification.

Al2NFeSi

Al2NFeSi show no traces of deformation structure and appears fully recrystallised (fig. 54) after annealing at 375°C for 30 minutes.
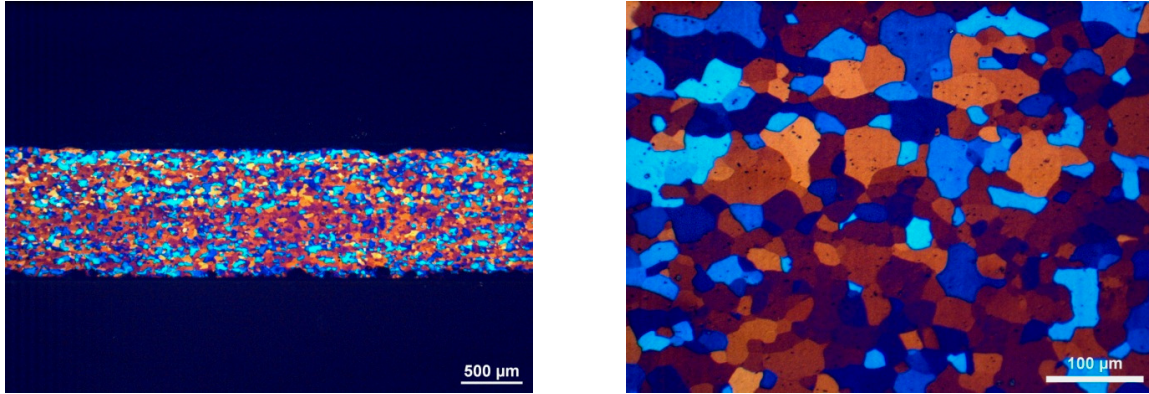
Figure 54: Al2NFeSi annealed at 375°C at 2.5X (left) and 20X (right) magnification.

Al2NFe2Si

Alloy Al2NFe2Si appears recrystallised as seen in figure 55. However a few areas showed some quite large narrow grains.
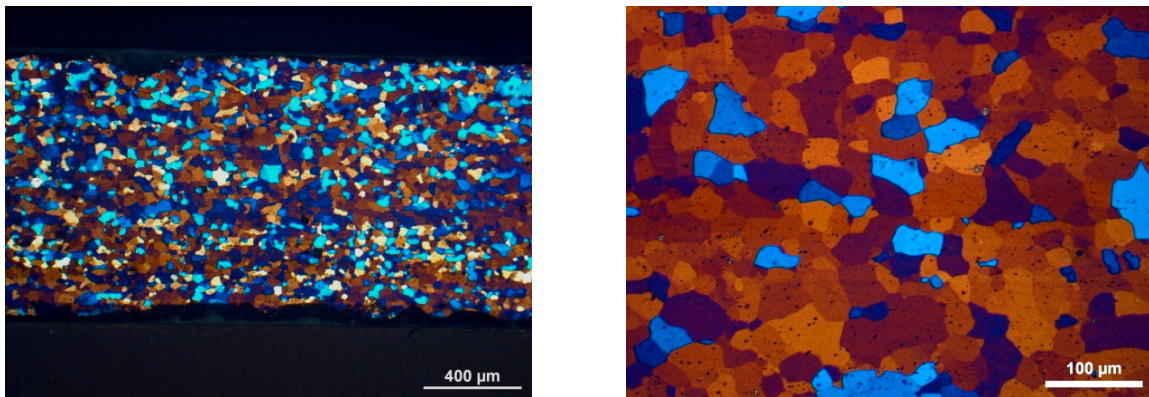
Figure 55: Al2NFe2Si annealed at 375°C at 5X (left) and 20X (right) magnification.

400 ^{o}C

To make sure the most alloyed material, Al2NFeSi, was in fact completely recrystallised, it was annealed in the 400 ^{o}C salt bath for 30 minutes. Alloy Al2NFe2Si appears fully recrystallised after annealing carried out at a temperature of 400°C (figure 56). Compared to the 375 ^{o}C treatment the grains were slightly smaller and showed no traces of deformation, i.e. large narrow grains. As no grain growth was registered the 400 ^{o}C treatment was preferred.
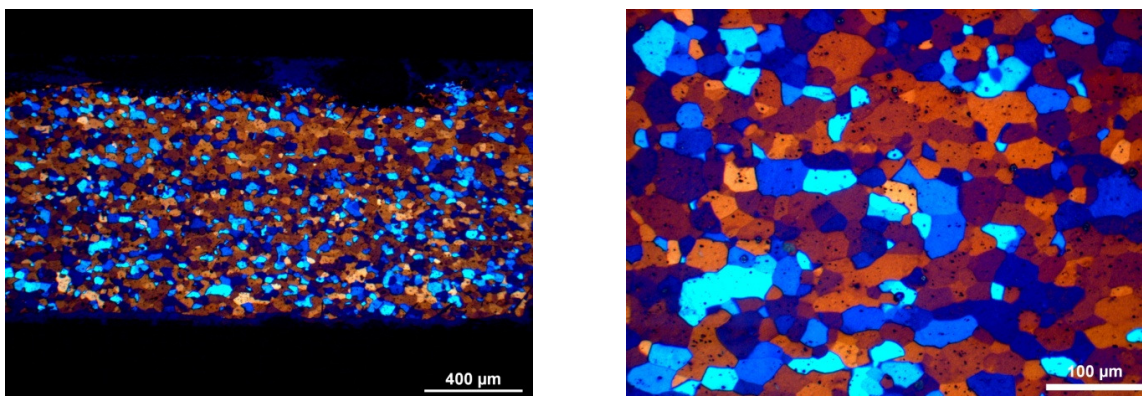
Figure 56: Al2NFe2Si annealed at 400°C at 5X (left) and 20X (right) magnification.

Recrystallisation temperature

Based on the annealing/hardness experiment and the corresponding microscope results a suitable annealing was determined. Tensile specimens of alloys Al5NFeSi and Al2NFeSi were annealed at 375°C for 30 minutes. Specimens of alloy Al2NFe2Si were annealed at 400°C, also for 30 minutes. However, it is likely that 375 ^{o}C would have been sufficient to recrystallise alloy Al2NFe2Si, based on the microscope results. The grains are slightly smaller after the 400 ^{o}C treatment, i.e. no grain growth.

Alloy Al5N showed a very low softening. It is likely that alloy Al5N, based on its purity, recrystallised during rolling or shortly thereafter. The recrystallisation temperature is probably so low that the heat transfer from the rolling cylinder has caused a dynamic recrystallisation during the process. The grain size development, given in table 6 below, showed that the grains became larger with higher annealing temperatures. This alloy was annealed for 30 minutes in a 350°C salt bath as relatively small grains were measured after this treatment.

Table 6: Grain size development of rolled Al5N during the annealing experiment.

Average grain size of alloy Al5N		
Holding time (min)	Temperature (^{o}C)	Grain size (µm)
30	20	~149
30	350	~163
30	375	~232

5.2. Grain sizes and grain size effect

Based on the micro structural results and measures of hardness an estimation of the expected mechanical properties can be made. For quantification the Hall Petch relation is convenient. The direct impact of grain size on the yield strength can be found as the last fraction in the relation.

Hall-Petch (equation 1)[11]:

$$\sigma_0 = \sigma_I + k \cdot \frac{1}{\sqrt{D}}$$

Where σ_0 is the yield stress, σ_I is the stress due to lattice friction, k is a constant and D is the grain size. The contribution to the yield stress from the grain size decreases with increasing grain size. In table 7 the average grain sizes for all the alloys in this work are given.

Table 7: Grain size and grain structure description for rolled, extruded and cast alloys.

Processing	Alloy	Grain size		Sub grain size		Description
Rolled	Al5N	167	µm			Recrystallised
Rolled	Al5NFeSi	27	µm			Recrystallised
Rolled	Al2NFeSi	30	µm			Recrystallised
Rolled	Al2NFe2Si	22	µm			Recrystallised
Extruded	Al5N	136	µm			Recrystallised
Extruded	Al5NFeSi	81	µm			Partly recrystallised
Extruded	Al2NFeSi	119	µm			Partly recrystallised
Extruded	Al2NFe2Si	51	µm	8.3	µm	Fibre structure
Cast	Al5N	5600	µm			Extremely large grains
Cast	Al5NFeSi	830	µm			Random structure
Cast	Al2NFeSi	1420	µm			Segregation structure
Cast	Al2NFe2Si	530	µm			Segregation structure

Comment table: Alloys Al5NFeSi and Al2NFeSi were partly recrystallised and the smaller grains were measured along with the larger ones which are due to the extrusion that the material has undergone. Alloy Al2NFeSi consisted of a distinct fibre-like grain structure and both fibre grain width and sub grain size are given. The table contains grain sizes fore cast, rolled and extruded alloys.

By isolating the section from (equation 1) the Hall-Petch relation which considers the grain size contribution;

$$k \cdot \frac{1}{\sqrt{D}}$$

...we can quantify the theoretical contribution in each of the cast, extruded and rolled/recrystallised alloys. The constant k for pure aluminium is ~ 0.08 kP/mm$^{3/2}$ and ~ 0.13kP/mm$^{3/2}$ for commercial purity[18]. From the results given in the table 8 we see that the contribution increases with decreasing grain size as the theory suggests.

Table 8: Hall-Petch, strength contribution from grain size in extruded and rolled alloys. Note that the grain sizes are averages. The factor k used in the table is 0.08 kP/mm$^{3/2}$ for pure aluminium (Al5N and Al5NFeSi) and 0.13 kP/mm$^{3/2}$ for commercial alloys (Al2NFeSi and Al2NFe2Si)[18].

Processing	Alloy	Grain size		Strength (k*1/√D)	
Rolled	Al5N	167	µm	2.0	MPa
Rolled	Al5NFeSi	27	µm	4.9	MPa
Rolled	Al2NFeSi	30	µm	7.5	MPa
Rolled	Al2NFe2Si	22	µm	8.8	MPa
Extruded	Al5N	136	µm	2.2	MPa
Extruded	Al5NFeSi	81	µm	2.8	MPa
Extruded	Al2NFeSi	119	µm	3.8	MPa
Extruded	*Al2NFe2Si*	51	µm	5.8	MPa
Cast	Al5N	5600	µm	0.3	MPa
Cast	Al5NFeSi	830	µm	0.9	MPa
Cast	Al2NFeSi	1420	µm	1.1	MPa
Cast	Al2NFe2Si	530	µm	1.8	MPa

5.3. SEM microscopy

In this section the results from the SEM microscope are presented. The extruded and rolled alloys were investigated by EBSD. It is natural to start with the extruded alloys as the texture caused by the extrusion deformation affects the texture of the rolled alloys. The rolled specimens were in addition studied by EDS to find particles and their composition. Two pole figures and the ODF map are shown for each alloy, both extruded and rolled, and a quick assessment regarding texture is made. Some extra SEM images (IPF, IQ) are included in the appendix page A.

In sections 5.3.1 and 5.3.2. a detailed explanation concerning a specific texture will not be repeated once introduced. If the texture reappears in another alloy this will simply be stated as it has already been explained.

5.3.1. Texture, extruded aluminium

Al5N, extruded:
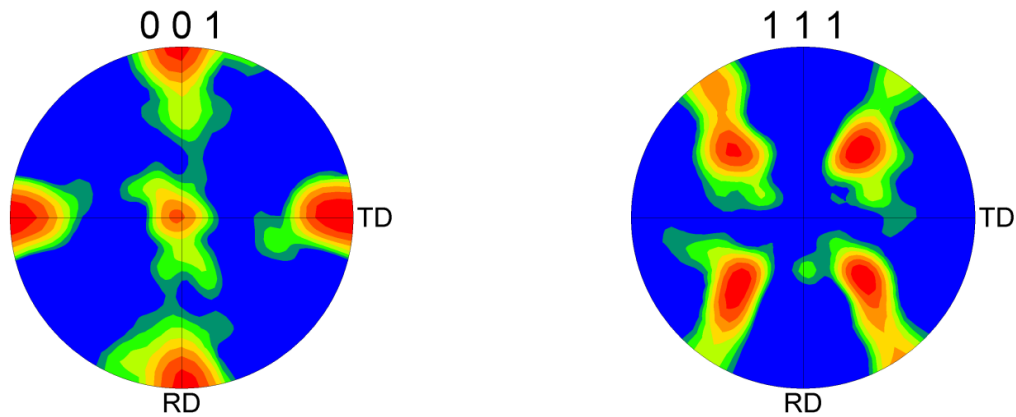
Figure 57: 001 and 111 pole figures for Al5N extruded.
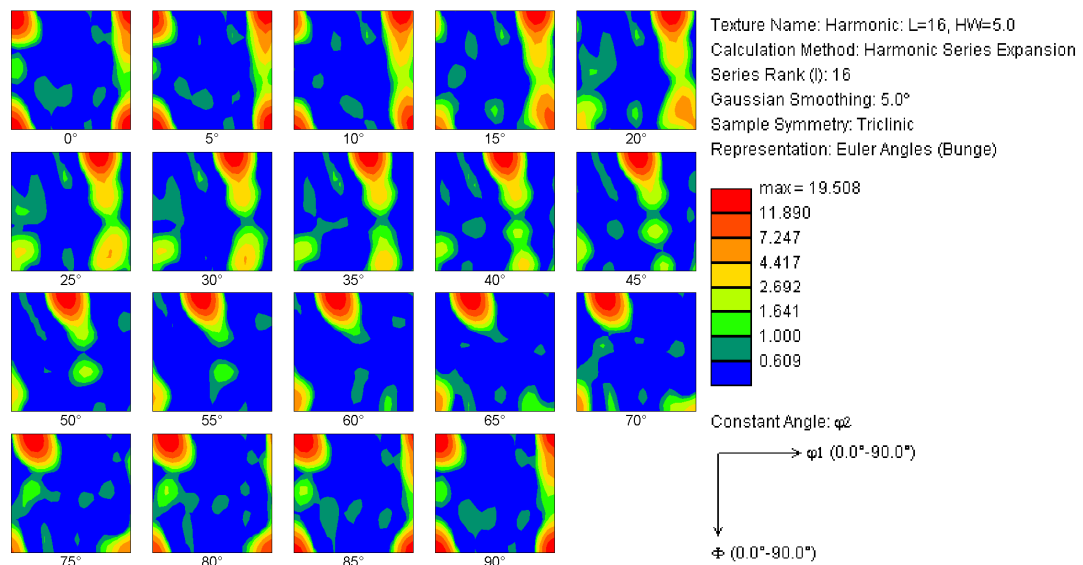
Figure 58: ODF map alloy Al5N extruded.

Based on the pole figures and the ODF map (Fig. 57 & 58) the governing texture in extruded Al5N is strong *cube texture*. The reflections (red levels) from the <100> planes are placed respectively 0, 90, 180 and 270 degrees relative to the centre of the 001 pole figure. In addition the reflection from the upper plane of the cube is shown in the centre. The 111 pole figure and the ODF map further supports these findings by the corner reflections at constant $\varphi_2=0^o$ in ODF and in the pole figure by the inclined reflections from the <111> planes[28].

Al5NFeSi, extruded:

Alloy Al5NFeSi has a strong cube texture in addition to a moderate β-fibre. The reflections from the β-fibre can be seen in the 001 PF (fig. 59) as a triangle between the cube reflections and the orange circle in the ODF map (fig. 60) by the position (Euler angles at roughly $\phi=45^o$, $\varphi_1=35^o$ and $\varphi_2=0^o/90°$)[28].
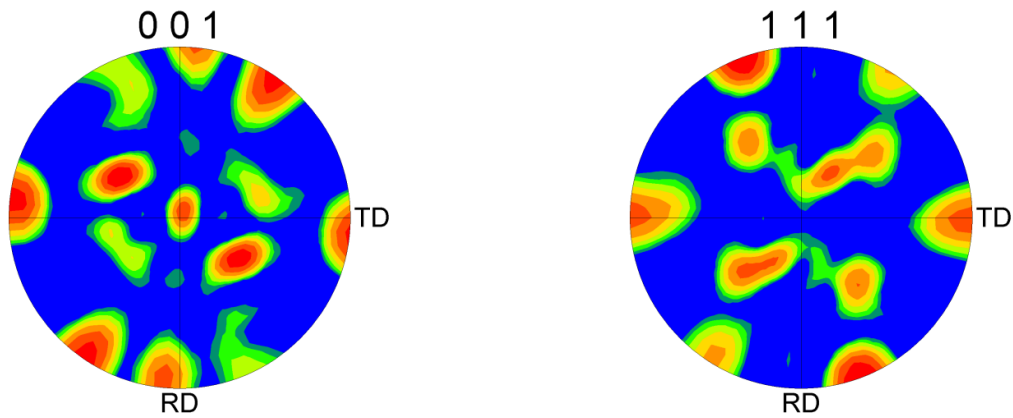
Figure 59: 001 and 111 pole figures for Al5NFeSi extruded.
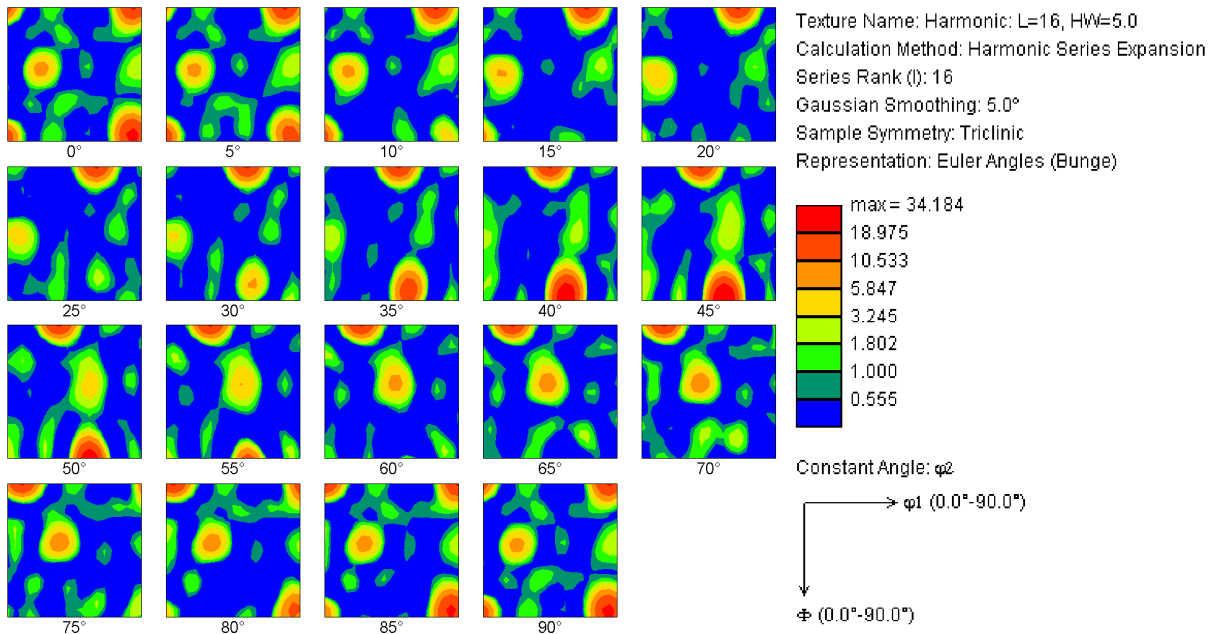
Figure 60: ODF for alloy Al5NFeSi extruded.

Al2NFeSi, extruded:

Figure 61 and 62 show the pole figures and the ODF map for the extruded alloy AL2NFe2Si. The alloy shows a strong β-fibre texture, best seen in the ODF map (figure 62) by the strong reflection in the β-fibre position as for the previous alloy (Al5NFeSi). There may also be a weak cube texture vaguely visible in the 4 corners of the ODF at constant Euler angle $\varphi_2 = 0°$[28].
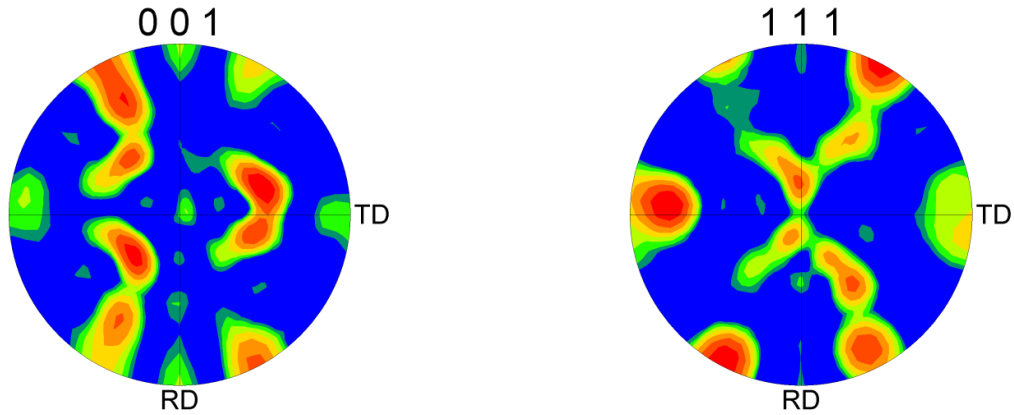
Figure 61: 001 and 111 pole figures for Al2NFeSi extruded.
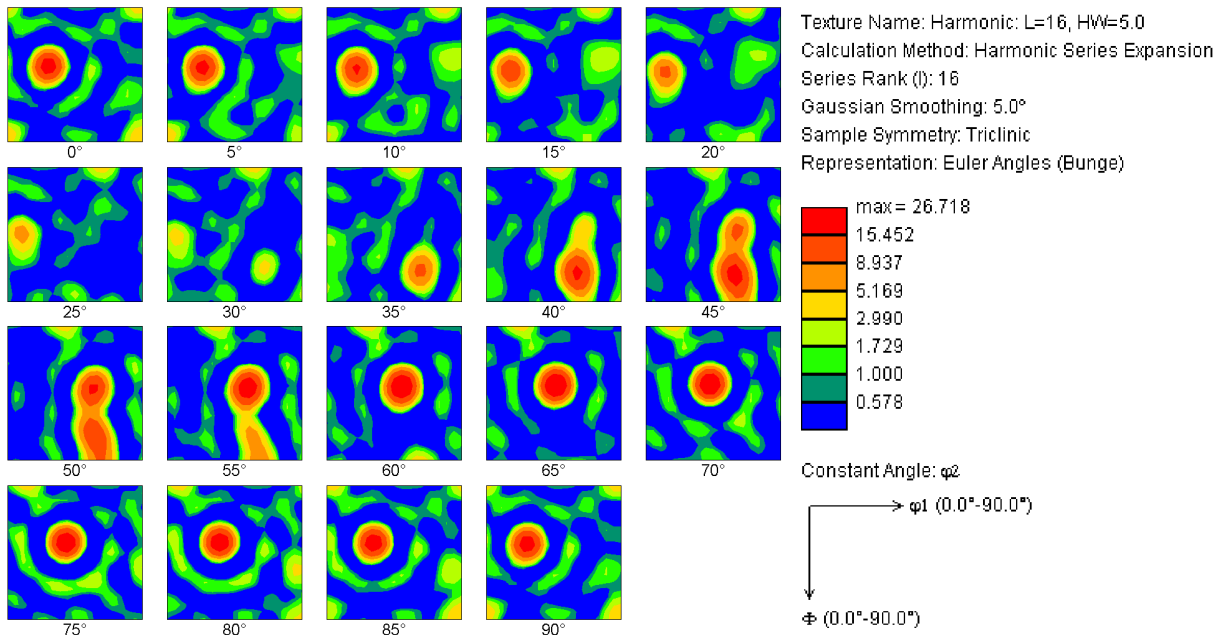
Figure 62: ODF for alloy Al2NFeSi extruded.

Al2NFe2Si, extruded:

Based on figures 63 and 64 the fibre-like alloy Al2NFe2Si shows a typical deformation texture by the many green narrow and long levels. The cube texture is the most apparent by the strong reflections in the corners of the ODF map and in the 001 PF. In addition a moderate R-texture seems to be present, which is a common deformation structure[28]. This may be seen in the 111 pole figure by what should be 8 concentrated reflections.
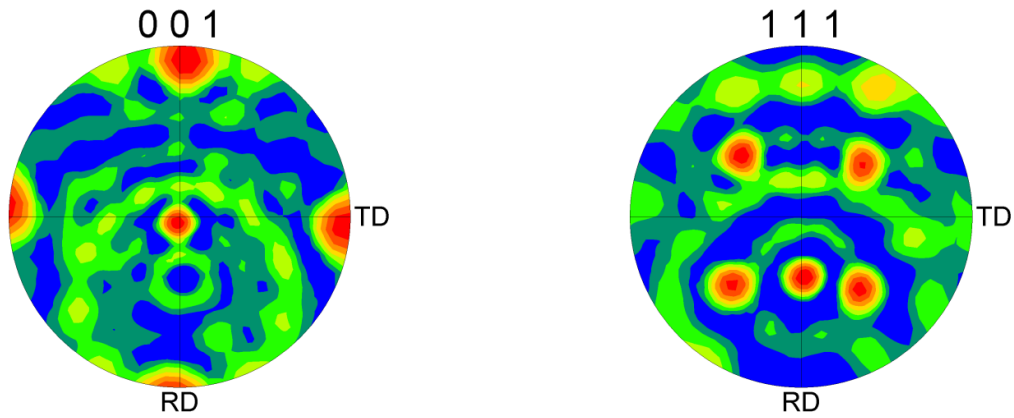
Figure 63: 001 and 111 pole figures for Al2NFe2Si extruded.
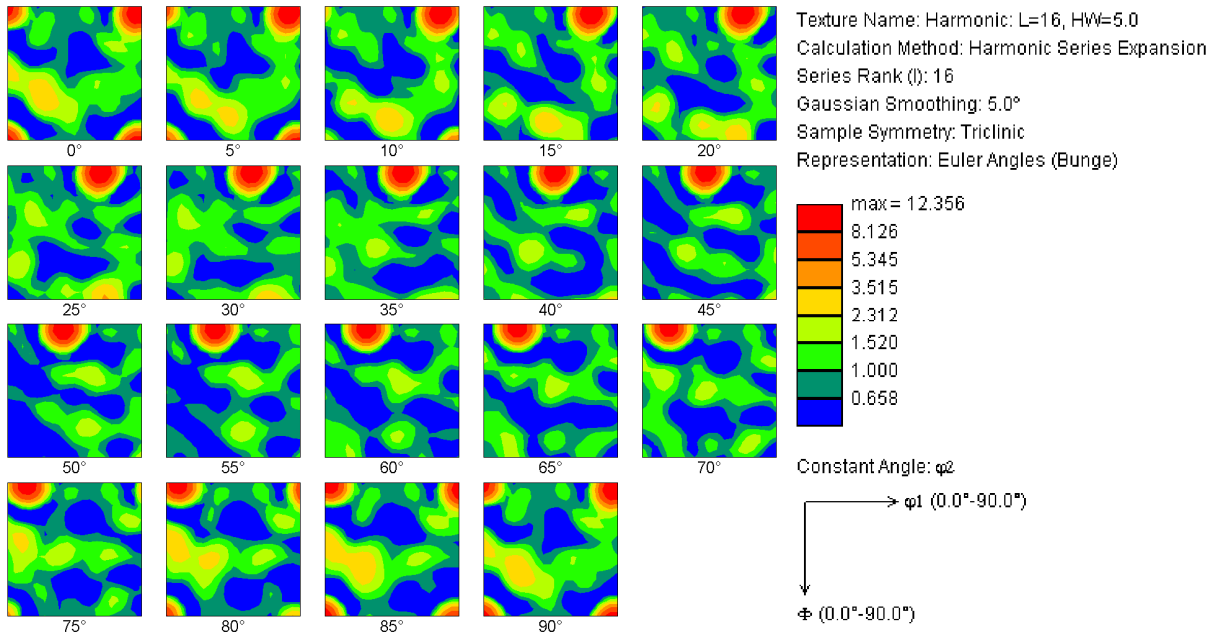
Figure 64: ODF for alloy Al2NFe2Si extruded.

Figure 65 shows the reflections, black circles, corresponding to the R-texture with miller indices {124} <211>. Although the levels have different intensities in the pole figure, the R-texture is likely present. The R-texture may be slightly displaced downward in the figure.
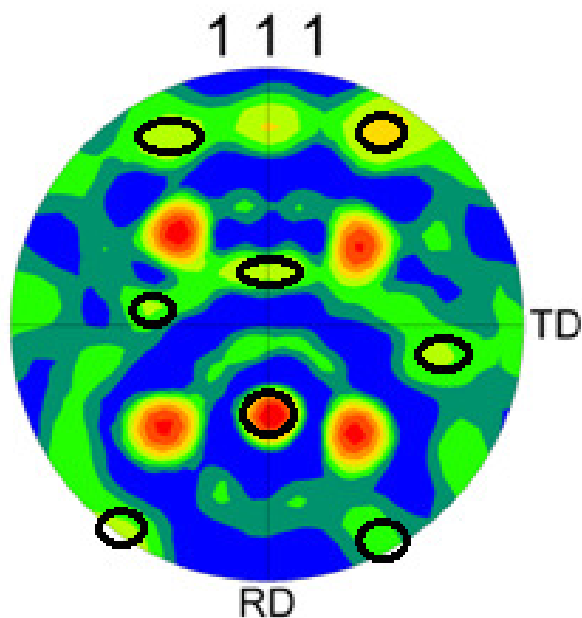
Figure 65: Pole figure 111 for Al2NFe2Si extruded showing what appears to be an R-texture in addition to a strong cube texture. The black circles point to where the reflections are usually found for the R-texture. The red intensity levels mark the cube texture.

5.3.2. Texture, rolled aluminium

Al5N, rolled:

Based on the pole figures and ODF (fig. 66 and 67) the cube texture is the most likely. However, this scan included too few grains to conclude this with any certainty. The cube and R-textures are common for recrystallised aluminium alloys[28].
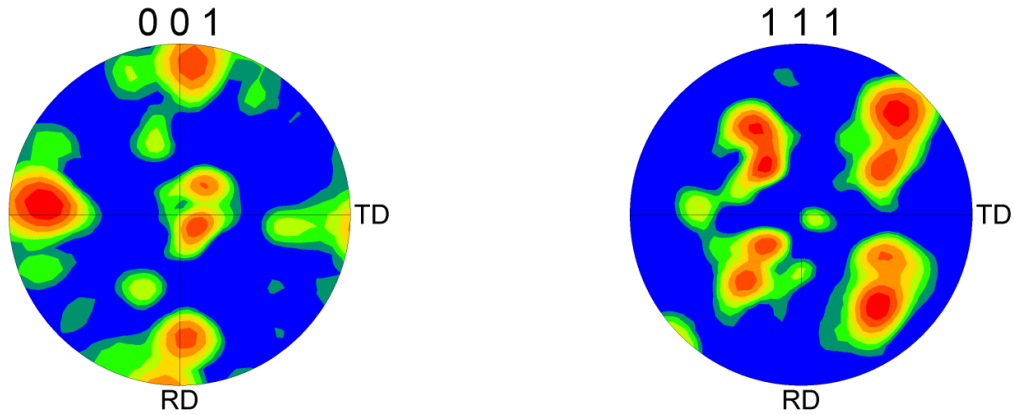
Figure 66: 001 and 111 pole figures for Al5N rolled.
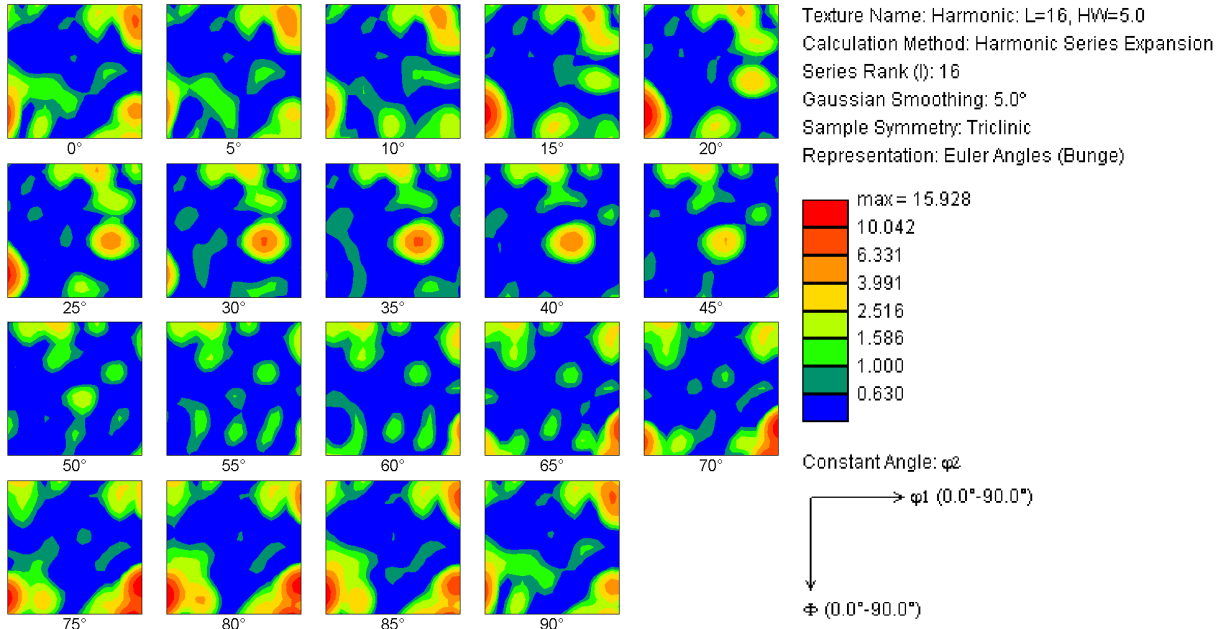
Figure 67: ODF for alloy Al5N rolled.

Al5NFeSi, rolled:

Based on figure 68 and 69 a TD rotated cube with weak β-fibre seems to be the texture of alloy Al5NFeSi. The red reflections in the 001 pole figure indicate that the cube is rotated roughly 45 degrees about the TD axis. This is further supported by the 111 pole figure. From the ODF maps there appears to be what looks like a weak β-fibre at $\varphi_2 = 0^o$.
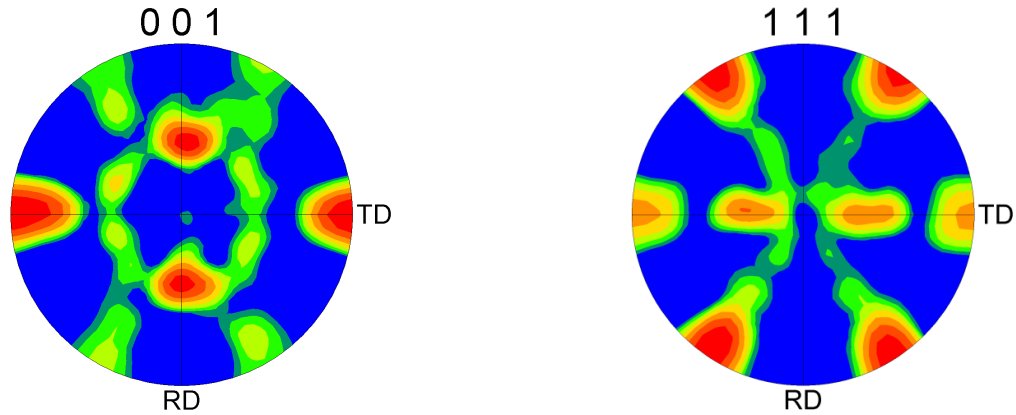
Figure 68: 001 and 111 pole figures for Al5NFeSi rolled.
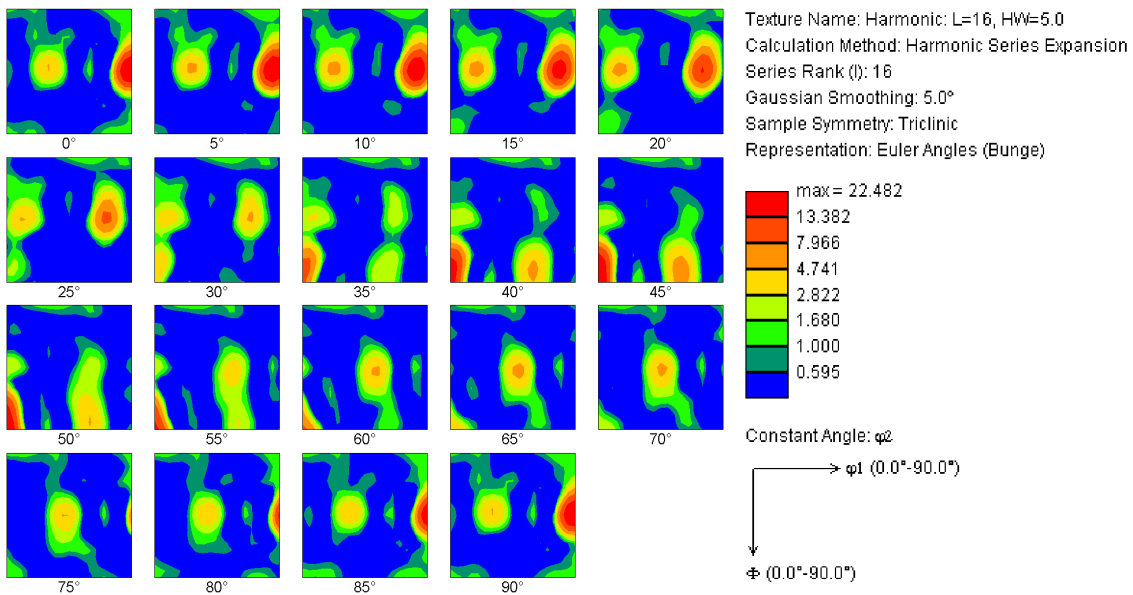
Figure 69: ODF for alloy Al5NFeSi rolled.

Al2NFeSi, rolled:

Based on figures 70 and 71 the texture of Al2NFeSi rolled seems to be the TD rotated cube texture with a weak β-fibre.
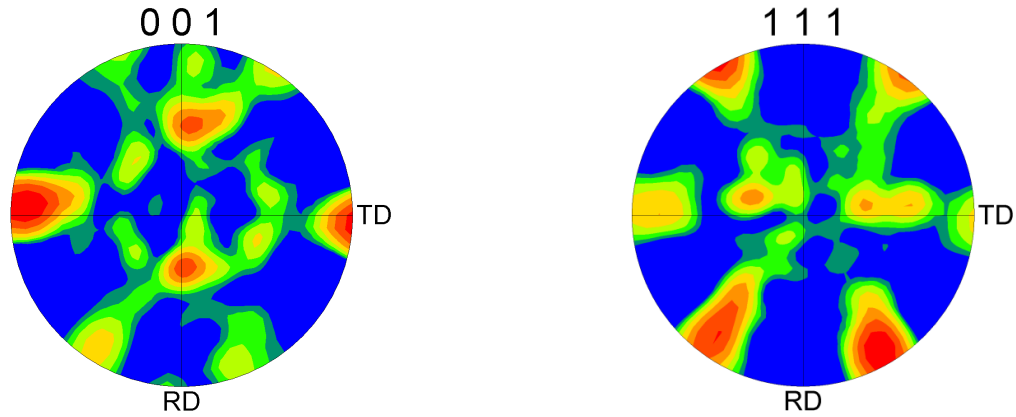
Figure 70: 001 and 111 pole figures for Al2NFeSi rolled.
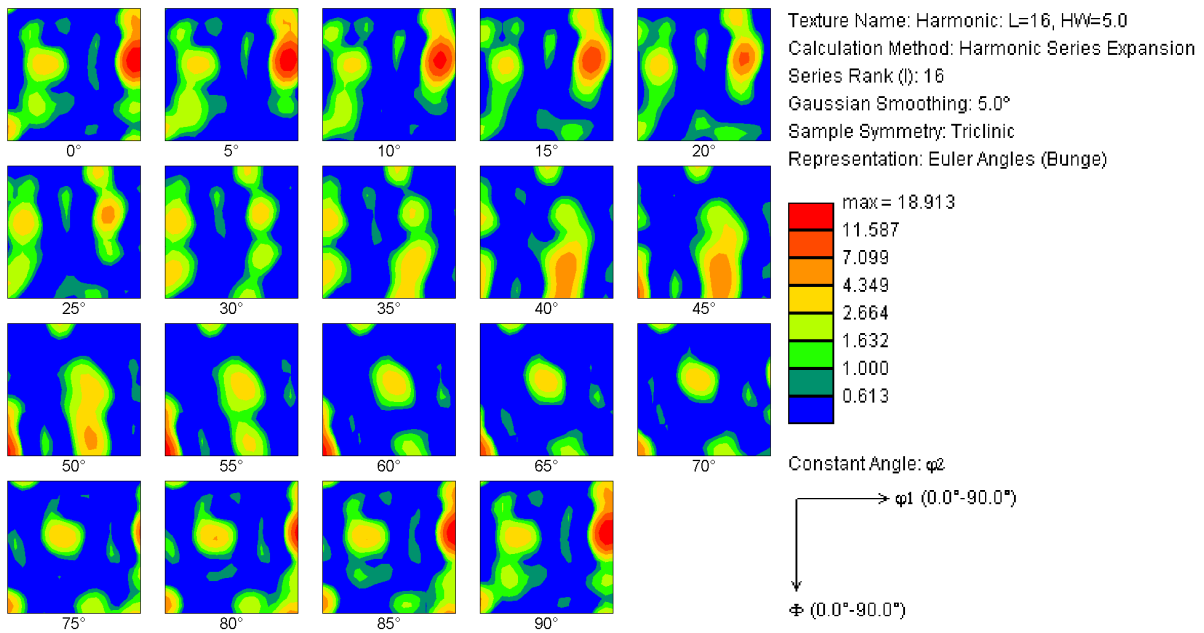
Figure 71: ODF for alloy Al2NFeSi rolled.

Al2NFe2Si, rolled:

Figure 72 and 73 show a TD rotated cube texture for rolled Al2NFe2Si.
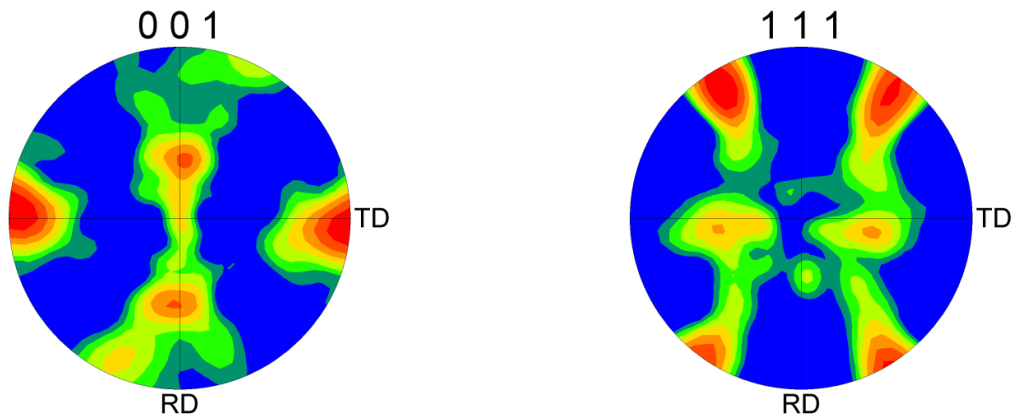
Figure 72: 001 and 111 pole figures for Al2NFe2Si rolled.
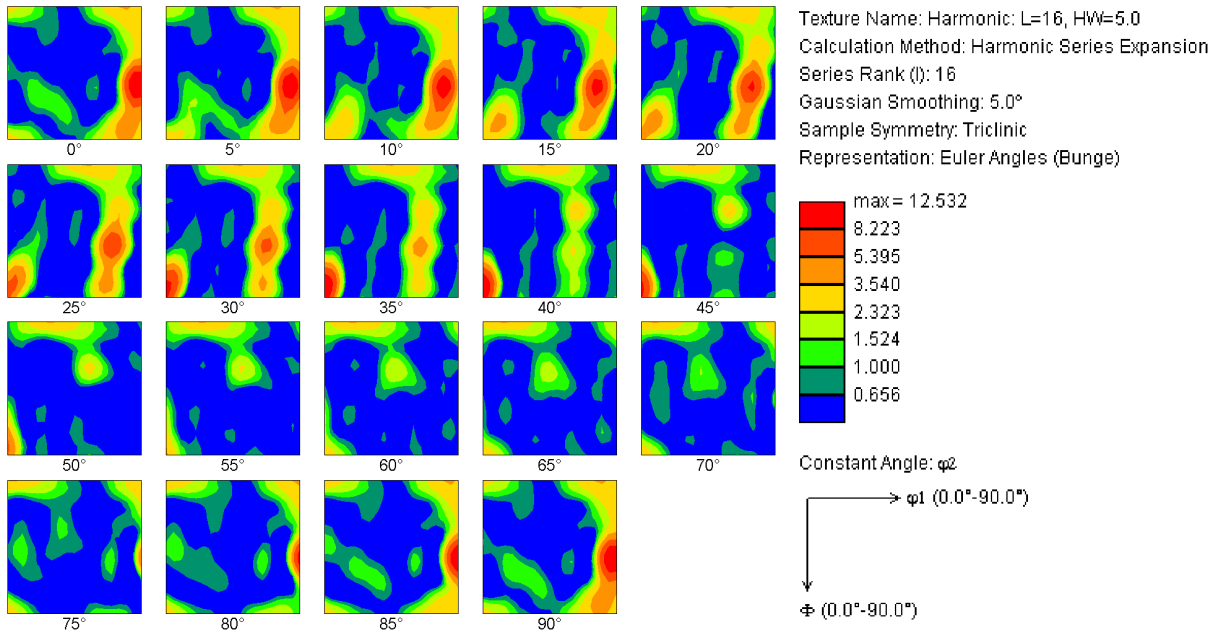
Figure 73: ODF for alloy Al2NFe2Si rolled.

5.3.3. Particles found in rolled alloys

By using the ESD technique in the SEM the characteristic radiation from the elements are depicted as peaks and the software calculates the atomic and weight % of the elements involved. The rolled material was studied. Rolled Al5N, however, was not studied because of the ultra high purity; it should not contain any particles. In the same way as for the optical microscope pictures the direction of deformation is parallel to the length (horizontal vector) of the pictures.

Figure 74 shows a part of the surface of rolled **Al5NFeSi** studied in SEM. Grains are visible and numerous particles are visible by their light/white colour. Some holes are visible likely due to oxygen bubbles during electro polishing. The average distance between particles seems to be quite large.
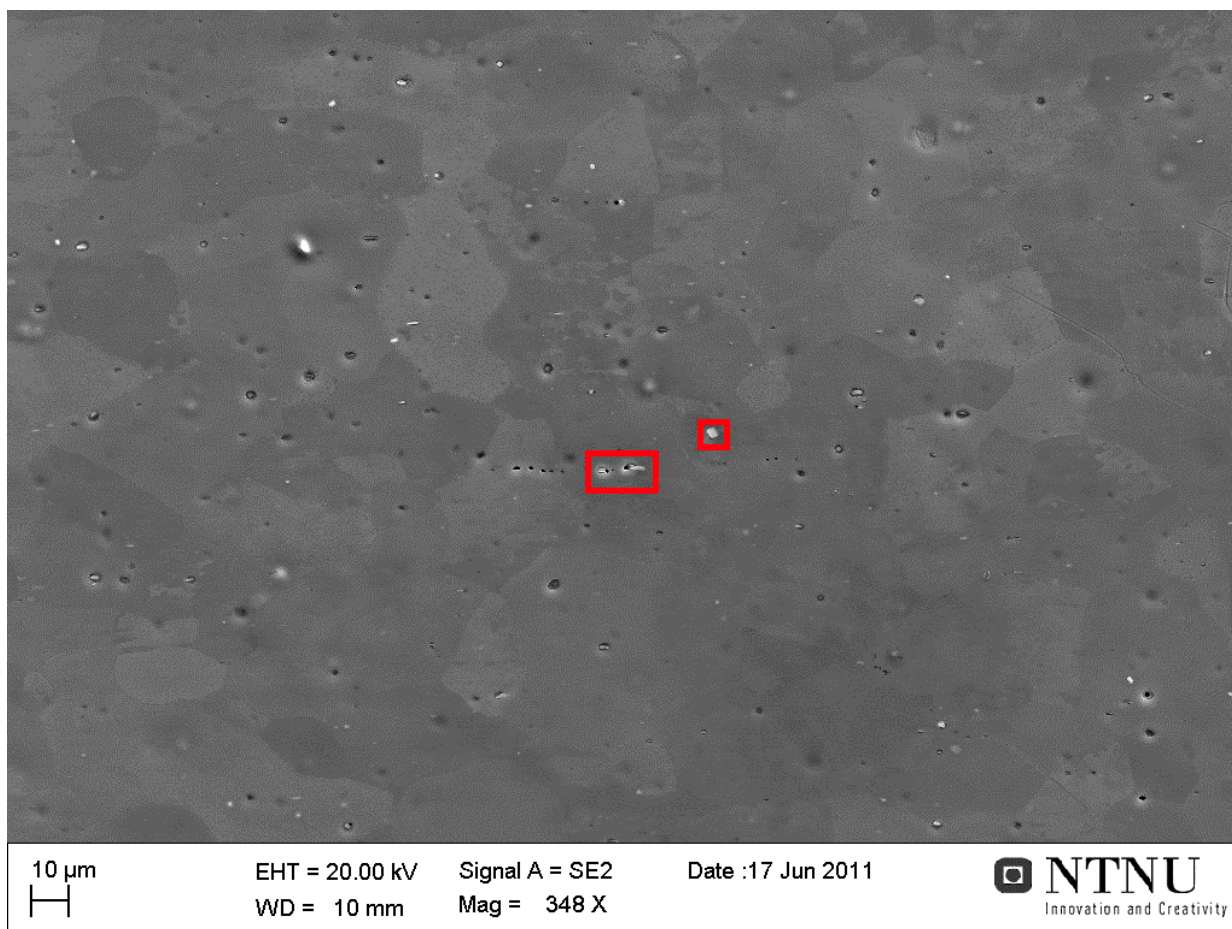
Figure 74: Particles in Al5NFeSi. 3 studied particles are marked by two red squares.

In figure 75 a rather big particle is visible. The particle is mainly submerged with a big ditch surrounding an area not covered by the surface. The size of the square-like particle is roughly 2x3µm. The gray circular zone is due to the elevated temperature which arises by large magnifications. In figure 74 the particle is vaguely visible in the right red square.
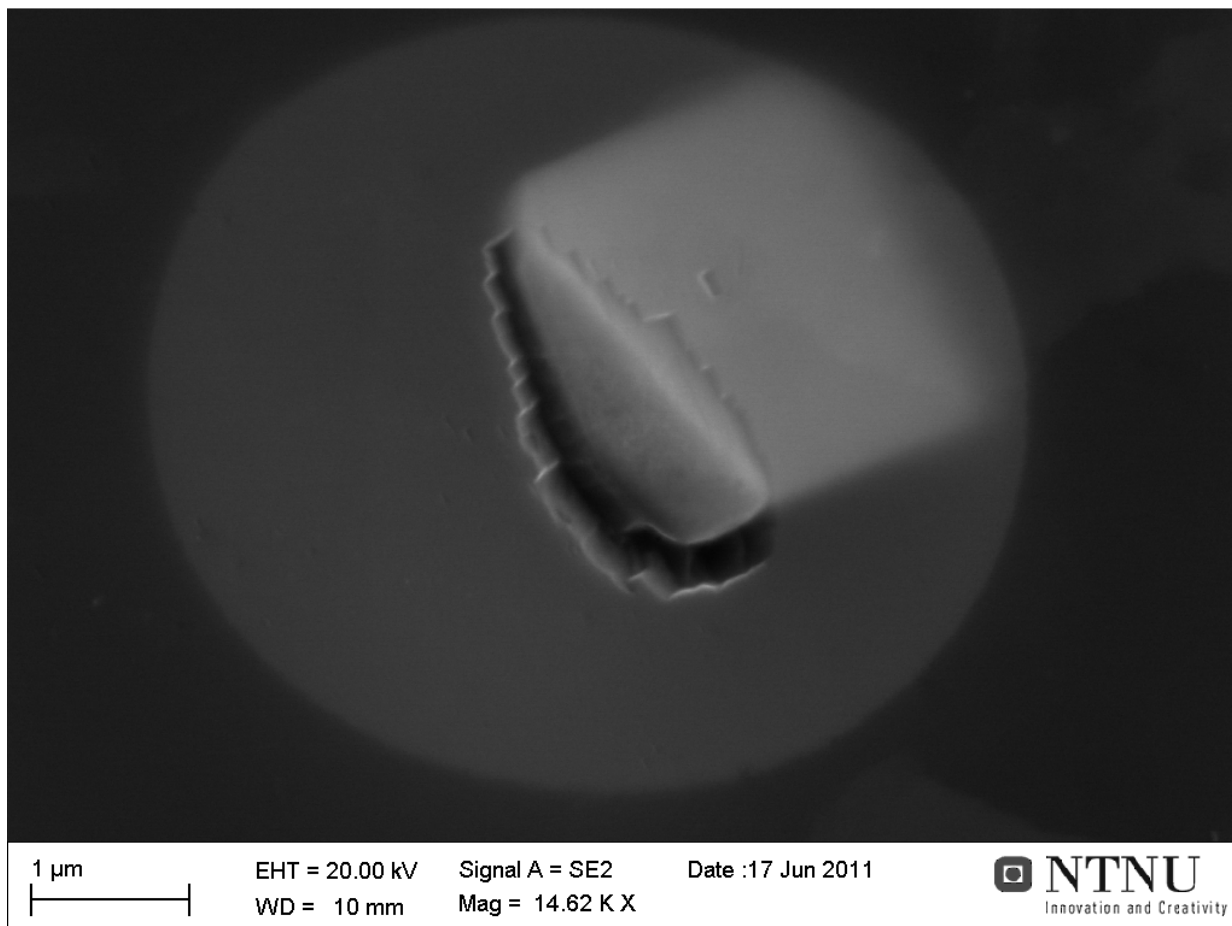
Figure 75: Partly submerged particle in alloy Al5NFeSi.

By EDS software calculations the particle should contain the relative amounts of elements given in table 9.

Table 9: Al5NFeSi-particle: element quantification given by EDS software in SEM.

Element	wt %	at %
Al	92.34	94.76
Si	2.94	2.90
Fe	4.72	2.34

Two different particles were found in the vicinity of the previous particle, these can be seen in figure 76 below and inside the left red square in figure 74. The particles lie partly logged in the material with a surrounding ditch and a free surface. In addition large holes have formed between the two particles. The lengths of the particles are difficult to decide based on the picture, but the areas not covered by the matrix are roughly 2 µm and 4 µm long.

| 1 µm | EHT = 20.00 kV | Signal A = SE2 | Date :17 Jun 2011 | NTNU |
| | WD = 10 mm | Mag = 7.69 K X | | Innovation and Creativity |
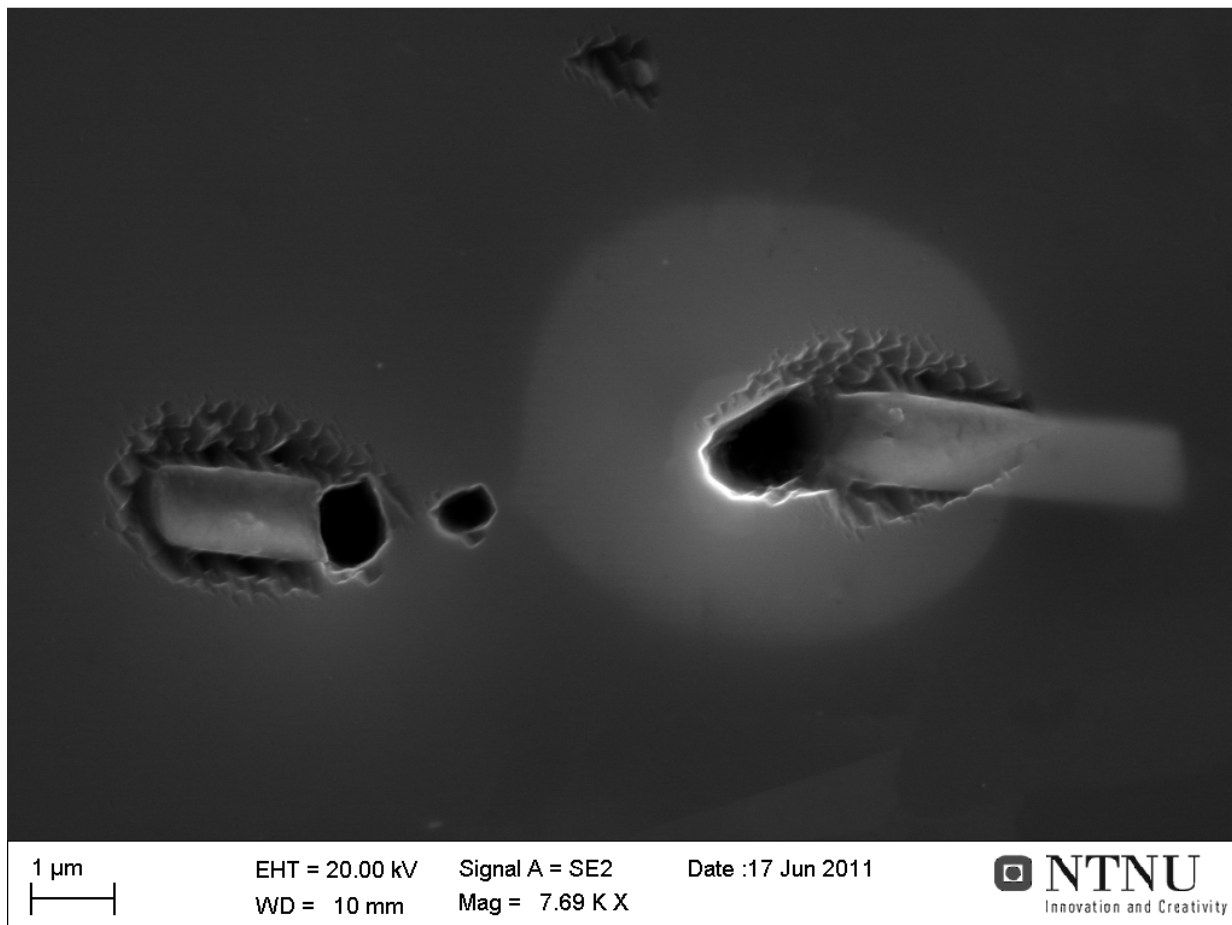
Figure 76: Two large particles found in alloy Al5NFeSi.

By EDS calculations the quantities of elements found in the two particles above are given in table 10.

Table 10: Al5NFeSi-particles: element quantification given by EDS software in SEM.

Particle	Element	wt %	at %
P_{left}	Al	92.89	94.48
	Si	4.17	4.07
	Fe	2.94	1.44
P_{right}	Al	94.17	95.47
	Si	3.45	3.36
	Fe	2.38	1.16

Figure 77 shows an overview of the particles found in alloy **Al2NFeSi**. The average particle spacing is still large, although the particle density seems to have increased ever so slightly compared to alloy Al5NFeSi. The particles are easily distinguishable by their white "shining" colour and a characteristic surrounding ditch. The red square area indicates the location of two particles which were studied by EDS.
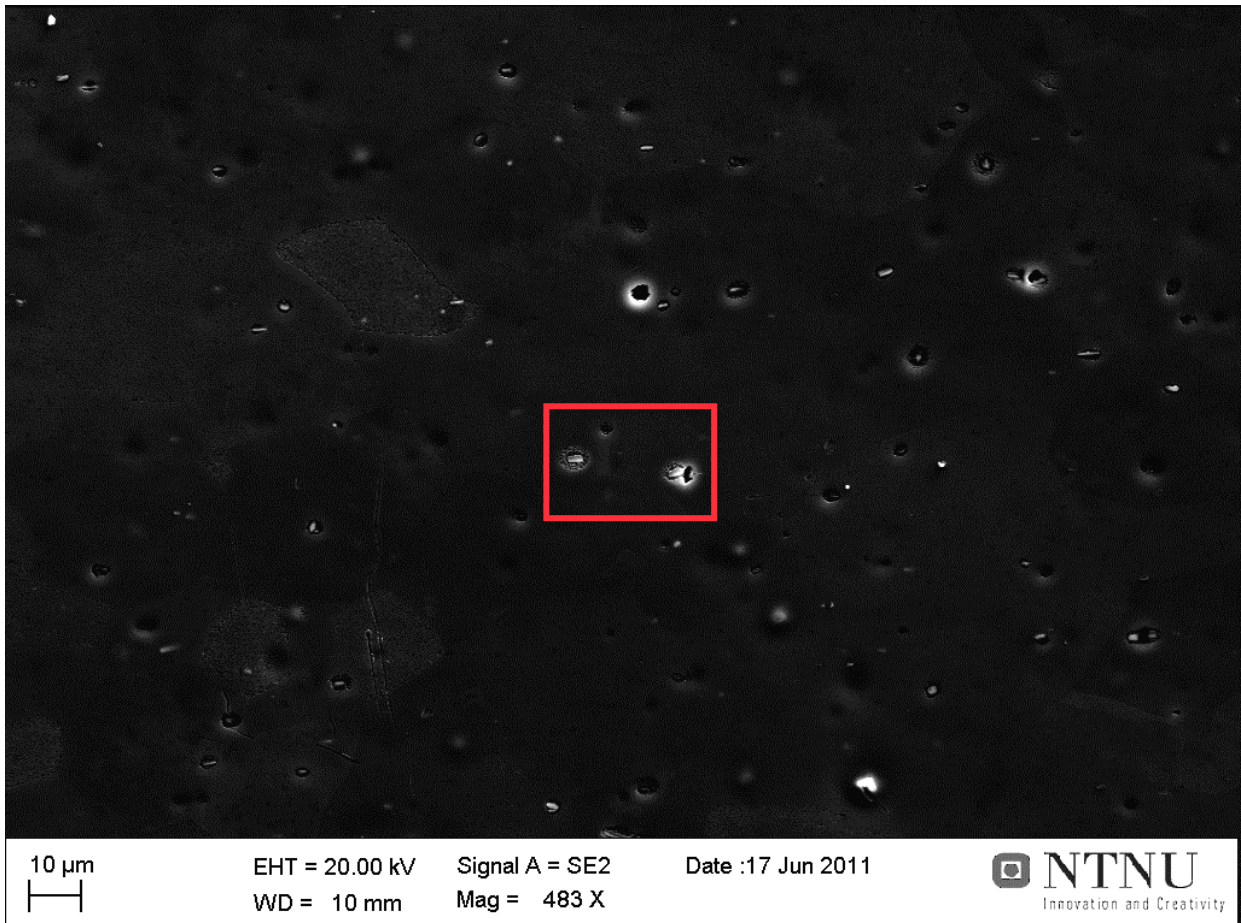
Figure 77: Particles in alloy Al2NFeSi. The particles are distinguishable by their white colour and usually a surrounding ditch.

Figure 78 shows two large particles and one smaller particle. The two biggest appear to be about 3 µm long and the smallest about 1 µm. The particles are also visible inside the red square area of figure 77.
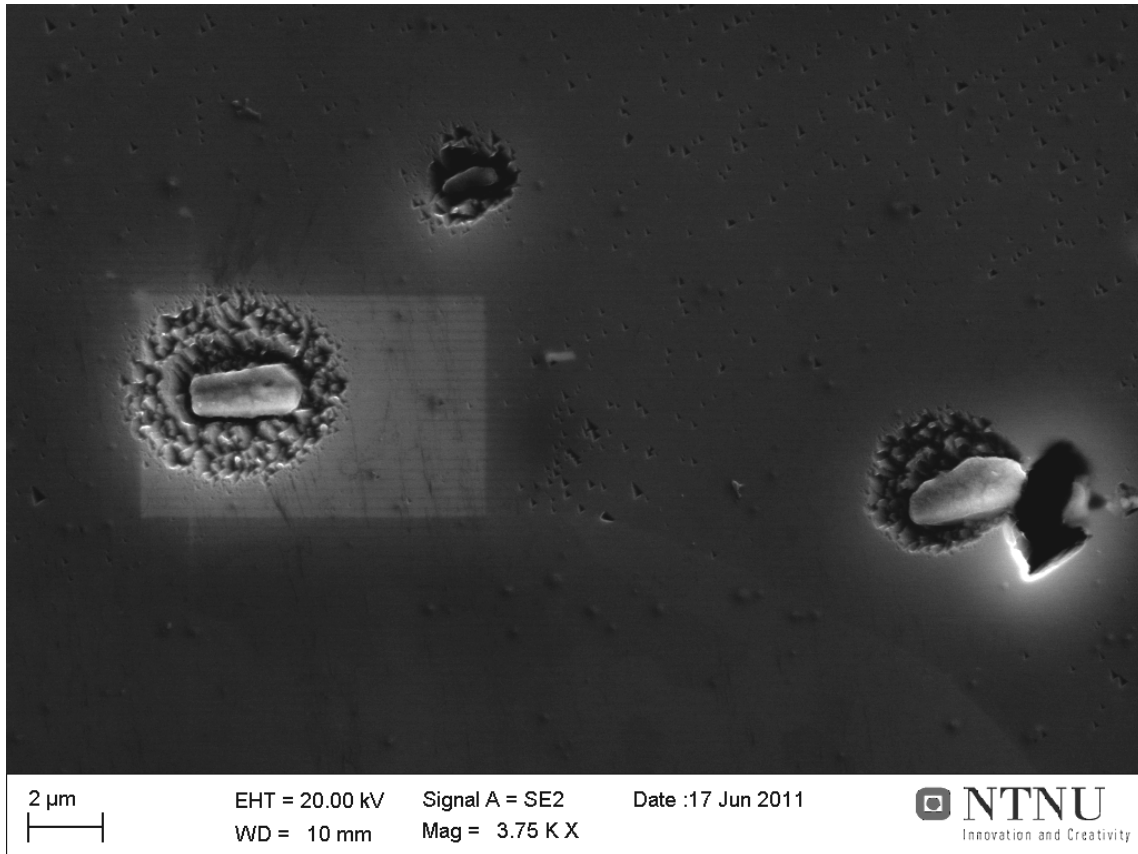
Figure 78: 3 visible particles found in alloy Al2NFeSi. The two biggest particles were examined by EDS.

Table 11 shows the values for relative amount of elements found in the two particles.

Table 11: Al2NFeSi-particles: element quantification given by EDS software in SEM.

Particle	Element	wt %	at %
P$_{left}$	Al	93.04	94.62
	Si	4.04	3.94
	Fe	2.93	1.44
P$_{right}$	Al	86.87	89.04
	Si	9.11	8.97
	Fe	4.02	1.99

In figure 79 three different "particles" in alloy Al2NFeSi are shown. The biggest two were discarded as dirt or contaminations. The white "particle" on the left had an iron content of about 40wt% and the black "particle" yielded a silicon content of 60wt% and is may likely be traced to the diamond spray used for polishing.

Figure 79: Small particle found in alloy Al2NFeSi, located in the lower part of the image slightly left of the centre.

The smaller particle located slightly to the left of the vertical middle was subjected to investigation and the quantities of elements are given in table 12. The particle is recognisable by the large surrounding ditch. The length of the particle is roughly 2 µm.

Table 12: Al2NFeSi-particle: element quantification given by EDS software in SEM.

Element	wt %	at %
Al	83.86	87.13
Si	9.61	9.59
Fe	6.53	3.28

In figure 80 the particle located in the centre of the image is visible by a part pointing out of the surface. The rest of the particle is submerged in the Al2NFe2Si material. To the right a particle which is completely submerged is vaguely visible. The "free" part of the centre particle was investigated by EDS.

1 µm	EHT = 20.00 kV	Signal A = SE2	Date :17 Jun 2011	⊙ NTNU
	WD = 10 mm	Mag = 12.11 K X		Innovation and Creativity
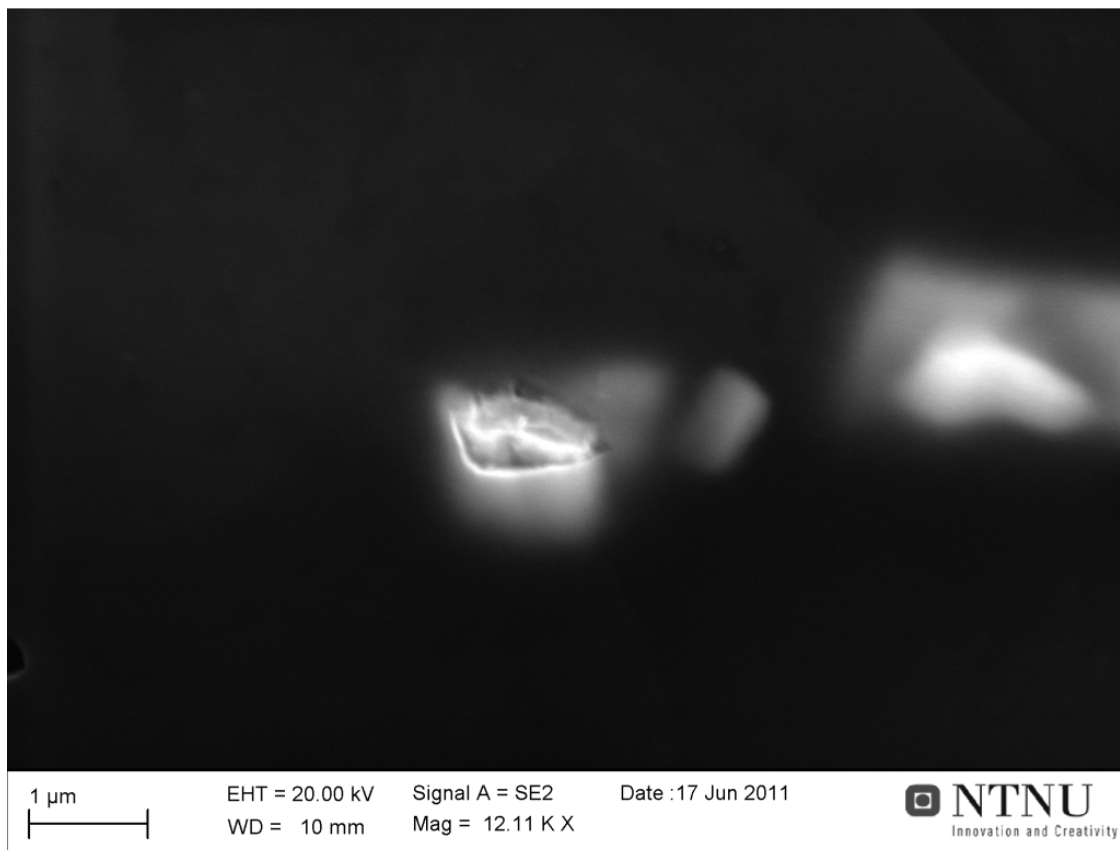
Figure 80: Submerged particles found in alloy Al2NFe2Si. The particle to the right is completely submerged while a small part of the left particle is elevated from the surface.

In table 13 below the relative amounts of elements found in the centre particle are given.

Table 13: Al2NFe2Si-particle: element quantification given by EDS software in SEM.

Element	wt %	at %
Al	87.53	91.10
Si	5.30	5.30
Fe	7.17	3.61

The final particle which was investigated is shown in figure 81. It is surrounded by a big ditch and recognisable by several cracks in the surface. The surface area visible in the figure measures roughly 3x1.5µm. The grain is located close to a grain boundary.
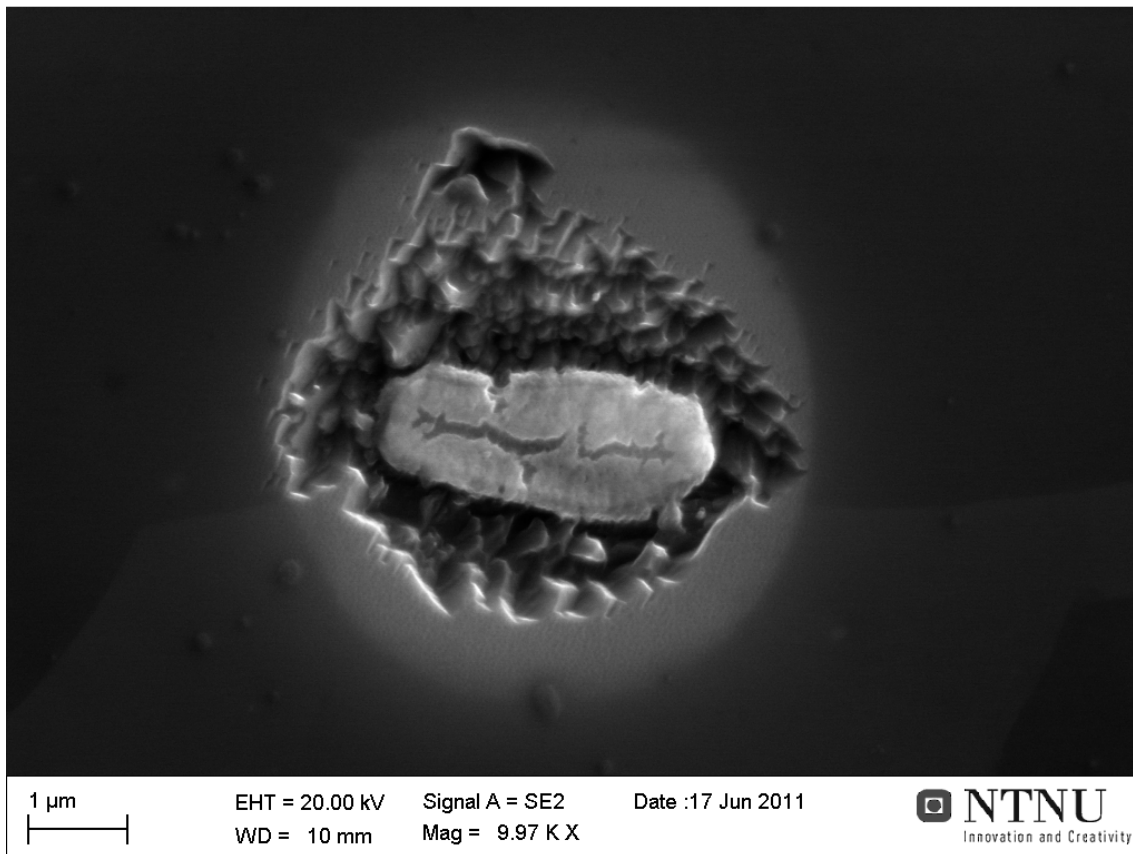
Figure 81: Large particle found in Al2NFe2Si at ~ 10000 X magnifications.

In table 14 the relative amounts of elements in the particle are shown.

Table 14: Al2NFe2Si-particle: element quantification given by EDS software in SEM.

Element	wt %	at %
Al	93.96	96.04
Si	1.99	1.96
Fe	4.05	2.00

Table 15 summarises the Fe/Si-ratio values for all particles found in the rolled alloys. This ratio was used to discuss what kind of particles they were and this is covered in chapter 6.4.

Table 15: Fe/Si-ratio for particles found in alloys Al5NFeSi-Al2NFe2Si. The particles are given in chronological order as the important aspect is to decide which kind of particles are present.

Particle found in	Fe/Si-ratio wt %	Fe/Si-ratio at %
Al5NFeSi	1.6	0.8
Al5NFeSi	0.71	0.35
Al5NFeSi	0.69	0.35
Al2NFeSi	0.73	0.36
Al2NFeSi	0.44	0.22
Al2NFeSi	0.68	0.34
Al2NFe2Si	1.35	0.68
Al2NFe2Si	2.04	1.02

Strengthening contribution:

From SEM overview pictures a rough estimate of the average particle spacing was carried out. The stress contribution due to non-shearing particles was then calculated for rolled Al5NFeSi-Al2NFe2Si by applying the formula[11]:

$$\tau_p = \frac{Gb}{\lambda} \qquad (23)$$

By including the Taylor, from $\sigma = M\tau$ *(24)*, factor we get the corresponding stress equation:

$$\sigma_p = \frac{GbM}{\lambda} \qquad (25)$$

Where M is the Taylor factor ($M_{Al} \approx 3$), G is the shear modulus ($G_{Al} \approx 25$ GPa), b is the Burgers vector ($b_{Al} \approx 2.86 \times 10^{-10}$ m) and λ is the particle spacing (µm). Table 16 shows the particle strengthening contributions for the 3 alloys were particles were found.

Table 16: Particle spacing and strength contribution due to hard non-shearing particles

Alloy	Average λ [µm]	σ_p [MPa]
Al5NFeSi	42	0.51
Al2NFeSi	25	0.85
Al2NFe2Si	4.1	5.27

5.4. Tensile testing: cast alloys

The cast tensile specimens proved to yield very different results. From microscopy results it was evident that the material was not homogenous and the microstructure varied over vast areas of the investigated samples. Due to the lack of correlation in tensile test results, these will only be treated briefly in this section as the results are poor. Figure 82 shows the tensile results for the 12 cast specimens, 3 of each alloy, at constant strain rate $10^{-3}s^{-1}$. Figure 83 shows the results at constant strain rate $10^{-2}s^{-1}$.
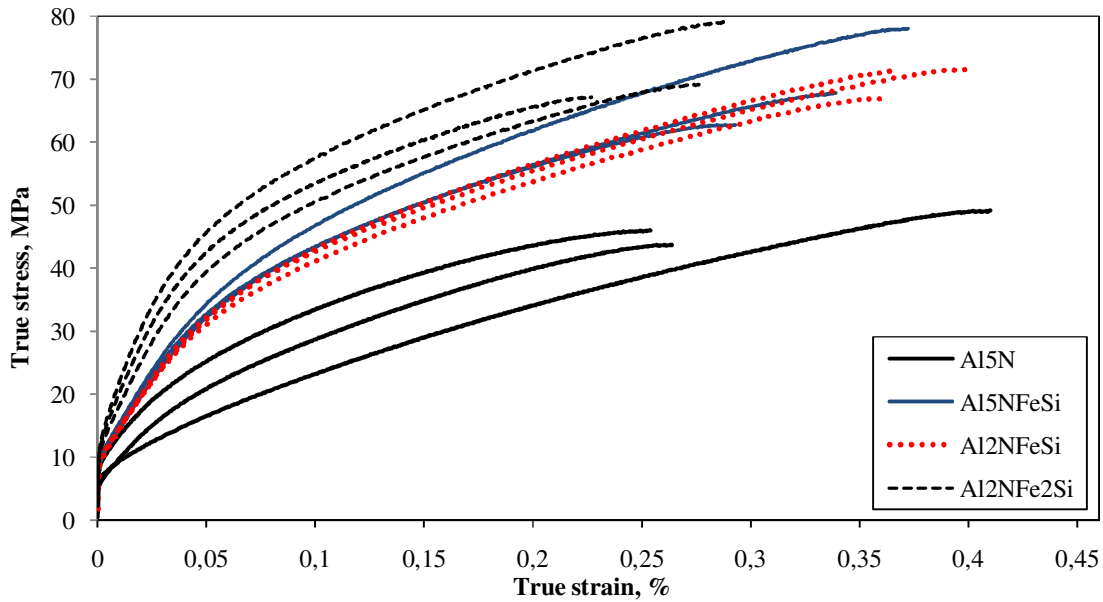
Figure 82: Cast aluminium flow curves at constant strain rate of $10^{-3}s^{-1}$.
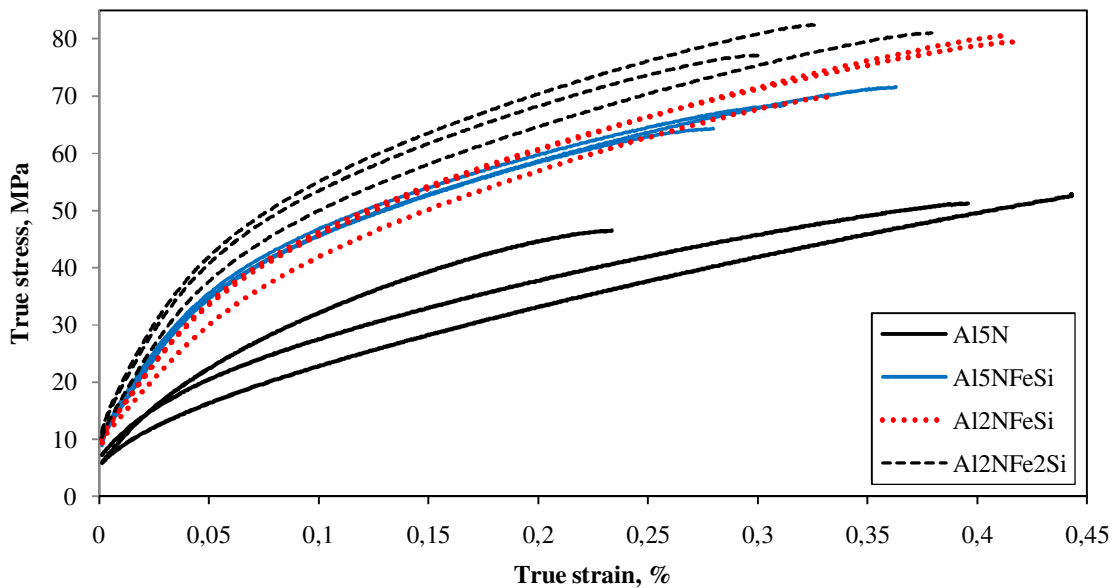
Figure 83: Cast aluminium flow curves at constant strain rate of $10^{-2}s^{-1}$.

Rather than a needle-like necking, which is characteristic for this type of material, the deformation seems to be planar.

Figures 84 and 85 show that while alloy Al5N deforms locally at several areas the other 3 alloys deform by plane necking at one initiation point/area. Also visible from the pictures is that the specimens appear to have undergone some twisting. Whether this motion is traceable to the material or the tensile machine leaves room for speculation. Alloy Al5N shows a planar like deformation rather than the more common needle like necking. The elongation of the specimens seems to vary greatly. This is most evident for alloy Al5N as seen in the pictures below.

Figure 84: Al5N (left) and Al5NFeSi (right) specimens after tensile tests.

Figure 85: Al2NFeSi (left) and Al2NFe2Si (right) specimens after tensile tests.

Table 17 is considered largely misleading as the average values given are based on 3 specimens per alloy which varied extensively. The table serves more as a very rough estimation of the mechanical properties found through tensile tests.

Table 17: Mechanical properties of cast alloys based on tensile testing. Note that these values are averages based on, in most cases, very different results. The data given in the table are more a rough estimate.

Alloy	R_{p02}	UTS	Uniform elongation
Al5N	7.7	46.3	0.31
Al5NFeSi	10.3	69.5	0.33
Al2NFeSi	10.1	70.0	0.38
Al2NFe2Si	12.8	71.8	0.26

5.5. Tensile testing: rolled and recrystallised aluminium

The tensile test results from the "slow" speed setting, i.e. constant strain rate at $10^{-3}s^{-1}$, are studied in detail. These results are the most valid since materials are sensitive to the strain rate and might deviate from ideal behaviour with elevated speeds. Starting with the ultra pure alloy, 2 and 2 alloys are paired together in diagrams to show the change by increased iron and silicon content and/or trace elements. Figure 58 below shows the flow curves for alloys Al5N and Al5NFeSi.
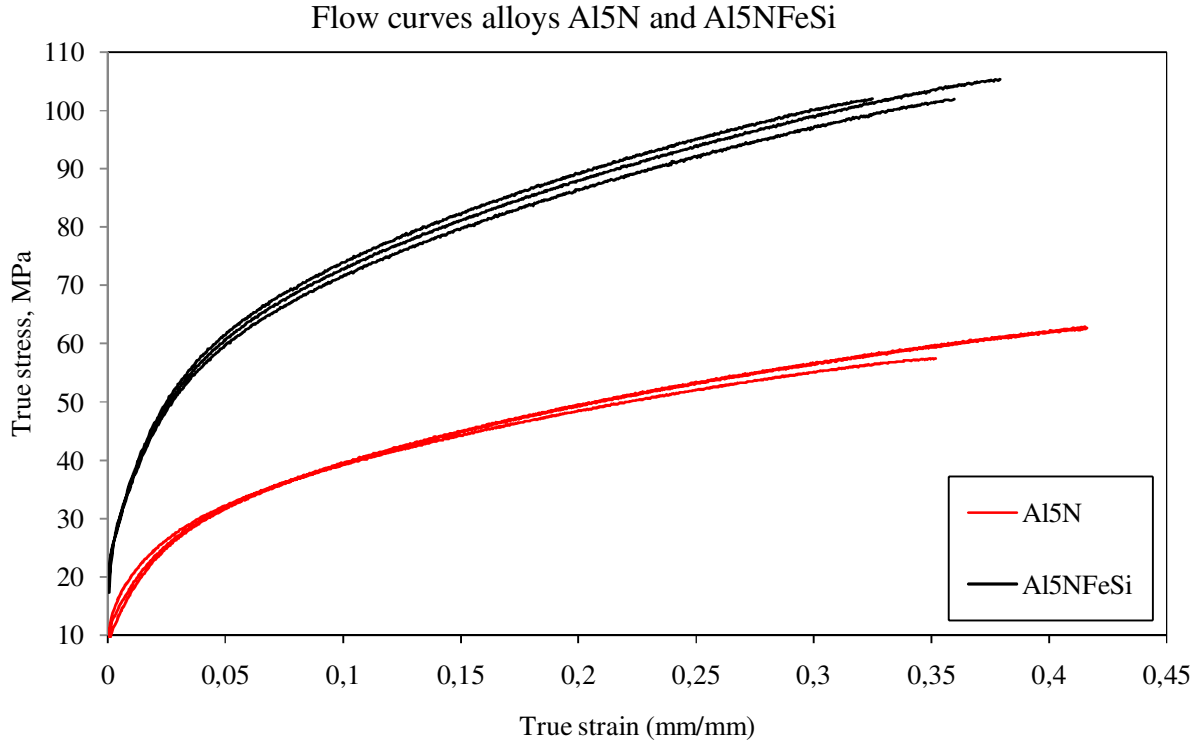
Figure 86: Flow curves for alloys Al5N and Al5NFeSi at constant strain rate of $10^{-3}s^{-1}$.

Alloy Al5N, which is the purest alloy free of trace elements, showed a relatively low work hardening rate and yielded YS around 10.8-13.8 MPa and UTS between 57.4-62.9 MPa. Tensile testing showed good consistency in the results regarding work hardening rate and elastic behaviour. However, the uniform elongation varied from 35% to 42%, roughly. The good consistency is evident in the 2 upper curves for alloy Al5N which almost completely overlap in the plastic region.

Once iron and silicon were introduced there was a dramatic increase in both work hardening rate and subsequently increased strength. Alloy Al5NFeSi, which contains 0.66 wt % Fe and 0.68 wt % Si, displayed YS of about 25.4-25.7 MPa while the UTS was estimated to be in the region 101.9-105.3 MPa. As for the purest alloy the uniform elongation varied, from about 33 % to 38 %. The work hardening rate in the plastic region was not consistent for the three tested specimens, but the miscorrelation was still small (4.6 MPa). However, alloy Al5NFeSi showed improved correlation in results in the elastic region compared to alloy Al5N.

As seen in figure 87 alloys Al5NFeSi and Al2NFeSi show distinctly similar tensile properties. This result was expected as the findings in the project work[5] carried out on extruded plate profiles during autumn 2010 indicated that these 2 alloys had similar tensile properties. However, the results were inconclusive because of large variations in results and several possible outcomes. The results from the rolled and recrystallised alloys show a much more satisfactory correlation and subsequently one can more safely conclude that the alloys are quite similar. Alloy Al2NFeSi was found to have a YS of 25.7-26.0 MPa and UTS between 101.5-104.2 MPa while the uniform elongation varied from 0.33-0.38 %. The elongation properties were quite close to those of alloy Al5NFeSi.
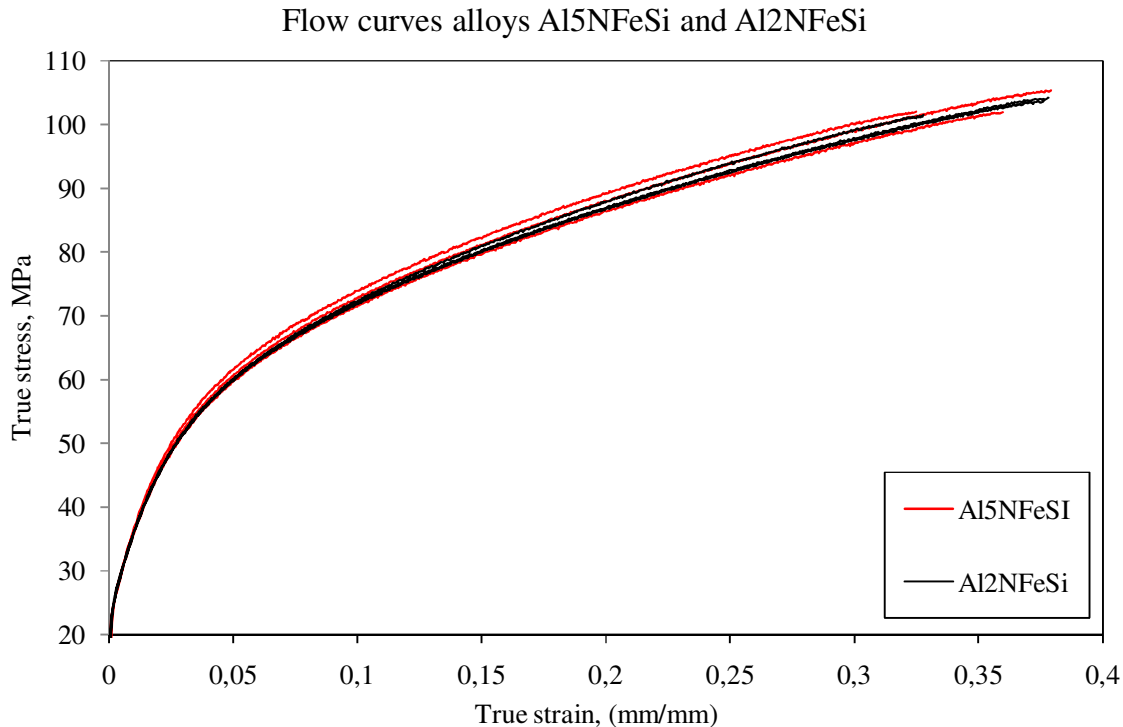
Figure 87: Flow curves for alloys Al5NFeSi and Al2NFeSi at constant strain rate of $10^{-3}s^{-1}$.

The final alloy comparison, seen in figure 88, between the two commercially pure alloys, Al2NFeSi and Al2NFe2Si, showed slightly improved strength properties for alloy Al2NFe2Si. The alloy displayed YS between 24.2-25.2 MPa and the UTS varied in the region 99.8-108.2 MPa. The uniform elongation was found to be in the area 29-39 %.
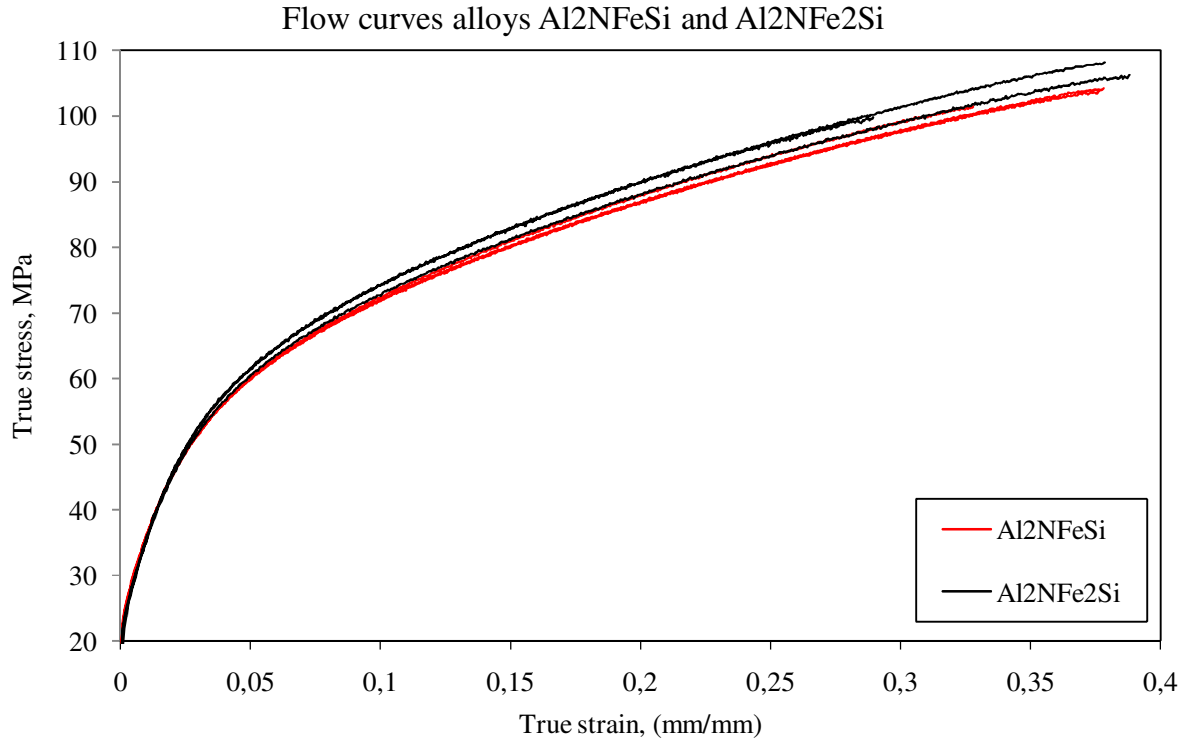
Figure 88: Flow curves for alloys Al2NFeSi and Al2NFe2Si at constant strain rate of $10^{-3}s^{-1}$.

Figure 89 includes the flow curves for all of the 4 rolled alloys tested at a constant strain rate of $10^{-2}s^{-1}$. The results show slightly elevated values for the YS and UTS, however the trends from the tests carried out at a lower strain rate are the same. As for the slow tests, the results are showing good correlation.

Flow curves cast alloys, const. strain rate at $10^{-2}s^{-1}$
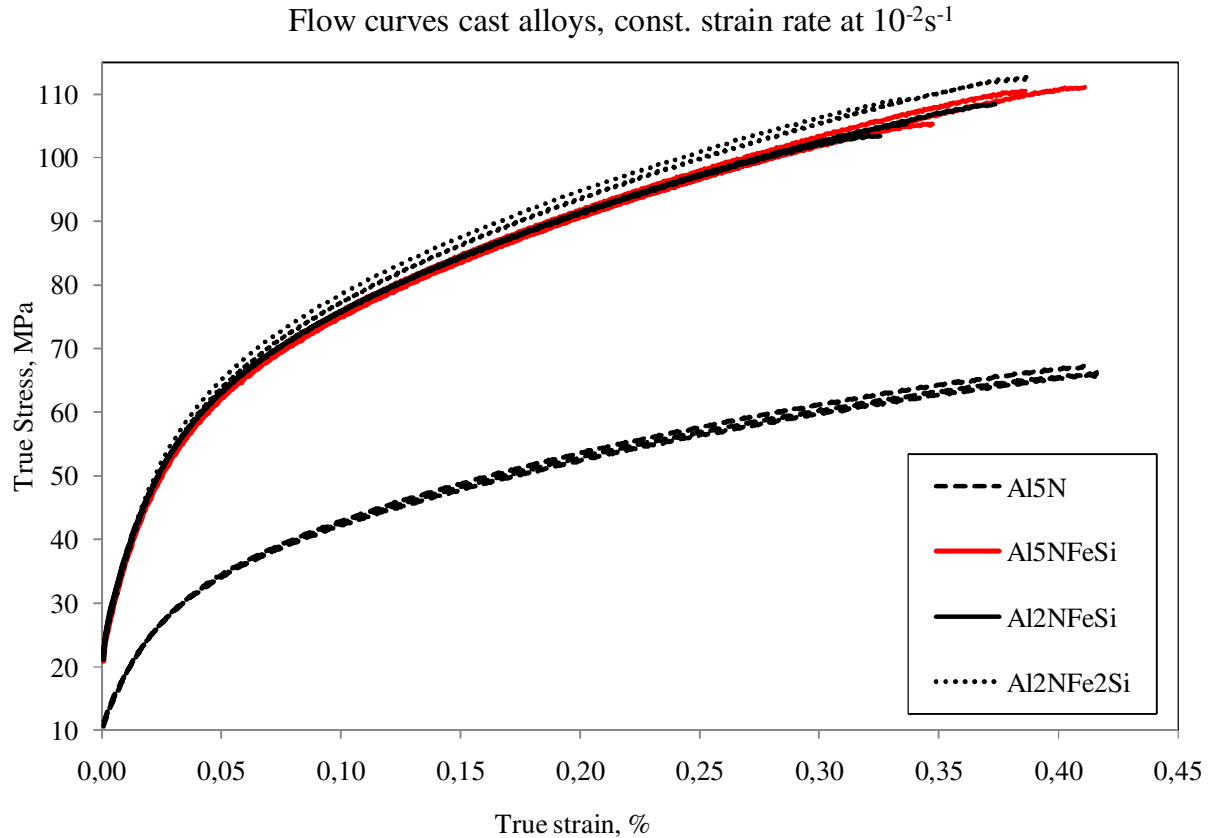
Figure 89: Flow curves for alloys Al5N-Al2NFe2Si at constant strain rate of $10^{-2}s^{-1}$.

The average values for the measured mechanical properties are given in table 18. The average approach is satisfactory as the results from 3 tested specimens per alloy show little relative deviation, i.e. the curves have a good fit and represent the alloys flow curves in a good way.

Table 18: Average mechanical properties gathered from tensile tests of rolled aluminium

Alloy	R_{p02}	UTS	Uniform elongation
Al5N	12.4	61.0	0.39
Al5NFeSi	25.6	103.1	0.35
Al2NFeSi	25.8	103.1	0.36
Al2NFe2Si	24.7	104.8	0.35

5.6. Tensile testing: the Haasen Plot for rolled material

Before the results from the alternating strain rate test and the Haasen plot are presented some attention to the data collection and processing will be outlined.

Each shift in strain rate was examined and the under-overshoot, which proved unavoidable, was corrected by means of extrapolating the curves. The curve regions which were subjected to extrapolating were located just before the shift and just after. By applying a vertical tangent between the upper and lower extrapolations the σ-values for the intersections could easily be determined by reading the values on the ordinate axis (as shown in figure 90).
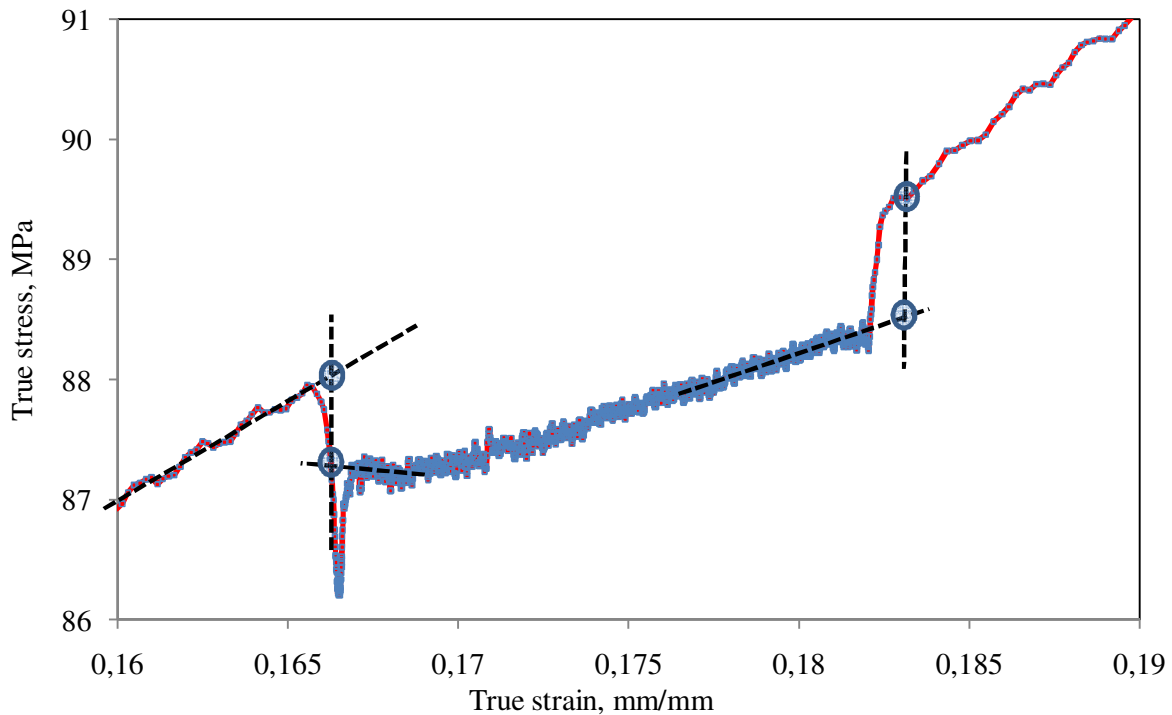
Figure 90: Data processing: extrapolation of true stress-true strain curves. Black curves are extrapolations of the curve while the blue circles indicate the intersections where the true stress values were read.

To establish the exact strain rate in each shift of the alternating strain rate test the strain rate was plotted as a function of true strain. This is visible in figure 91. The red circles and the corresponding values show were the data was measured. The figure shows two transitions or shifts, a downward and an upward shift, respectively.
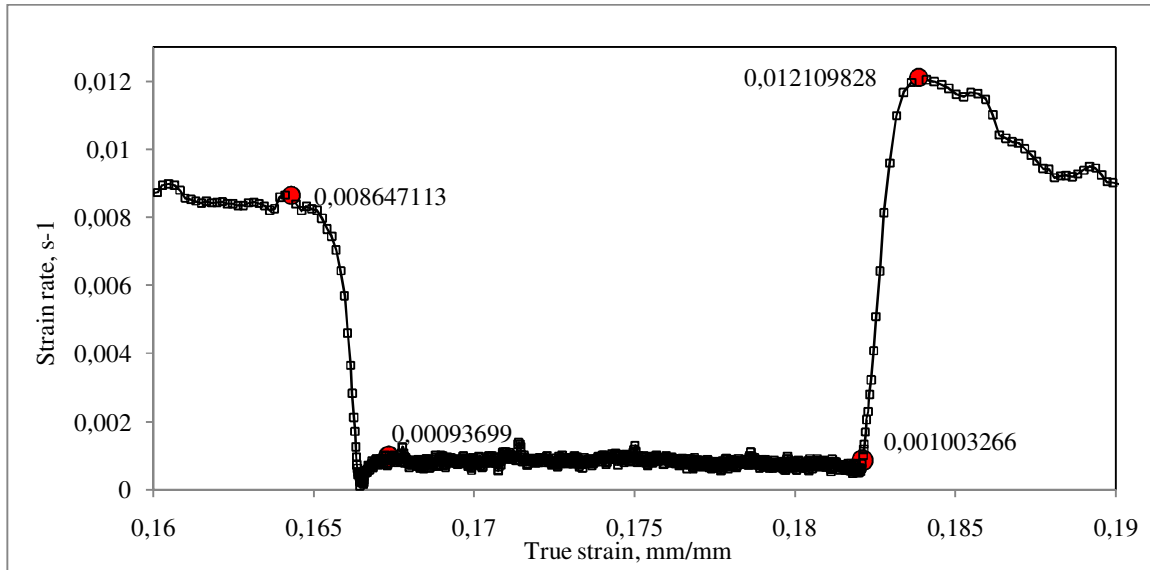
Figure 91: Data processing: Strain rate as a function of true strain.

Figure 92 shows a different "Haasen"-experiment and the corresponding stress-strain curves. The enlarged figures show how the delta sigma value was collected. The method is very similar to the one used in this work. However, the short intervals may not describe the full picture. The transient during a shift is better described by equal and longer intervals to gather the response of the material during the abrupt changes in strain rate.
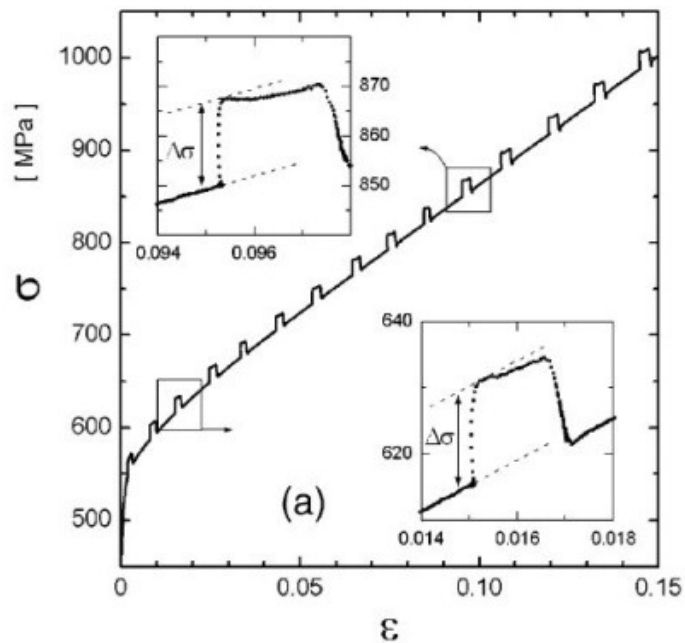
Figure 92: Data collection approach for a tensile test with short jumps rather than equal intervals[19].

Figure 93-96 shows the Haasen plot for the 4 rolled alloys as points representing upward and downward shifts by triangles calculated from $\Delta\sigma/\Delta ln\dot{\varepsilon}$. The red triangles indicate a shift upward, while the black triangles represent a downward shift. The plots are all based on 3 tensile tests per alloy to secure satisfying results. The linear line, usually used to represent an alloy, in the Haasen plot is based on all these points.
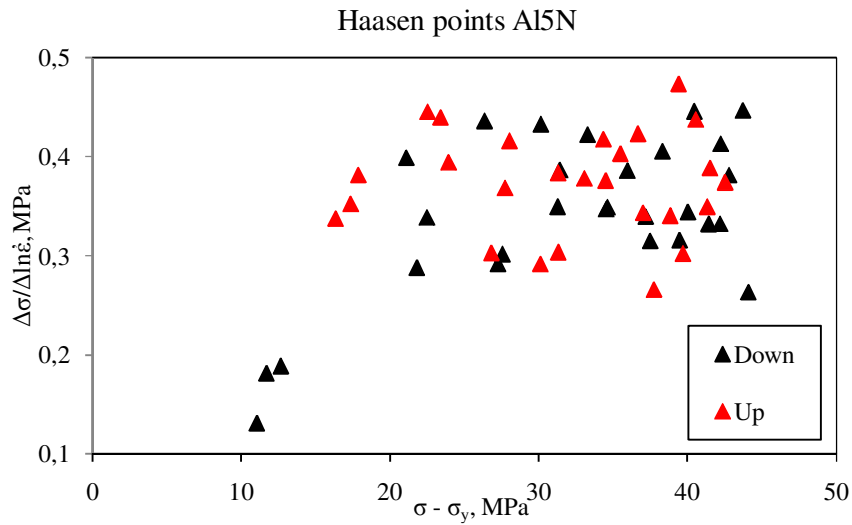
Figure 93: Haasen plot for 3 tensile specimens of Al5N. The black triangles represent a downward shift in strain rate and the red indicate an upward shift.
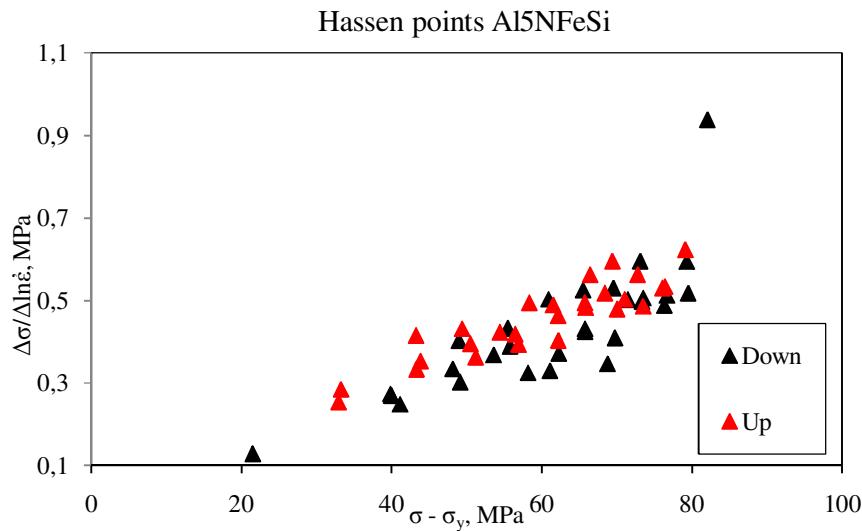
Figure 94: Haasen plot for 3 tensile specimens of Al5NFeSi. The black triangles represent a downward shift in strain rate and the red indicate an upward shift.
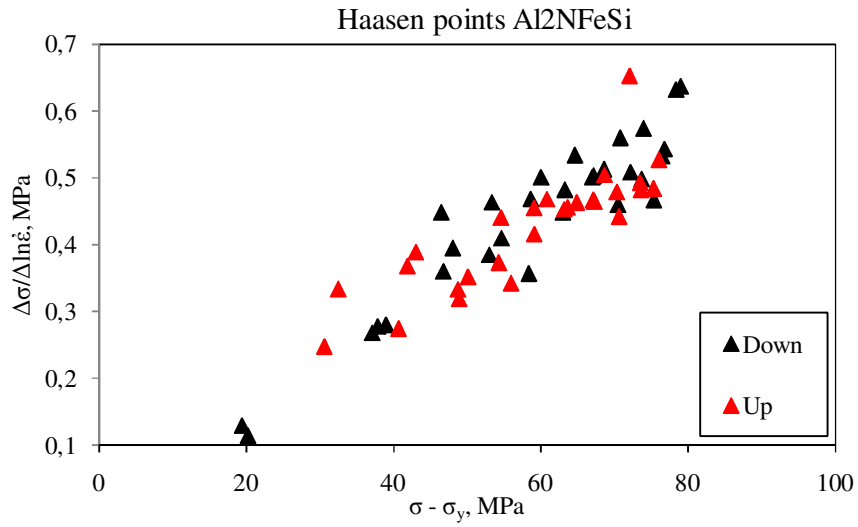
Figure 95: Haasen plot for 3 tensile specimens of Al2NFeSi. The black triangles represent a downward shift in strain rate and the red indicate an upward shift.
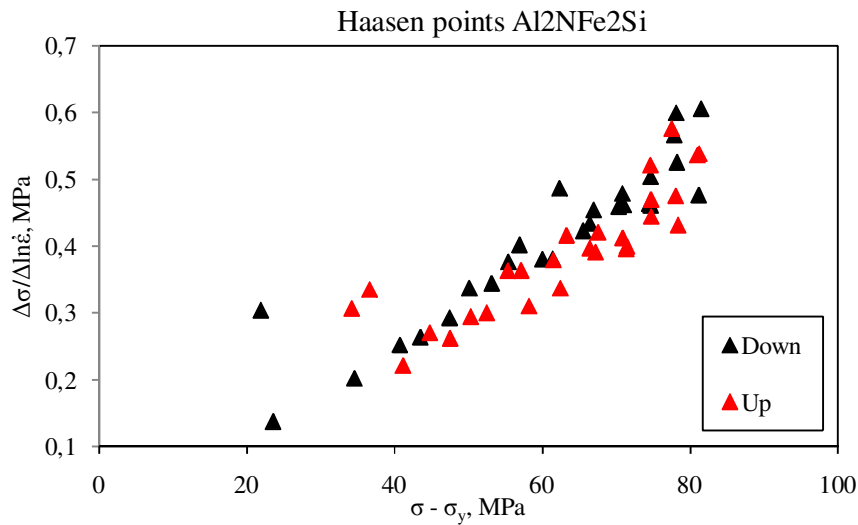
Figure 96: Haasen plot for 3 tensile specimens of Al2NFe2Si. The black triangles represent a downward shift in strain rate and the red indicate an upward shift.

Figure 97 shows the Haasen plot for the rolled alloys based on the points from figures 93-96. Alloys Al5NFeSi-Al2NFe2Si seem to display close to equal values both for the slope and the intersection with the ordinate axis. Alloy Al5N however, distinguishes itself from the others by its slope and ordinate axis intersection value. This alloy is of ultra pure quality and pure aluminium has been extensively[20] tested and the widely accepted behaviour is that of a line crossing in $\Delta\sigma/\Delta\ln\dot{\varepsilon} = 0$ with a low value for the slope. The slope of the linear line representing alloy Al5N is more similar to the mentioned findings for pure aluminium. The reason for the deviation will be discussed in chapter 6.6.
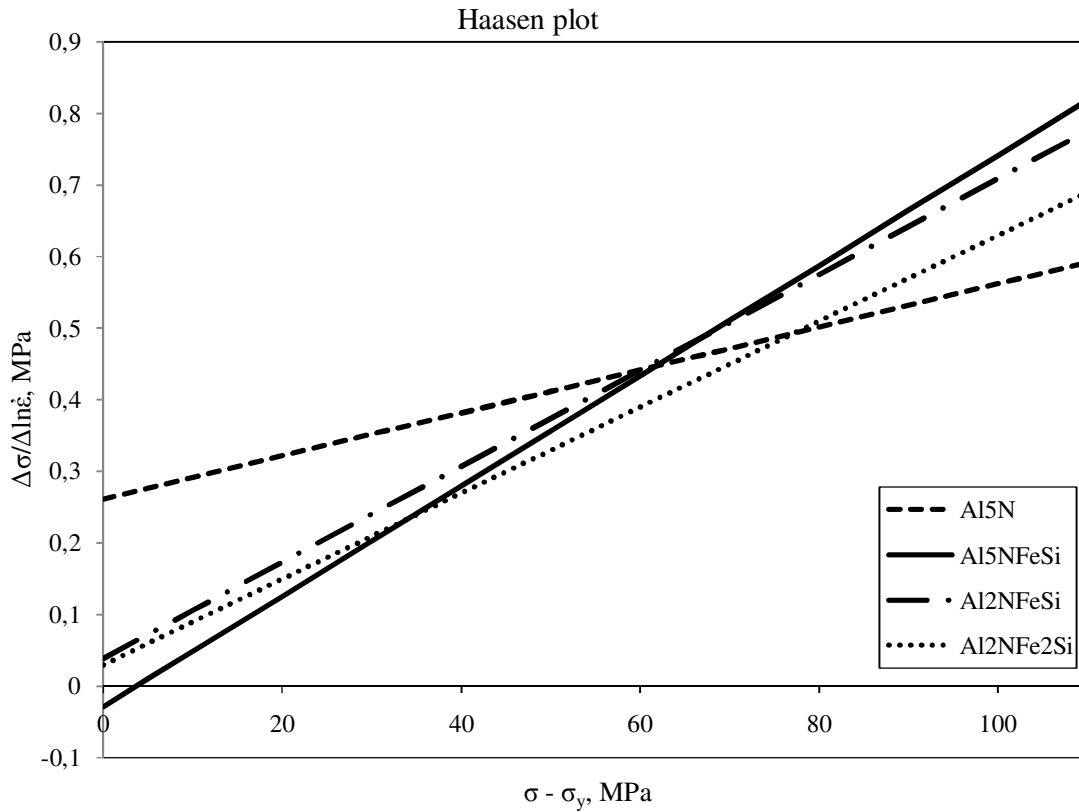
Figure 97: The Haasen plot for alloys Al5N-Al2NFe2Si.

Figure 98 shows the Haasen plot with a correction for alloy Al5N as the linear line for the alloy found in figure 97 puts too much weight into the three first points, the red line in the diagram gives a slightly improved description for alloy Al5N based on previous findings[20].
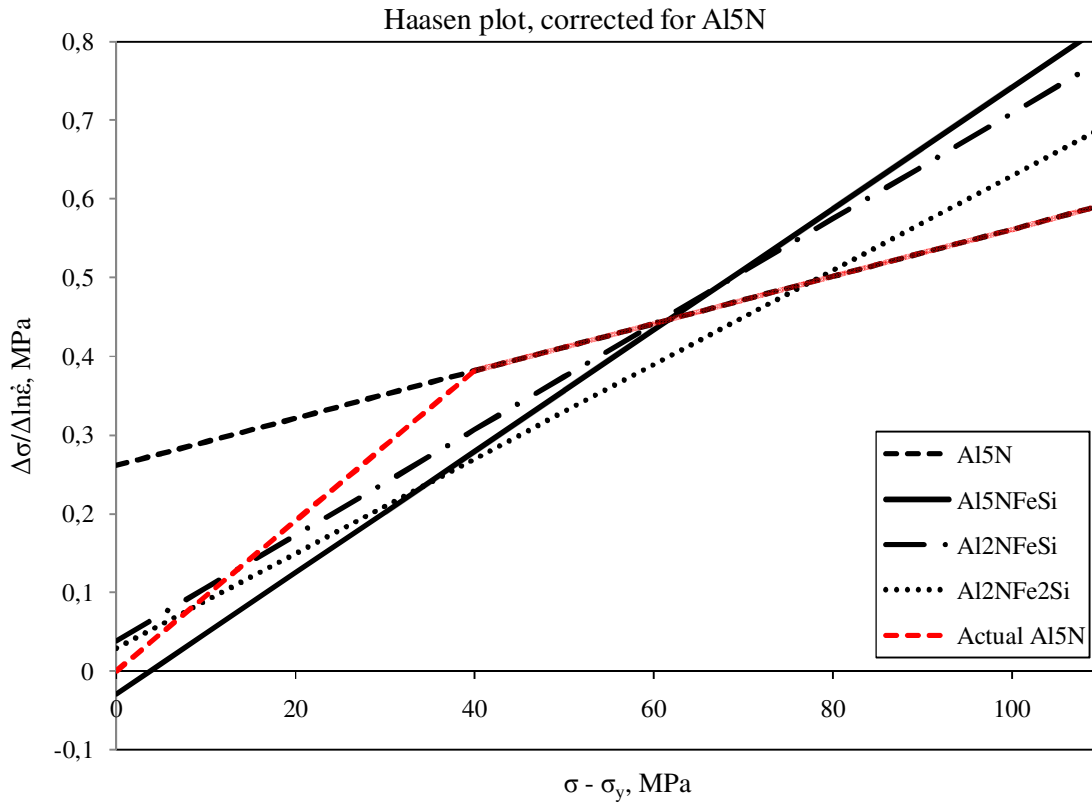
Figure 98: Haasen plot for alloys Al5N-Al2NFe2Si, corrected for Al5N.

Table 19 shows the values for the instantaneous strain rate sensitivity, B, the intersection with the ordinate axis, A, and the activation volume due to elements in solid solution, V_s.

Table 19: Instantaneous strain rate sensitivity, B, intersection with vertical axis, A, and activation volume, Vs, for rolled alloys Al5N-Al2NFe2Si. See formulae chapter 2.6. for B, A and V_s, equations (17, 21).

Alloy	B	A (MPa)	V_s (J)
Al5N (not corrected)	0.0030	0.2614	1.35E-18
Al5NFeSi	0.0077	- 0.0288	5.26E-19
Al2NFeSi	0.0067	0.0386	6.04E-19
Al2NFe2Si	0.0060	0.0293	6.75E-19

6. Discussion

In this chapter the results from chapter 5 are discussed. Firstly, in this section, a short description of the results from the project work[5] will be given. These results are included as they are highly comparable and useful to give a more detailed assessment regarding the effects of Fe and Si in aluminium.

6.1. Previous work: Extruded Alloys

The present work is a continuation of the report *"Study on the effect of Fe and Si content in Aluminium Alloys as a result of increased recycling - testing of high purity aluminium alloys in uniaxial tension"*[5]. The same alloys were used, in the form of the extruded flat profiles. It is therefore convenient to include some of the results here. 3 different tensile tests named "slow", "fast" and "alternating speed/Haasen" were run. These tests were carried out under the same conditions as the tensile tests in this work. The microstructure of the extruded flat profiles have already been covered in chapter 5.1.2.

6.1.1. Particles

To establish grain size and distribution, new samples were polished and studied in the optical microscope for this work and are given in chapter 5.1.2.

The figures 99-102 below show the amount of particles. The red circles indicate particles and the black circles indicate particles from the diamond spray used for polishing. The easiest way to distinguish between them is by studying the colour. The iron rich particles are light grey, while the diamond particles are black (and bigger). Diamond particles are of sizes equal to the diamond spray applied, i.e. 1, 3 and 6µm. Two such 6µm particles can be seen in the upper right corner in figure 102.

Al5N is free of particles and the visible black spots are particles from the diamond spray. As this alloy is in an ultra pure form this was a likely result (fig. 99).
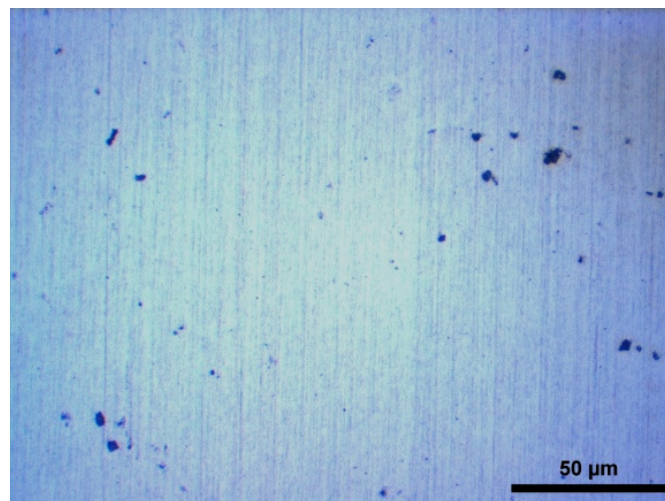
Figure 99: Particles introduced through sample preparation of alloy Al5N at 50X magnification [5].

In alloy Al5NFeSi the introduction of iron and silicon has lead to some particle formation. Their grey colour indicates an iron rich form of particle (fig. 100).
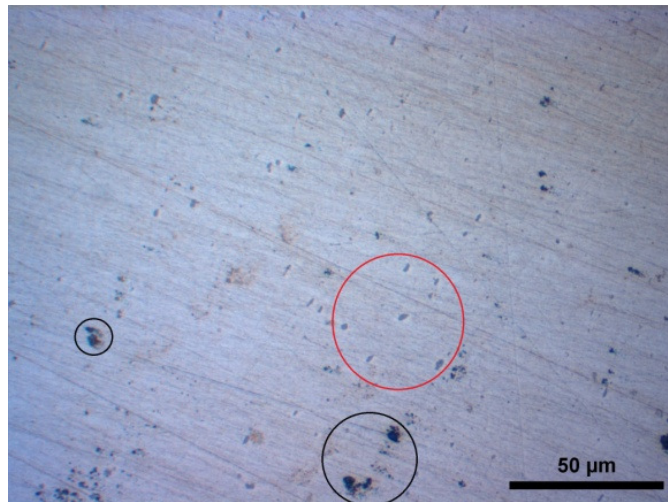
Figure 100: Particles found in alloy Al5NFeSi at 50X magnification. The red circle marks some of the grey iron rich particles while the black circles mark the particles introduced through sample preparation[5].

Compared to alloy Al5NFeSi, alloy Al2NFeSi contains a slightly higher amount of particles. Also, some of the particles appear to be larger, these may also be clusters (fig. 101).
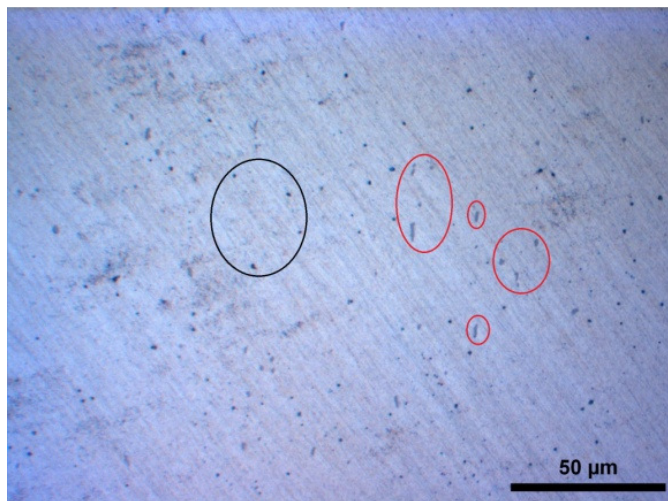
Figure 101: Particles found in alloy Al2NFeSi at 50X magnification. The red circle marks some of the grey iron rich particles while the black circles mark the particles introduced through sample preparation [5].

Alloy Al2NFe2Si which has an increased amount of wt % iron relative to the 3 other alloys shows a significant increase in particle density (fig. 102).
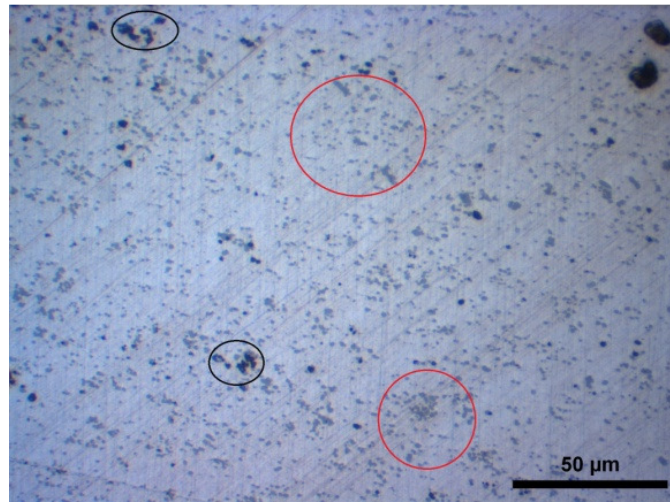
Figure 102: Particles found in alloy Al2NFe2Si at 50X magnification. The red circle marks some of the grey iron rich particles while the black circles mark the particles introduced through sample preparation [5].

6.1.2. Tensile tests

The results from the tensile tests performed in the project work are given in figure 99. Apart from alloy Al5N and partly Al2NFe2Si the results were too inconclusive to give a general description on a satisfactory basis. The curves in figure 99 are not the actual results, but rather trend lines based on 1-4 test specimens per alloy. The reason for the inconsistency was likely the difference in degree of recrystallisation (chapter 5.1.2). 3 of the alloys were only partly recrystallised and in that sense, not homogenous and uniform throughout the material. Alloy Al5N and Al2NFe2Si appeared fully recrystallised and not recrystallised respectively (some initiation points for recrystallisation were visible in alloy Al2NFe2Si) and hence the results appear more satisfactory and similar. In those 2 cases the trend line gives a good description of the tensile properties. Alloys Al5NFeSi and Al2NFeSi were only partly recrystallised and showed large deviations in results.
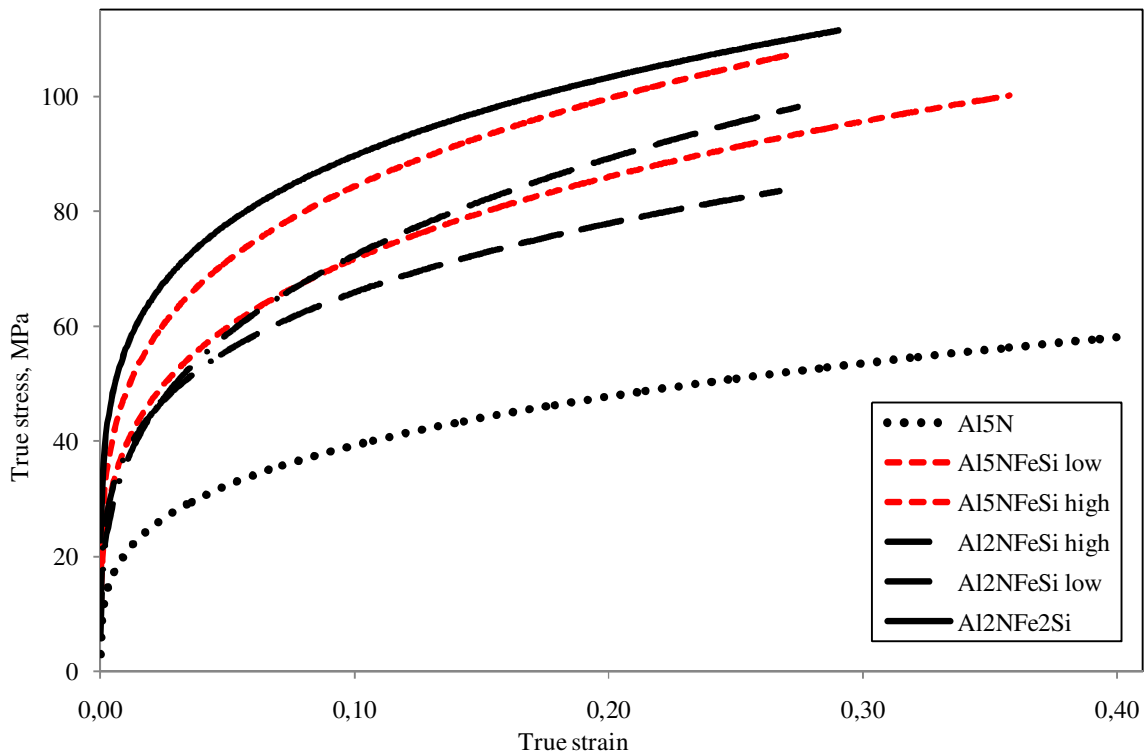
Figure 103: Flow curves for extruded alloys Al5N-Al2NFe2Si at const. strain rate: $10^{-3}s^{-1}$ [5].

Table 20 shows the average values for the most significant properties for extruded alloys Al5N-Al2NFe2Si. The tensile properties are somewhat misleading as they are calculated on the basis of several possible outcomes; they are given more as a rough estimate.

Table 20: Tensile properties and grain size of extruded material tested during fall 2010[5].

Alloy	Yield Strength [MPa]	Ultimate Tensile Strength [MPa]	Uniform Elongation [%]	Strain Rate Sensitivity, m	Average grain size [μm]	Average particle size [μm]
Al5N	13.5	57.8	39.9	0.0026	136	-
Al5NFeSi	36.5	99.3	28.9	0.0050	81	2
Al2NFeSi	27.0	90.2	26.9	0.0036	119	2
Al2NFe2Si	50.0	107.7	28.7	0.0059	51	2-5

From the tensile results it was concluded that an initial introduction of small amounts of iron and silicon lead to a dramatic increase in strength and reduction in uniform elongation. A further increase seemed to affect these parameters in a much less dramatic way. The results also indicated a similar tensile behaviour in the 2 alloys Al5NFeSi and Al2NFeSi as a possible solution. The only difference between these 2 alloys was that Al2NFeSi contained trace elements and a 40% increased wt % iron. The effect, if any, of a further increase of iron and the introduction of trace elements was therefore considered questionable.

6.1.3. Haasen Plot
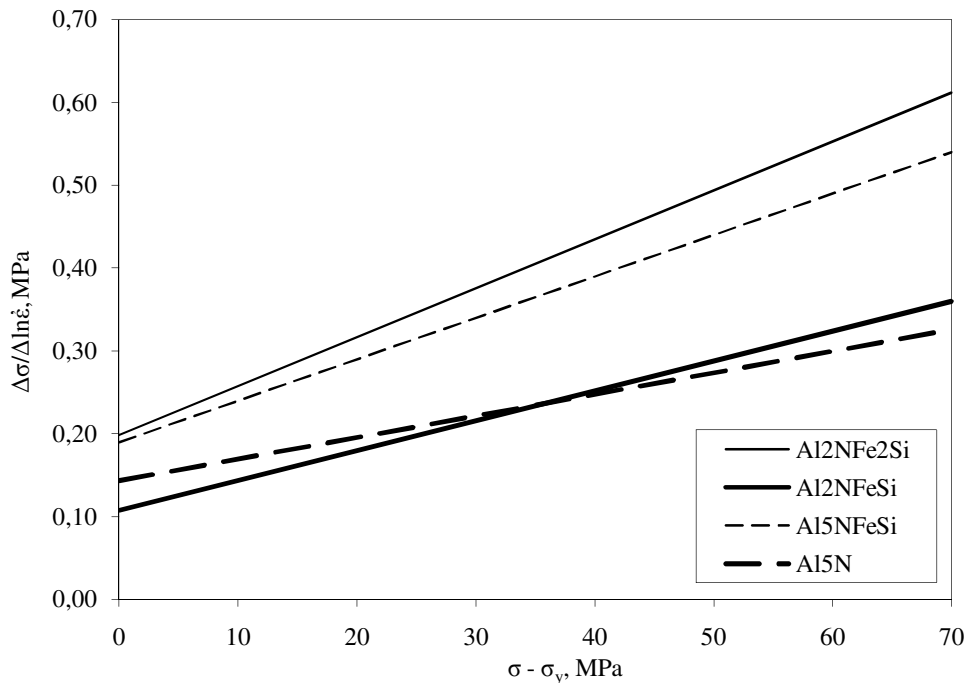
Figure 104: Haasen plot for the extruded alloys, performed during project work[5].

The results from the Haasen plots for the extruded alloys tested in the project work will be discussed in chapter 6.6. The characteristic values collected from these Haasen plots are given in table 21.

Table 21: Instantaneous strain rate sensitivity, B, intersect with y-axis, A, and activation volume, Vs, for extruded alloys Al5N-Al2NFe2Si.

Alloy	B	A	V_s [J]
Al5N	0.0026	0.1434	1.56E-18
Al5NFeSi	0.0050	0.1897	8.10E-19
Al2NFeSi	0.0036	0.1080	1.12E-18
Al2NFe2Si	0.0059	0.1984	6.86E-19

6.2. Microstructure

Cast alloys:

The results from the optical microscope showed that Al5N contained extremely large grains compared to the other cast alloys. The likely reason for the large grains is the lack of a grain refiner in the casting process and the low recrystallisation temperature. The grains are free to develop and grow during casting and solidification. There is a "single-grain" effect, the grains are so large that they behave like single crystals and there are no or few areas for nucleation. Homogenisation was carried out at 600°C and during cooling the alloy has undergone extensive grain growth until near room temperature in the specimen has been restored.

The initial introduction of iron and silicon to Al5NFeSi affects the grain size and structure dramatically. Since the only difference between Al5N and Al5NFeSi is the Fe/Si content, the changes in microstructure are directly traceable to the iron and silicon. As iron and silicon both have a low solubility in aluminium a small amount is likely solved in the aluminium matrix while the rest forms intermetallic phases and particles. The grain sizes decrease dramatically in alloy Al5NFeSi compared to alloy Al5N as more areas for nucleation are present.

The two 5N alloys displayed the best "resistance" against segregation. Resistance is a false term as it is the low recrystallisation temperature which more or less erases the cast or segregation structure. In alloy Al5NFeSi recrystallisation has been initiated but not completed. In addition, silicon in aluminium cast processes compensates, depending on the amount, for the volume reduction caused by aluminium shrinkage during casting and shortens the saturation interval. Silicon expands heavily during solidification[29]. Based on these to alloys it is likely that iron and silicon increases the recrystallisation initiation temperature.

Alloy Al2NFeSi was heavily affected by the casting process; the grains were large, coarse and had no distinct shape. Big segregated grains dominated while a few areas were found where small grains had started to form on grain boundaries by initiation of recrystallisation. Al2NFeSi contains a relative increase in wt % iron of roughly 40% compared to alloy Al5NFeSi. In addition Al2NFeSi contains various trace elements corresponding to roughly >330 wt ppm. These additions may be the cause of the coarse nature of the microstructure. Whether the trace elements or the iron increase is the specific cause is harder to determine. However, the likely explanation is a further increase of recrystallisation initiation temperature caused by increased iron content and in addition to *no* further increase in silicon content.

Alloy Al2NFe2Si has an increase in iron wt % content of about 60% and the amount of trace elements has increased from >330 to >430 (compared to alloy Al2NFeSi). The grain structure showed smaller segregated grains also with areas where nucleation has started. As the structure is considered "finer" compared to that of alloy Al2NFeSi and the biggest relative difference is in the form of iron increase, the trace elements may cause more coarse segregated grains. The presence of Vanadium in the alloy is very small 118 wt ppm, some minor effect of this element which is commonly used in aluminium as a grain refiner might also explain the reduction in grain size. However, this is highly unlikely as the previous alloy contained 89 wt ppm Vanadium. The iron increase is believed to be responsible for the smaller grains by leaving more areas for nucleation.

Based on the microscope results for the cast alloys it appears that iron and silicon affects the degree of recrystallisation. Alloy Al5N has likely recrystallised during air cooling after the homogenisation process. The pure state has allowed the grains to grow freely during cooling. The same explanation is applicable to the 3 other alloys and their varying degree of recrystallisation. The temperature during cooling may have been sufficiently high to start recrystallisation. The presence of elements have increased the recrystallisation temperature so that they appear partly recrystallised to a varying degree. Al2NFe2Si and Al2NFeSi show the least recrystallised grain structure and contain the highest amounts of elements with respect to both iron and trace elements.

The grains in the cast alloys are all too big for the Hall-Petch effect to apply.

Extruded alloys

The extruded alloys are briefly discussed in connection with various degrees of recrystallisation and remaining deformation structure. This limitation is done on the basis that they have not been tested in the uniaxial tension machine for this master thesis.

Due to the purity alloy Al5N requires a very low temperature in order for recrystallisation to occur. Even room temperature, $20^{\circ}C$, is a rather high temperature for this alloy. The extrusion process requires a low applied force, in this case, and it is possible that the alloy is recrystallised through dynamic recrystallisation or recovery. The heat arising from the extrusion is possibly elevated enough to cause the material to recrystallise during the process or the temperature in the material shortly after extrusion is sufficient for recovery. The grain structure is made up of large equiaxed grains due to the lack of obstacles against grain growth and few areas for nucleation.

Alloy Al5NFeSi and Al2NFeSi were partly recrystallised when studied in the OM. It is likely that they have started to recrystallise after the extrusion procedure. The required temperature for recrystallisation to occur is dependent on the amount of alloying elements and this may be slightly increased by the addition of iron, silicon and/or trace elements so that the recrystallisation has been initiated but not been completed. The deformation structure is still visible and quite dominant.

Alloy Al2NFeSi displayed a typical deformation structure where large narrow grains deformed by extrusion cover most of the specimen. Several areas were registered as initiation of recrystallisation on grain boundaries; however these were few and far between. Higher magnifications revealed a sub structure network inside the narrow fibre grains. The extensive increase of iron is the likely cause of the deformation structure. Further increase of the temperature at which recrystallisation may occur as a result of increased relative amounts of trace elements and iron.

The findings that the iron and silicon addition affects the degree of recrystallisation are further supported by the results for the cast alloys.

Rolled alloys

The rolled alloys were recrystallised and by the annealing experiment shown in figure 47 the similar properties regarding the three alloys Al5NFeSi-Al2NFe2Si became apparent. The alloys followed roughly the same recrystallisation curve and the hardness measurements were similar at the different temperatures.

Al5N appeared fully recrystallised at room temperature and the annealing only lead to grain growth which was not desirable. The grains were roughly of equiaxed shape and varied greatly in size across the examined area in the optical microscope.

The recrystallisation development and temperature for alloy Al5NFeSi was greatly affected when iron and silicon were solely added. This supports the statement made for the extruded alloys that alloying elements increases the temperature for initiation of recrystallisation. Furthermore, the introduction of iron and silicon lead to increased hardness values by about 250% compared to alloy Al5N. A further introduction of iron, silicon and trace elements only lead to moderately increased values for hardness.

The recrystallisation temperature for alloys Al5NFeSi-Al2NFe2Si was not affected by the relative differences in elements as they all seemed to have the same temperature for complete recrystallisation at 375°.

6.3. Texture

The cube texture was found in varying degree of intensity in all of the extruded alloys. This texture is a typical recrystallisation texture usually found in cold rolled al-alloys[28]. This corresponds well with the findings in the micro structural assessment made in the previous chapter. All of the extruded alloys showed some degree of recrystallisation. Al5N showed a very strong cube texture and appeared fully recrystallised after extrusion. Alloy Al5NFeSi and Al2NFeSi both displayed a partially recrystallised state and the cube texture decreased in intensity along with increasing amount of iron, silicon and trace elements. While the cube texture was still strong in alloy Al5NFeSi it was substantially weaker in alloy Al2NFeSi. Alloy Al2NFe2Si showed only a few initiation areas for nucleation but still displayed a strong cube texture. One explanation might be either the sub grains or a scanning area which included too few grains, i.e. to many nuclei relative to the rest of the specimen surface.

In addition to the cube texture, which was found to some degree in all four extruded alloys, two other textures were found in the three alloys which contained iron and silicon. The β-fibre which is a typical deformation structure was found with high intensity in alloy Al2NFeSi while in alloy Al5NFeSi the intensity was moderate. As these two alloys are a combination of long narrow grains and sections of smaller grains it might be possible that these would create different textures.

In addition to the strong cube texture in alloy Al2NFe2Si another weaker texture type was found, believed to be an R-texture. This is usually a typical recrystallisation texture. The few areas containing nuclei might explain the existents of the texture and its low intensity.

The analysis carried out for *rolled* Al5N was based on too few grains to conclude the texture with any certainty. However, the results indicated a cube texture, which is likely considering the results for the extruded version. The 001 pole figure in figure 66 showed a slightly TD rotated cube texture.

The rolled alloys Al5NFeSi-Al2NFe2Si all showed a strong TD rotated cube. The cube seems to be rotated roughly 45° about the TD axis. The result is highly probable as these alloys are rolled versions of the extruded material. If the texture is stable, the deformation caused by rolling leads to

rotation of the cubes. Furthermore, this is supported by the fact that the cube structure is hard to "get rid of" once introduced. The β-fibre found in extruded Al5NFeSi and Al2NFeSi was still visible in the ODF maps (figure 69 & 71) for the rolled versions and have decreased in intensity. This further supports their presence in both alloys.

The rolled alloy Al2NFe2Si has several lower intensity areas which might be explained by the reflections of several differently TD rotated cubes (figure 72). This is based on the strong reflections lying on the horizontal edges of the circle frame, while the reflections inside the 001 pole figure are varying in intensity. In addition to the TD cube, the R-texture has almost vanished but is slightly visible by the same points suggested by figure 65.

6.4. Particles

Big coarse particles of sizes varying in the region 1-5µm were found during EDS investigation. Apart from alloy Al2NFe2Si, which has a substantially higher amount of particles, the particle strengthening contribution from Al5NFeSi and Al2NFeSi is considered insignificant. The spacing between the particles for these two alloys is too large for the strengthening through non-shearing particles by the Orowan mechanism to occur.

From table 16 the strengthening contribution from the alloy particles showed that only Al2NFe2Si-particles would contribute to strength increase by a significant amount. This may be one explanation for the slightly elevated flow curves seen for alloy Al2NFe2Si compared to the two other alloys which contained particles. This is based on the fact that the grain sizes were very similar after annealing and recrystallisation, i.e. the grain size effect would not explain this difference.

Al5NFeSi, know that this alloy should only contain two elements capable of creating particles in aluminium as it is virtually free of trace elements.

Most of the particles found were square shaped with rounded edges and the longest sides were oriented parallel to the rolling direction. This implies that the particles were deformed during rolling and the ditch area surrounding most particles may be the result of a former circular shaped particle. Particles found in the extruded material (section 6.1.1) were distinctly more circular. From the introduction of iron and silicon to the ultra pure alloy Al5N we get Al5NFeSi and it follows that the particles which are created must be a form of AlFeSi. The particles found in the two other alloys are believed to be of the same nature and their colour (light grey) indicates that they are iron rich. The trace elements are likely not of significant quantity to create particles of significant sizes with iron and silicon.

As mentioned in the theory section (2.7.3.) the characterisation of the particles is a difficult task. The table below (table 22) considers the Fe/Si ratio believed to represent the α- and β-AlFeSi particles by findings from various sources collected by S. Bunkholt[26]. The assessment is made difficult by the various conditions under which the Fe/Si-ratios were obtained. During the particle investigation in this master thesis 20kV was used for accelerating voltage of the beam, while the values in the table were obtained by 15kV. Whether the ratios are given by the wt% or at% is also not given.

Table 22: The Fe/Si-ratio representing α- AlFeSi and β-AlFeSi particles according to three different sources are given below their names. To the left the Fe/Si-ratio from wt% values in the particles found in the three rolled alloys are given. (x) denotes that the ratio found corresponds well, (-) denotes the possibility. For references see[26].

		Samuel et al.		Claeves et al.		Claeves et al.		Osada et al.	
		0.7	0.4	0.55	0.14	1.71	0.81	> 5.2	<3.3
Alloy Particle	Fe/Si-ratio wt%	α	B	α	β	α	β	α	β
Al5NFeSi	1.60					x			-
Al5NFeSi	0.71	x		-			-		-
Al5NFeSi	0.69	x		-			-		-
Al2NFeSi	0.73	x		-			-		-
Al2NFeSi	0.44		x	-					-
Al2NFeSi	0.68	x							
Al5NFe2Si	1.35					-			-
Al5NFe2Si	2.04								-

The corresponding table for at % values was also used for characterisation but was not considered as likely as the one given. The Fe/Si ratios deviated more from the ratios found by the authors, and the table is therefore not included here.

From microscopy the presence of particles is unquestionable but whether they are α-AlFeSi or β-AlFeSi is hard to conclude based on table 22. If one considers Samuel et al.[26] to be correct the particles found are mainly α-AlFeSi particles. This seems likely based on the similarity in Fe/Si ratio, but the sources do not say anything about the values used (wt % or at %).

6.5. Constant strain rate tensile tests

Cast

Both set of tests performed with the cylindrical cast specimens yielded very inconclusive results. Most evident was the difference in elongation, but the strength also varied in specimens from the same alloy. The contributing factors to this instability are believed to be results of the casting and or the homogenising. The cast material has coarse and large grains and may include impurities from the process. In theory the material should be isotropic and homogenous in the area from which the samples had been cut out. However, both the micro structure characterisation and the tensile tests indicated the opposite. The results from the cast tensile tests will be covered briefly in the following as they are considered more or less useless for the purpose of determining the effects of elements on tensile behaviour.

The largest grains found in alloy Al5N were measured to be in the region 5-15mm. Since the cross-section of the cylindrical tensile specimens had a diameter of 6mm, some specimen areas may contain only a few grains in the area of parallel length during tensile tests. In fact, the behaviour would resemble that of a single crystal or rather a series of single crystals. The extreme scenario would be that one tensile specimen would contain no more than 2-3 grains in the parallel area. The varying microstructure combined with the large grains is the reason for lack of correlation in tensile test results for alloy Al5N. The random structure and grain size are due to the casting process and the lack of a grain refiner in the ultra pure alloy to prevent grain growth.

The strongest alloy based on the tensile test was the most alloyed Al2NFe2Si, as expected. The main strengthening contribution is likely the increased amount of iron compared to Al2NFeSi. The amount of trace elements is only slightly higher compared to the "weaker" 2N-alloy and the silicon content is the same for the 2 alloys. It is evident, in this case, that even relatively small amounts of iron affects the properties, and especially the strength parameters. Even though the amount of iron in alloy Al2NFe2Si is 0.149 wt %, it showed improved YS and UTS compared to alloy Al2NFeSi which contains about 0.094 wt % iron.

The most valuable findings in the cast tensile tests were the similar tensile behaviour displayed by alloys Al5NFeSi and Al2NFeSi. This is supported by the project work[5] on the extruded alloys as a plausible outcome. For 12 tested specimens of the two alloys 11 of the flow curves were within the same region. These 11 curves displayed a maximum deviation by only 5-6MPa relative to each other for the two tensile set ups (figures 82 and 83). The similarity in work hardening rate indicated that the increase of relative iron amount and the introduction of trace elements have little effect on these two alloys. The elongation varied extensively due to the non-uniform grain distribution, and subsequently the UTS varied to larger degree.

The grains in the 4 alloys were too large to register any noticeable Hall-Petch effect as seen by the low values in table 8.

The twisting motion during testing as mentioned in the results chapter was likely due to a combination between the dimension of the cross heads and the softness of the material. The tension machine seemed to twist the specimen slightly during clamping. The result was visible by the specimen cross heads by a crooked deformation.

In retrospect these cast tensile tests should not have been carried out under the conditions applied. One way of improving the results would be to make larger tensile test specimens and improve the conditions during homogenisation.

Rolled

The results from the rolled and recrystallised were by far the most relevant and satisfactory to make a good assessment regarding the effects of elements and impurities in the tested alloys.

Rolled Al5N was found to have low strength values and the highest elongation. This was expected based on the micro structure which revealed large grains compared to the other alloys. The alloy contains close to no elements other than aluminium and the large grains and low strength lead to high ductility. No contributions from particles or Hall-Petch effect in addition to dislocation density reduction by annealing are the likely contributors to the low mechanical strength properties. The alloy displayed average values for YS of 12.4MPa, UTS of 61MPa and uniform elongation of 39%. The average approach is a good model to describe these values because of the good correlation in flow curve results.

The introduction of 0.066 wt % iron and 0.068 wt % silicon to alloy Al5NFeSi leads to a dramatic increase in strength properties and only a moderate reduction in ductility compared to the ultra pure alloy without the elements. The YS improved by about 100-110% from 12.4MPa to 25.6MPa, the UTS was improved by roughly 70% from 61MPa to 103.1MPa while the reduction in ductility was estimated to be about 10% from 39% to 35% elongation. The isolated effect of an initial introduction of small amounts of iron and silicon to an "element free" alloy is directly traceable and gives a substantial change in mechanical properties. The altering of the microstructure resulting in increased grain boundary area causing dislocation pile ups and the Hall-Petch (table 8) effect are possible contributors to the improved properties. However, the main contribution comes from a small amount of elements, Fe and Si, in solid solution. Iron is known to increase the dislocation density by a substantial amount[8]. The contributions from Hall-Petch and grain boundary area are far too modest to account for such an extensive strength improvement. The particle content is also too low to contribute (table 16).

Al5NFeSi and Al2NFeSi showed close to equal results from the tensile testing. The maximum deviation in UTS for the two alloys was calculated to be only 3.8MPa. The average values for UTS were identical and the YS deviated by 0.2MPa while the uniform elongation differed by 1% relative to the elongation of Al5NFeSi. As the only difference between the two alloys is a slight increase in the wt % iron from 0.066 to 0.094 and the introduction of pollutions (trace elements) in Al2NFeSi relative to Al5NFeSi, the assumption that this introduction does not significantly affect the mechanical properties seems to apply. This is partly supported by the findings in the project work[5] on extruded versions of the material. Although, this was hard to conclude with any certainty as there were several possible outcomes because of miscorrelation in the flow curves. Still, it was considered a likely outcome and the findings in this work are even more conclusive. The results from the cast tensile tests may further support this theory as the same alloys displayed close to similar tensile behaviour. In addition previous work such as Westvold's thesis which registered the same effect of magnesium[7]. One explanation for the lack of change in tensile properties may be that maximum solid solubility has already been reached for iron in the aluminium matrix so that the excess iron may only be present as particles or intermetallic compounds. The Si content is

virtually unchanged. Another likely explanation would be that iron and silicon form inclusions rather than forming by elements in solid solution. The amount of formed particles is too low to contribute any strengthening due to the small relative amounts of the elements added.

The yield strength of alloy Al2NFe2Si was in fact found to decrease by roughly 4%, while the UTS increased by about 2% and the uniform elongation was estimated to be about the same, 35% elongation (compared to Al2NFeSi). The slightly elevated values for UTS may be explained by the large increase in particle density. From the calculations(table 16) made in chapter 5, although very rough estimates, the particle strength contribution of about 5MPa seems to fit in well with the theory that there in fact is a moderate particle strengthening effect. Another explanation would be the Hall-Petch effect which appears to be present for the rolled material (table 8). However, the alloy does not distinguish itself from the other alloys to the same extent as for the particle strengthening values.

The formation of an increased amount of particles might further support the assumption that the maximum solubility has already been reached for iron in aluminium and a further increase would only lead to more particles. It is also possible that silicon forms particles with iron rather than forming by elements in solid solution. This would explain the dramatic increase in particle density in alloy Al2NFe2Si compared to Al5NFeSi and Al2NFeSi. Alloy Al2NFe2Si contains 0.149 wt % iron which is a substantial increase compared to the other alloys.

6.6. Haasen Plot of rolled specimens

Of the 4 *rolled* alloys included in the Haasen plot, 3 displayed a linear line which roughly had the same value for the slope and intersected the ordinate axis in y=0. Based on the theory outlined in chapter 2.6. this implies that the constant (equation17) *A* is roughly zero. The variable V_s corresponds to the fraction of activation volume resulting from elements in solid solution. A low contribution from the V_s corresponds to a large distance between solute atoms. According to the theoretical background the thermal contribution at room temperature (which was the condition for the tensile test) is zero and therefore the contribution must come from some form of initial dislocation density or dislocation network (due to sub structure) stored in the material. This is a paradox seen in light of the heat treatment which the rolled alloys have undergone. These were all annealed and dislocation density should decrease as a consequence. However, this remains a possibility leading to the conclusion that for these three alloys Al5NFeSi-Al2NFe2Si the dominating mechanism is the dislocation-dislocation interaction by either an initial dislocation density or a sub structure containing a network of dislocations.

Rolled alloy Al5N shows a different phenomenon. This alloy is of ultra pure quality and pure aluminium has been extensively[20] tested and the widely accepted behaviour is that of a line crossing in y=0 with a low value for the slope. The reason for this deviation is clearly visible from figure 93 where three distinct points, likely one point from each test, is located a great distance relative to the other points. The three points represent the first downward shifts and a possible explanation may be the settings concerning the initiation of loops, i.e. the PID settings, or it may be the result of the softness of the material during clamping as this was done manually. However, since the points likely come from three equal specimens it is more likely that this is an actual response in the material which cannot be overlooked. If these three points were discarded, a linear line similar

to the line found in most Haasen experiments for polycrystalline pure aluminium would be the result. As the alloy is free of elements in solid solution the elevated A-value, if considered to be correct, must come from some initial dislocation density or a network of dislocations due to some form of sub structure. This is however not seen in the microscope results and therefore the corrected curve given in figure 98 is considered a more likely solution. Curved Haasen lines have been reported in past studies[19].

Except for the case of alloy Al5N the introduction and further increase of iron and silicon along with trace elements seemed to have little effect on the instantaneous strain rate sensitivity and activation volume.

The Haasen plot for the *extruded* material should according to theory be equal (see figure 104). This is not the case and the results for all 4 extruded alloys involve an intersection with the ordinate axis located above y = 0. This positive intercept indicates that there is a contribution from an increased amount of solute atoms. The solute atoms distribute a breaking force on the dislocations. The increase of the constant A, which is the intercept with the ordinate axis, in alloy Al2NFe2Si can be explained by the increased density of particles found in this alloy. The precipitation process is more thermal. The elevated A-value for alloy Al5NFeSi compared to alloys Al5N and Al2NFeSi is accredited to the initial introduction of iron and silicon which likely involve a rapid increase in solute atoms. The conclusion for alloy Al5N and its deviation from "ideal" behaviour is roughly the same as for the rolled version of the alloy, either there is an initial dislocation density or sub structure or some error by the experimentalist has been made. From the chemical analysis and all other results it is evident that a contribution from elements in solid solution cannot account for the elevated curve.

6.6. Recycling

The results from the work conducted in this thesis are of a quite positive nature seen from a recycling perspective. Although the introduction of iron and silicon to a pure metal changes the mechanical properties and affect the grain structure the effects of a further increase up to 0.149wt% does not affect these properties significantly. The strength is high and the formability is only slightly decreased. The recrystallisation temperature is hardly affected by the increase. The reproducibility of low alloyed aluminium alloys does not seem to be greatly affected by an increase of trace elements or iron/silicon once these have been introduced. These conclusions are largely based on the results from the rolled experiments which yielded the best results.

6.7. Further Work

Suggestions for further work include an optimisation of the regulations (PID) and conditions for running an alternating tensile test for Haasen plot analysis should be established, a more thorough characterisation of the amounts of elements in solid solution by measuring dislocation density and electrical resistivity and a further variation in the conditions and amounts for trace elements, iron and silicon content. In addition, a further characterisation of the particles present in pure alloys containing iron and silicon should be conducted. Further tensile testing of cast aluminium by using large tensile specimens and an optimised heat treatment, might be something to consider.

7. Conclusions

- The initial introduction of iron and silicon seemed to affect the grain structure of both cast and extruded material greatly. A further increase of these elements along with small amounts of trace elements also affected the grain structure and grain sizes for both types of material. For the cast material the risk of segregated grains increased by increased amounts of elements. For the extruded alloys the degree of recrystallisation, post extrusion (recovery), also decreased along with an increase in elements. Ranging from large equiaxed grains in alloy Al5N to a typical deformation structure in alloy Al2NFe2Si (fibre structure).

- The effect of iron and silicon on recrystallisation temperature and hardness was extensive by the initial introduction for rolled specimens. The hardness values for Al5NFeSi increased by as much as 250% compared to alloy Al5N. The temperature for start of recrystallisation for the latter alloy increased from roughly room temperature to between 200-250°C. A further increase in relative amounts of iron and silicon along with the introduction of trace elements did not seem to affect the temperature for start and completion (about 375°C) of recrystallisation and the hardness values only increased slightly. The same effect was registered for the cast aluminium.

- The initial introduction of iron and silicon affected the texture by a varying degree. The introduction affected the micro structure and subsequently the texture of the extruded alloys which in turn affected the rolled textures. The most dominant texture component found in all of the extruded alloys was the Cube texture. The introduction of Fe and Si resulted in a strong β-fibre. By a further increase the β-fibre intensity was weakened and by a final increase the β-fibre vanished and a weak R-texture became visible. The combination with the cube and the β-fibre was likely the result of a mixed grain structure, consisting of both fibres and smaller grains found in alloys Al5NFeSi and Al2NFeSi. The R-texture was believed to be traced to the deformation structure in alloy Al2NFe2Si. The textures in the extruded alloys resulted in mainly a TD rotated cube texture in the *rolled* alloys and a weakening of the additional textures.

- The particles found in rolled alloys Al5NFeSi-Al2NFe2Si were categorised as either α- or β-AlFeSi. The alloys likely contained both, but the α-AlFeSi particles were considered the most common. However a conclusive assessment was difficult and the findings remain uncertain. The effect of the introduction of iron and silicon on particle density resulted in a few coarse grains, a further addition of elements increased the particle density slightly, and the final increase resulted in a great boost in particle density for alloy Al2NFe2Si. The strengthening contribution from the particles, by the Orowan mechanism, was only of significance in the latter alloy due to particle spacing.

- Tensile testing of cast aluminium yielded poor results and these were likely due to casting, specimen geometry and microstructure. However, an indication that alloys Al5NFeSi and Al2NFeSi displayed similar tensile behaviour was of interest. This was outlined as a possible solution during the project work, fall 2010[5]. The tensile tests performed on the recrystallised and rolled specimens showed and initial increase of about 100% for the YS,

70% for the UTS and a decrease in uniform elongation of only 10% once iron and silicon was introduced. Fe and Si in solid solution were found to the likely cause of this increase. Further additions of iron and silicon along with trace elements did not affect the tensile properties by a substantial amount. The strength was high, UTS and YS of about 103MPa and 25MPa, respectively, and the uniform elongation was measured to be about stabile around 35% for the three alloyed rolled materials. The introduction of pollutions represented by the small amounts of trace elements in the two commercial alloys did not affect the tensile results for the rolled alloys.

- Instantaneous strain rate sensitivity experiments by use of the Haasen plot showed that for the rolled alloys Al5NFeSi-Al2NFe2Si the value for the intersect with the ordinate axis was zero. The conclusion was that for these alloys dislocation-dislocation interactions or an initial dislocation density/network was the preferred mechanism. Alloy Al5N, which should cross the zero value of the ordinate axis, had a positive intersect with the ordinate axis and this must likely be due to some error in the analysis or an initial dislocation density. The alloy was annealed at 350°C even though it appeared fully recrystallised at room temperature and some grain growth might have lead to this increase. Iron, silicon and trace elements hardly seemed to affect the values for instantaneous strain rate sensitivity and activation volume.

- From a recycling perspective the findings in this work are uplifting. Once iron, silicon and trace elements are introduced into the material the mechanical properties are hardly changed. The tested alloys containing the mentioned elements showed stable and close to equal values for strength and formability.

8. List of figures and tables

8.1. Figures

8.2. Tables

9. References

1. Askeland, D. R., and Phulé, P. P. (2006) *The science and engineering of materials*, Fifth ed., Nelson, a division of Thomson Canada Ltd, USA.

2. URL. (13.06.2011) https://www.sciencephoto.com/media/97351/enlarge.

3. URL. (13.06.2011) http://scrapetv.com/News/News%20Pages/Science/Images/industrial-chimneys.jpg.

4. Furu, T. (2011) *Lecture: Recycling of Aluminium - possibilities and metallurgical challenges*, Hydro Aluminium.

5. Slagsvold, M. (2010) Study on the effect of Fe and Si content in Aluminium Alloys as a result of increased recycling - testing of high purity aluminium alloys in uniaxial tension, Trondheim.

6. Ryen, Ø. (2003) Work Hardening and Mechanical Anisotropy of Aluminium Sheets and Profiles, NTNU Norges teknisk-naturvitenskapelige universitet, Trondheim.

7. Westvold, F. (2000) The effects of alloying elements on mechanical properties and formability of recycled Aluminium sheet, Unipub forlag, Oslo.

8. Kovacs, I. (1990) *Effect of Iron and Silicon in Aluminium and Its Alloys*, Vol. 44 & 45 of Key Engineering Materials, Trans Tech Publications, Zürich, Switzerland.

9. Yamamoto, A., Tsubakino, H., Suehigo, A., and Watanabe, A. (2000) The Effects of Excess Si, Excess Mg and Fe on Precipitation in 6061 Aluminum Alloys during Recycling Process.

10. Davis, J. R., and Associates (1993) *Aluminum and Aluminum Alloys*, ASM International, Materials Park, OH.

11. Dieter, G. E. (1988) *Mechanical Metallurgy SI metric edition*, McGraw-Hill Book Company (UK) Ltd, Singapore.

12. Kalpakjian, S., and Schmid, S. R. (2008) *Manufacturing Processes for Engineering Materials*, Fifth ed., Prentice Hall Pearson Education South Asia Pte Ltd, Singapore.

13. URL. (18.06.2010) http://www.treehugger.com/aluminum-burtynsky.jpg.

14. URL. (18.06.2011) http://www.11thgillingham.btck.co.uk/Media/974/Logos%20and%20badges/aluminium.jpg.

15. URL. (18.06.2011) http://aliplast.en.made-in-china.com/product/HqgmptiSaeYo/China-Industrial-Aluminum-Profile-Aluminum-Products.html.

16. URL. (18.06.2011) http://www.alibaba.com/product-gs/428013744/New_Aluminum_Tiger_Design_Blade_case/showimage.html.

17. Gottstein, G. (2004) *Physical Foundations of Material Science*, Springer-Verlag Berlin Heidelberg.

18. Hansen, N. (1976) The Effect of Grain Size and Strain on the Tensile Flow Stress of Aluminium at room temperature, Pergamon Press, Great Britain.

19. Valle, J. A. d., Picasso, A. C., and Romero, R. (2003) The superposition of flow stress contributions in a precipitate hardened Ni-based alloy studied by strain rate sensitivity measurements.

20. Esmaeili, S., Cheng, L. M., Deschamps, A., Lloyd, D. J., and Poole, W. J. (2001) The deformation behaviour of AA6111 as a function of temperature and precipitation state.

21. Meetings (2011) *Lectures and meetings with supervisor: professor Bjørn Holmedal*.

22. URL. (16.6.2011) http://www.ebsd.com/ebsd-explained/images/beginners/insidesem.jpg.

23. URL. (16.6.2011) http://www.crystaltexture.com/jpg/IBP_1.JPG.

24. Haaland, B. (2007) Developments in mechanical and microstructural properties during deformation and annealing of accumulated roll-bonded aluminium alloys, Trondheim, Norway.

25. URL. (18.6.2011) http://aluminium.matter.org.uk/content/html/eng/default.asp?catid=100&pageid=1039432491.

26. Bunkholt, S. (2010) Microstructure and Mechanical Properties in Al-Mg-Si Alloys After Introduction of Post-Consumer Scrap, NTNU, Trondheim.

27. Norge, S. (2009) Norsk Standard NS-EN ISO 6892-1 2009: Metalliske materialer Strekkprøving Del1: Prøvingsmetode i romtemperatur.

28. Engler, O., and Randle, V. (2010) *Introduction to texture analysis : macrotexture, microtexture, and orientation mapping*, 2 ed., CRC Press, Boca Raton.

29. Solberg, J. K. (2010) *Technological metals and alloys*, Institute for Material Science, NTNU, Trondheim.
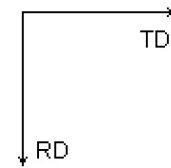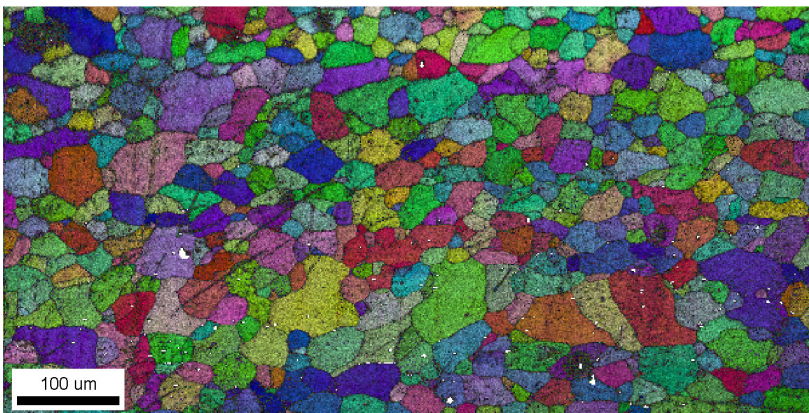
10. Appendix

10.A. SEM images of rolled alloy Al5NFeSi
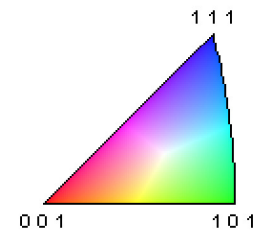

TD

RD
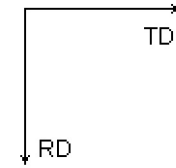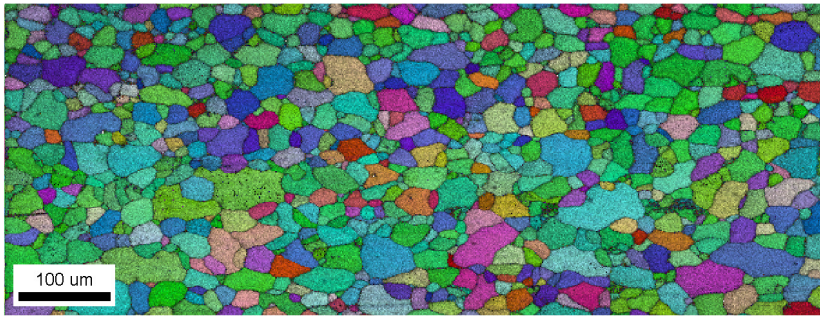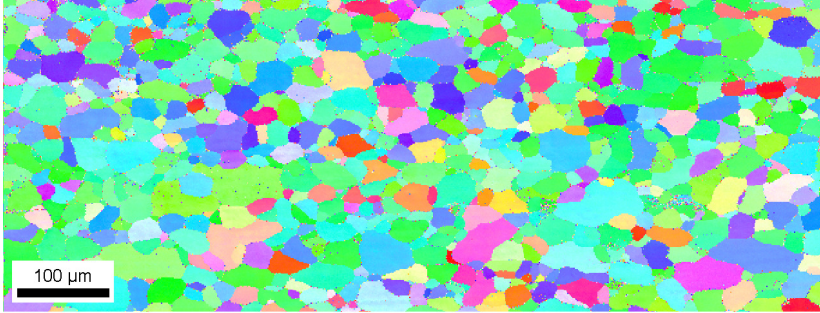
Color Coded Map Type:
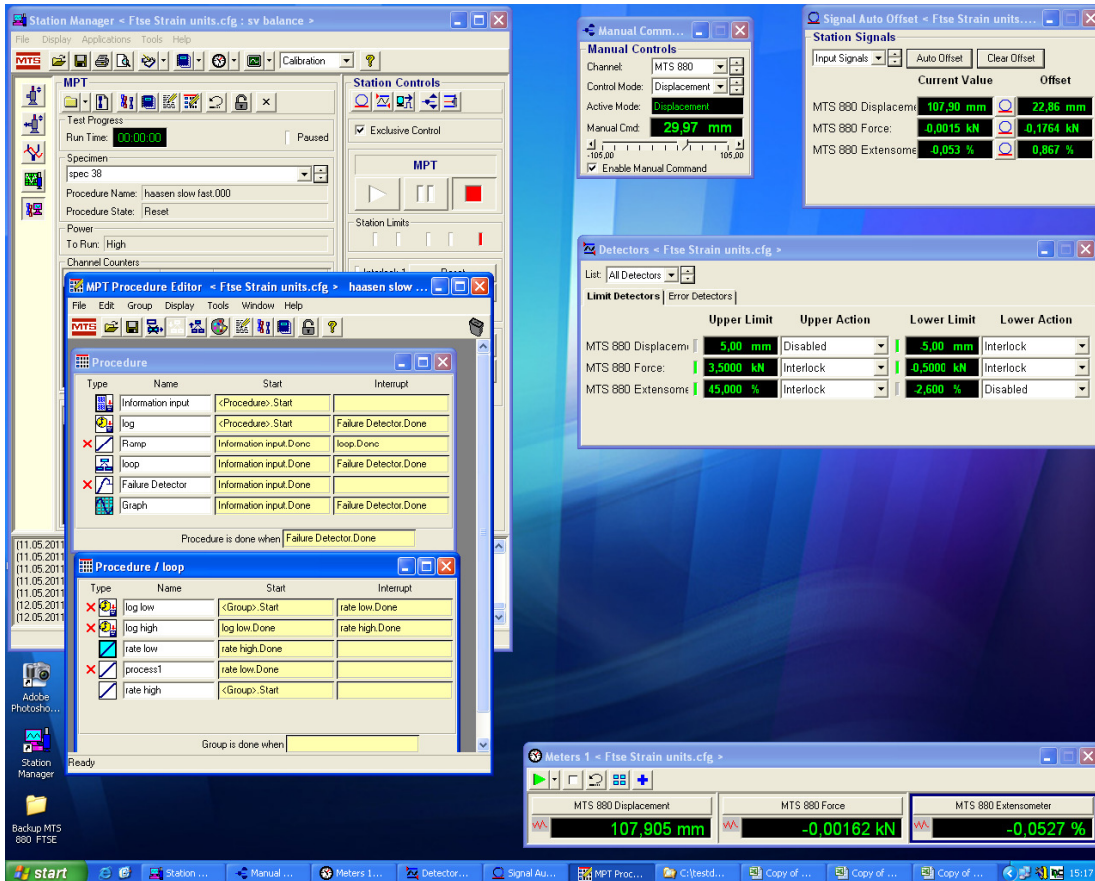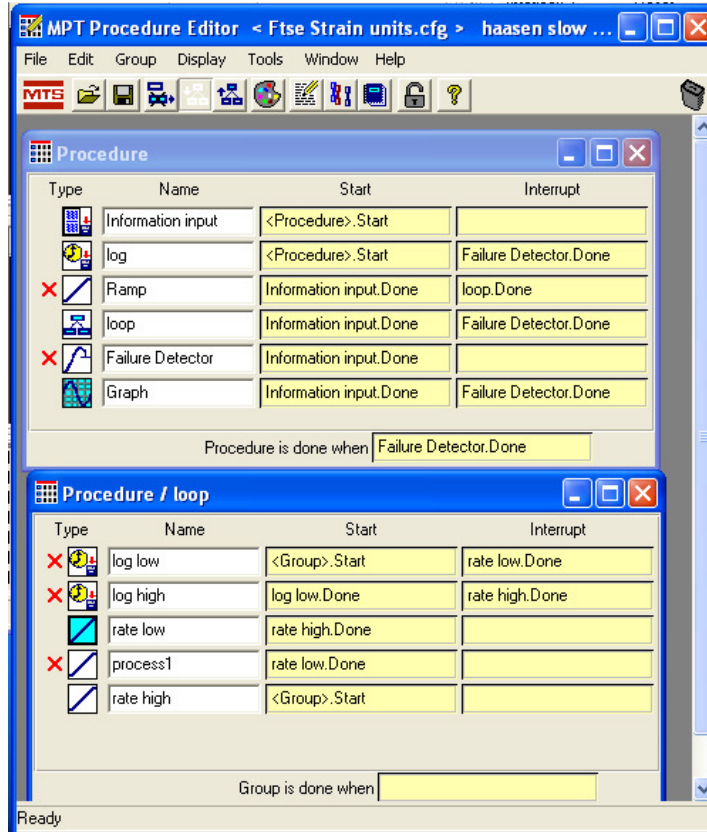Inverse Pole Figure [001]
Aluminum
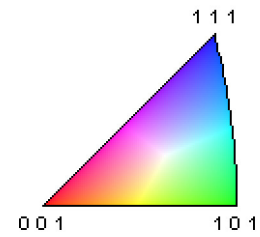
10.B. SEM images of rolled alloy Al2NFeSi

TD

RD

Color Coded Map Type:
Inverse Pole Figure [001]
Aluminum

A

10.C. Screenshots for programming of alternating strain rates

B

10.D. Chemical analysis-1

KJEMISK ANALYSE

Kallenavn		Al5N		Kallenavn		Al5NFeSi	
Prøvebetegnelse		**42442-O**		**Prøvebetegnelse**		**42443-O**	
Navn		**Al 5N**		**Navn**		**Al 5N**	
Legeringselement		**-**		**Legeringselement**		**0,067%Si+0,086%Fe**	
Legeringselementer		**Andel i %**	**Andel i ppm**	**Legeringselementer**		**Andel i %**	**Andel i ppm**
Ag	<	0,000001	0,01	Ag	<	0,000001	0,01
B	<	0,000020	0,20	B	<	0,000020	0,20
Ba	<	0,000004	0,04	Ba	<	0,000004	0,04
Be	<	0,000001	0,01	Be	<	0,000001	0,01
Bi	<	0,000070	0,70	Bi	<	0,000070	0,70
Ca	<	0,000020	0,20	Ca	<	0,000020	0,20
Cd	<	0,000010	0,10	Cd	<	0,000010	0,10
Cr	<	0,000010	0,10	Cr	<	0,000010	0,10
Cu		0,000037	0,37	Cu		0,000038	0,38
Ga	<	0,000010	0,10	Ga		0,000011	0,11
In	<	0,000030	0,30	In	<	0,000030	0,30
Li	<	0,000002	0,02	Li	<	0,000002	0,02
Mg		0,000093	0,93	Mg		0,000091	0,91
Mn	<	0,000010	0,10	Mn	<	0,000010	0,10
Na	<	0,000005	0,05	Na	<	0,000005	0,05
Ni	<	0,000020	0,20	Ni	<	0,000020	0,20
P		0,000164	1,64	P		0,000220	2,20
Pb	<	0,000020	0,20	Pb	<	0,000020	0,20
Sb	<	0,000080	0,80	Sb		0,000110	1,10
Sn	<	0,000030	0,30	Sn	<	0,000030	0,30
Sr	<	0,000007	0,07	Sr		0,000012	0,12
Ti	<	0,000010	0,10	Ti	<	0,000010	0,10
V	<	0,000020	0,20	V	<	0,000020	0,20
Zn	<	0,000100	1,00	Zn	<	0,000100	1,00
Zr	<	0,000005	0,05	Zr	<	0,000005	0,05
Sum		**0,000779**	**7,79**	Sum		0,000870	8,70
Fe		0,000072	0,72	**Fe**		0,066000	660
Si		0,000107	1,07	**Si**		0,068000	680
Renhet Al(eksl. Fe Si)		**99,999221**	% Al	Renhet Al(eksl. Fe Si)		**99,99913**	% Al

10.E. Chemical analysis-2

Kallenavn		Al2NFeSi	Kallenavn			Al2NFe2Si
Prøvebetegnelse		42444-O	Prøvebetegnelse			42480-O
Navn		Al 99,8 (2N)	Navn			Al 99,8-Al 5N
Legeringselement		0,067%Si+0,086%Fe	Legeringselement			-
Legeringselementer		Andel i %	Andel i ppm	Legeringselementer		Andel i %	Andel i ppm
Ag	<	0,0000010	0,01	Ag	<	0,00020	2,00
B		0,0002090	2,09	B		0,00030	3,00
Ba	<	0,0000040	0,04	Be	<	0,00010	1,00
Be		0,0000050	0,05	Bi	<	0,00100	10,00
Bi	<	0,0000700	0,70	Ca	<	0,00010	1,00
Ca		0,0000720	0,72	Cd	<	0,00030	3,00
Cd	<	0,0000100	0,10	*Co*		0,00040	4,00
Cr		0,0007970	7,97	Cr		0,00080	8,00
Cu		0,0005670	5,67	Cu		0,00060	6,00
Ga		0,0091600	91,60	Ga		0,01190	119,00
In		0,0000490	0,49	*Hg*	<	0,00020	2,00
Li	<	0,0000020	0,02	In	<	0,00020	2,00
Mg		0,0033800	33,80	Li	<	0,00010	1,00
Mn		0,0016400	16,40	Mg		0,00490	49,00
Na	<	0,0000050	0,05	Mn		0,00190	19,00
Ni		0,0032900	32,90	Na	<	0,00010	1,00
P		0,0014200	14,20	Ni		0,00450	45,00
Pb		0,0006110	6,11	P		0,00080	8,00
Sb		0,0001740	1,74	Pb		0,00080	8,00
Sn		0,0001060	1,06	Sb		0,00110	11,00
Sr		0,0000120	0,12	Sn	<	0,00100	10,00
Ti		0,0041800	41,80	Sr	<	0,00010	1,00
V		0,0089100	89,10	Ti		0,00370	37,00
Zn		0,0027100	27,10	V		0,01180	118,00
Zr		0,0008330	8,33	Zn		0,00470	47,00
Sum		**0,0382170**	**382,17**	Zr		0,00090	9,00
				Sum		0,05250	525,00
Fe		0,0940000	940,000				
Si		0,0690000	690,000	**Fe**		0,14900	1490,00
				Si		0,06500	650,00
Renhet Al(eksl. Fe Si)		**99,961783**	% Al				
				Renhet Al(eksl. Fe Si)		**99,94750**	% Al

D